A HIGH PRECISION ANGULAR ENCODER
BASED ON CAPACITIVE COUPLING

by

TODD SANKEY

B.A.Sc, The University of British Columbia, 1992

A THESIS SUBMITTED IN PARTIAL FULFILLMENT OF THE REQUIREMENTS FOR

THE DEGREE OF

MASTER OF APPLIED SCIENCE

in

THE FACULTY OF GRADUATE STUDIES

Department of Physics

We accept this thesis as conforming

to the required standard

THE UNIVERSITY OF BRITISH COLUMBIA

AUGUST 1994

In presenting this thesis in partial fulfilment of the requirements for an advanced degree at the University of British Columbia, I agree that the Library shall make it freely available for reference and study. I further agree that permission for extensive copying of this thesis for scholarly purposes may be granted by the head of my department or by his or her representatives. It is understood that copying or publication of this thesis for financial gain shall not be allowed without my written permission.

(Signature)

Department of Physics

The University of British Columbia
Vancouver, Canada

Date August 19, 1994

DE-6 (2/88)

Abstract

A method for measuring angular position based on sensing electrostatic fields is described. A device is presented which uses this method to achieve a resolution of 10^{-5} radians and is fabricated entirely from common electronic components mounted on printed circuit board.

The angular sensor consists of two coplanar, coaxial disks, one static and the other freely rotating. An electrostatic field is generated by N_r active radiator electrodes on the static disk. N_m passive modifier electrodes on the rotating disk determine the magnitude of the signals measured by a detector circuit for each of the radiators.

The relationship between N_r and N_m is chosen to be $N_m = \frac{N_r}{2} + 1$ which produces a vernier effect between the two disks. This effect determines the relationship between successive signals measured at a given rotor position. This relationship is shown to be most easily analyzed using Fourier analysis because the angle of the rotor can be entirely determined from phase of the single frequency component at $\omega = \pi - \frac{2\pi}{N_r}$.

Also presented are the effects of two different kinds of misalignment of the sensor: an offset in the centres of rotation of the disks and a tilt in the axes of rotation. The errors are characterized and a method for measuring and reducing their impact is shown.

Several tests of the sensor are presented and the results analyzed. A device simulator is used to examine the effect of changing the physical parameters of the sensor. A laser and spot detector are employed to test the accuracy of the sensor in measuring very small rotations. The repeatability of the sensor is examined by attaching the rotor to a stepper motor.

Finally the current design is extrapolated to suggest possibilities for a more precise sensor or a sensor better suited to different environments.

Table of Contents

List of Tables

List of Figures

1 Introduction

The aim of this thesis is to present a description of the resolving capabilities of an angular sensor based on an array of differential capacitance elements. The capacitances are modified when one array of electrodes is rotated relative to another, producing a set of electrical signals which are subsequently combined to determine the angular position.

A sensor is "any device designed to detect, measure, or record physical phenomenon."[1] A sensor converts one physical property, such as temperature, length, current, velocity, or pressure, into another in a predictable manner. For example, a mercury thermometer converts temperature into length through thermal expansion.

Sensors, both biological and manufactured, are based on many physical laws, such as thermal expansion, pressure variation, conservation of energy, and even quantum tunneling. Two properties of particular interest are photo-sensitivity and capacitance.

Photo-sensitivity is the basis for human vision. The retina of the eye translates incident light into electrical signals interpreted by the brain. It is also the basis for many manufactured sensors such as photographic plates, phototransistors, and charge-coupled devices.

Photo-sensitivity has several characteristics that make it desirable as the basis for a sensor. The field of optics is very well established. Optical sensors and the human vision system are intuitively related, which is helpful in design, implementation, and use. The use of light as the information carrier provides a very large channel for the transmission of information because of the high speed and large bandwidth available.

There are also difficulties with optical sensors, especially those intended to be very precise. Interpreting optical information can be difficult because the incoming signals can have a very large bandwidth. Preparing accurate optical instruments can be expensive as the components,

---

1 "Sensor," Webster's New World Dictionary of the American Language, p.1297.

such as lenses and mirrors, may need to be carefully ground and polished. Optical sensors may also be unsuitable for inspecting objects whose surface roughness is of the order of the wavelength of light or objects with dirty surfaces. Difficulties also arise in environments in which the intervening medium is either not transparent to the light, such as muddy water, or is highly inhomogeneous, such as a very turbulent atmosphere.

Capacitance is also the basis for many sensors. It is defined as the ratio of charge stored to potential difference. Mathematically capacitance is defined as:

$$C = \frac{Q}{V} = \frac{\int \nabla \cdot D \, dv}{\int E \cdot dl} \tag{1.1}$$

where Q is the charge stored in the device
V is the potential difference across the device
E is the electric field around the device
D is the electric displacement in the device
dv is a volume element
and dl is a path element

The capacitance of a device can be modified in two particular ways that make it useful as the basis for a sensor. The numerator in the above expression can by modified by changing the geometry of the capacitor. This action will change the amount of charge storage at a given voltage.

The second method is to modify the denominator by introducing a material or medium which can modify the electric field in the region of the device. Such a material can be either dielectric or conductive, which includes most materials and media. In typical capacitors the plates are separated by a vacuum, air gap, paper, or aluminum oxides but more exotic materials also work such as water, titanium dioxide, or plasma.

The first approach is used by most capacitive sensors. An example of this is a parallel plate capacitor where the capacitance, C, is approximated as:

$$C = \frac{\varepsilon_o A}{d} \tag{1.2}$$

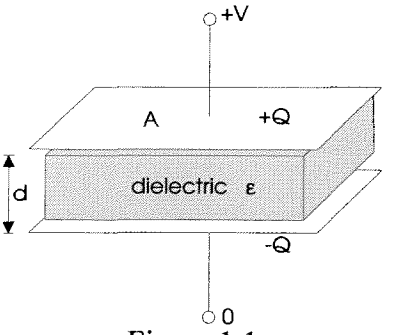

Figure 1.1
Parallel Plate Capacitor

where A is the area of the capacitor

d is the distance between the plates

ε is the dielectric constant of the material between the plates.

A sensor based on a parallel plate capacitor can effectively measure either changes in the distance between plates, assuming the area of the capacitor remains constant, or changes in the area assuming the separation is constant. These effects make a parallel plate capacitor a possible one dimensional position or motion sensor. Ultrasonic capacitance microphones have been built using this principle[2].

Optical sensors and capacitive sensors based on geometry modification are quite different. Capacitive sensors which use a field modifier, however, have significant similarities with optical sensors.

An object is "seen" optically with a sensor by observing light which has been generated by a light source and reflected by the object. The object is detected through the presence or absence of reflected light; that is, through a modification in the electromagnetic field.

An object can be "seen" capacitively as well. The basis for the vision is the electric field that exists between the plates[3] of a capacitor. An object[4] will modify this field. Consequently the

---

2 E.L. Meeks, R.D. Peters and R.T. Arnold, "Capacitance Microphones for Measurement of Ultrasonic Properties of Solids," Review of Scientific Instruments, XLII (October 1971), 1446-1449.

capacitive sensor can detect the presence of an object through its modification of the electric field.

Sensors based on this principle have been built before, the first of which was the Differential Inductometer designed by Michael Faraday in 1838[5] which could measure the dielectric effect of different materials based upon the deflection of two gold leaves. However, no such device has been built specifically as an alternative to optical vision. This is an idea put forward by Roger Dower[6], which he calls electrostatic imaging, or *antivision*.

While the concept of capacitive vision is foreign to humans, it does have a place in the animal kingdom. Some animals such as the mole-rat and the shark "see" by detecting electric fields. Sharks have electrosensory systems that are sensitive to gradients of less than five nanovolts per centimetre which they use to detect prey.

Other animals such as the African Mormyriformes have active sensory systems which consist of weak electric discharge organisms coupled with preferentially sensitive electroreceptors. These animals use their ability for communication as well as "electrolocation" analogous to echolocation used by many species of bats[7].

An electrostatic approach to vision has several potential advantages over optical vision. Dielectric and conductive properties tend to be constant with respect to the electric field strength and direction whereas colour and shade can be extremely sensitive to light intensity, wavelength, and the angle of the surface normal relative to the observer and the incident light. Transparent

---

3 Here "plates" is used in a general sense to include any set of objects between which there exists an electric field whose strength is proportional to the charge on the objects.

4 "Object" is also used in a general sense to include any material which has either dielectric or conductive properties. That is any material which can modify an electric field.

5 Faraday, Michael, Experimental Researches in Electricity I, 413-416.

6 Roger Dower, "Electrostatic Imaging Apparatus," Patent Application.

7 Joseph Bastion, "Electrosensory Organisms," Physics Today, XLVII (February 1994), 30-37.

materials can be difficult to detect optically yet may still have a significant dielectric constant. Also, capacitive devices can be manufactured inexpensively and accurately with etched printed circuit boards (henceforth called pc-boards).

Table 1.1
Comparison of Optical and Capacitive Vision

	Optical Vision	Capacitive Vision
carrier	electromagnetic wave	electrostatic field
field generator	EM radiation source	charge distribution
field modifier	surface of object	volume of object (dielectric) surface of object (conductive)
intermediate medium	index of refraction, n_{medium}	dielectric constant, ε_{medium}
requirement for clear vision	n_{medium} homogeneous $n_{object} \neq n_{medium}$	ε_{medium} homogeneous $\varepsilon_{object} \neq \varepsilon_{medium}$

This *antivision* concept has been generalized to include any sensor which operates based upon the principle of detecting a modified electric field[8]. In order for antivision to be useful, a quantitative description of its capabilities must be presented, and experimental tests to verify its predictions should be performed. This thesis attempts such a verification.

The approach taken in this thesis is to build a prototype sensor based on antivision and compare its capabilities with those of current state-of-the-art sensors. A reasonable starting point is a

8 Roger Dower, "Electrostatic Imaging Apparatus," Patent Application.

displacement sensor. Given an object with a fixed orientation, antivision is very sensitive to object position. Two candidate sensors are a linear displacement sensor and an angular displacement sensor.

An angular displacement sensor is a device which can measure absolute or incremental rotations. Commercially available angular sensors are based on a number of physical properties which include induction, electrical resistance, and photo-sensitivity. High precision capacitive angular sensors are not commercially available, but two devices hav been built by R.D. Peters[9] and a group at Delft University of Technology[10]. Mr. Peters' design is based upon the idea of changing the area of a capacitor. An antivision angular sensor operates by modifying the electric field by the presence of another object. The design from the Delft group is very similar in principle to the design presented here, however there are important distinctions which make the design described in this thesis more versatile.

An angular sensor is a suitable choice as a starting point for analyzing a sensor based on antivision because of its geometric simplicity and symmetry. In addition optical angular sensors with similar geometries are commercially available.

Some commercial angular sensors are capable of achieving accuracy in the micro-radian range, so an antivision angular sensor must be able to achieve similar results if it is to represent a technologically or commercially viable alternative to existing devices. Also, a thorough analysis of the errors associated with such an encoder is needed in order to extrapolate the usefulness of antivision to new domains.

---

9 R.D. Peters, "Linear rotary differential capacitance transducer," Review of Scientific Instruments, LX (August 1989), 2789-2793.

10Gerben W. de Jong et. al., "A smart capacitive absolute angular-position sensor," Sensors and Actuators A, XLI (1994), 212-216.

Following is a thorough analysis of an antivision angular sensor. Chapter 2 provides the theoretical basis for the sensor. Chapter 3 contains a description of the various components. Chapter 4 provides a detailed explanation of test procedures. Chapter 5 is a description of the experiments conducted and a report of the results. It also contains a comparison with existing devices, and proposes improvements on the current design. Chapter 6 suggests uses for this device and other sensors which utilize the same principles.

2 Theory of Operation

Electrostatic imaging, or *antivision*, is the idea that the surface profile of an object can be determined from the effect that object has on a known electric field. It is possible because virtually all materials have dielectric or conductive properties which will modify an electric field.

An antivision sensor, therefore, must consist of several components:

- signal generators to control the characteristics of the electric field
- electrostatic radiators to generate the field
- a homogeneous background medium to carry the electric field
- an object to modify the field
- detectors to respond to the generated field
- a signal conditioner to extract the relevant information from the generated field

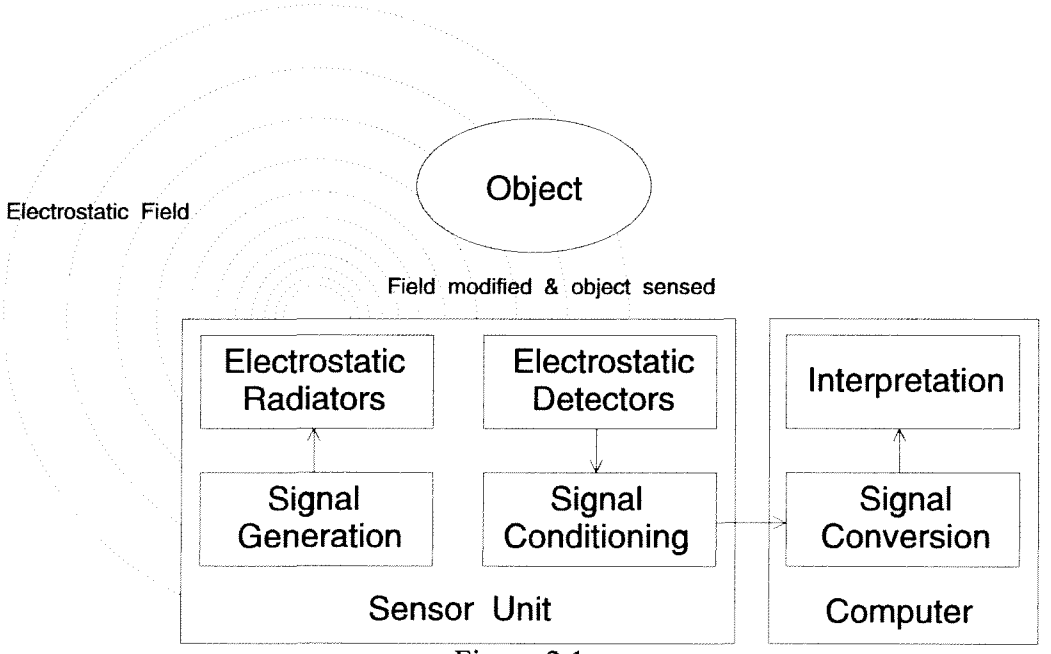

Figure 2.1
Concept of Electrostatic Imaging

- a signal converter to translate the information into a useful form

An electric field is set up between the radiators and the detectors. The modifier alters this field based on its geometry and dielectric properties. This change is reflected in the output of the detectors.

Many such sensors are possible[1]. An angular encoder can be implemented by creating an electrostatic radiator and modifier with circular symmetry. The phase relationship between the two would then be reflected in the output of the detector.

The current design consists of two co-planar, co-axial disks. The *stator* disk contains N_r radiators arranged symmetrically around the edge. It also holds the detector which is a single ring

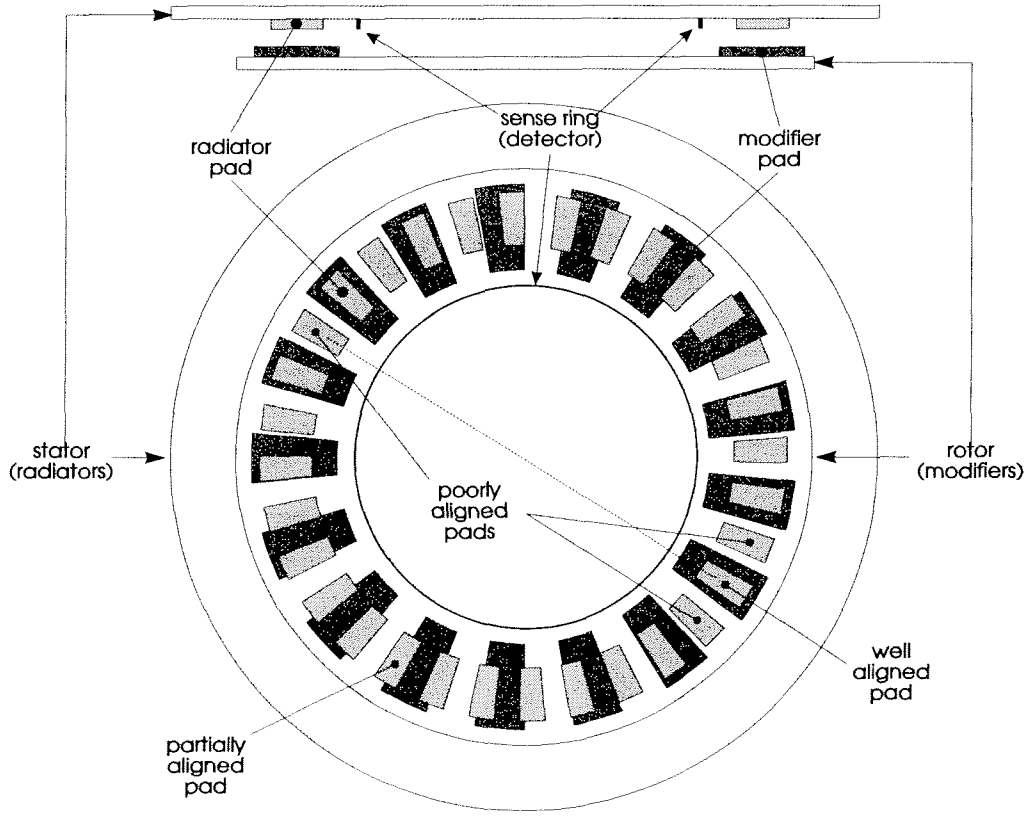

Figure 2.2
Side and Top Views of Stator and Rotor for $N_r = 32$, $N_m = 17$

1 Roger Dower, "Electrostatic Imaging Apparatus," Patent Application.

just inside the radiators. The *rotor* disk has $N_m = \frac{N_r}{2} + 1$ modifier pads similar to the radiators, and it is mounted such that it can rotate freely with respect to the stator.

Each radiator is sequentially driven to a specific voltage and the detector output is sampled while this voltage is maintained. The specific voltage is identical for all of the radiator pads. If a radiator pad aligns with a modifier pad then most of the electric field will be contained between the two and the detector will pick up very little. Conversely, if a radiator is not aligned with any modifier then the detector will feel a larger electric field.

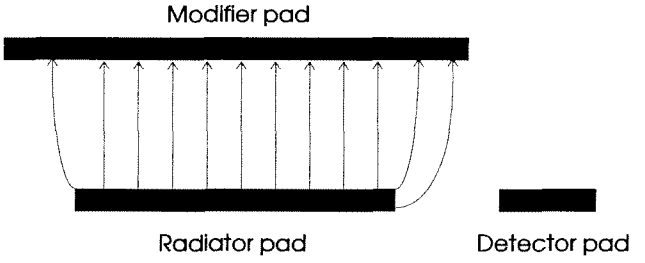

Figure 2.3
Electric Field for Well Aligned Pads

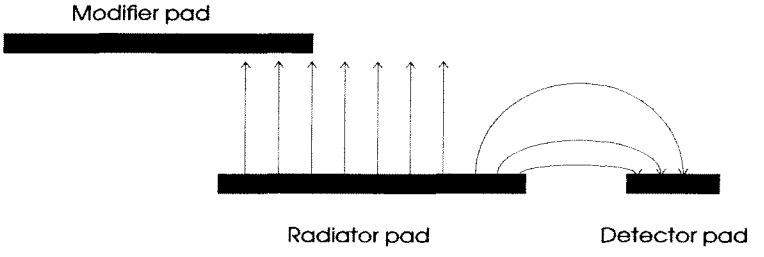

Figure 2.4
Electric Field for Poorly Aligned Pads

The number and geometry of pads on the rotor and stator are chosen to produce a vernier effect on the signal output. Where the stator has N_r radiator pads, the rotor has $N_m = \frac{N_r}{2} + 1$ modifier pads. This choice is intentional because it facilitates the interpretation of the sensor signals.

Because of the vernier effect of the geometry, a single stator pad will align maximally with one of the rotor pads. This stator pad will produce the minimal signal on the sense ring as most of the electric field will be contained between the stator pad and the rotor pad (see Figure 2.3).

Conversely a different stator pad will align minimally with another rotor pad. This radiator will produce the maximal signal on the sense ring (see Figure 2.4). Because of the layout of the pads and the relationship between N_r and N_m, this minimally aligned pad will be π radians away from the maximally aligned pad.

A rough calculation of the angular position of the rotor could be performed be collecting all N_r signals from the sensor and simply finding the maximum and minimum signals within the set. The angular position would then be determined to one part in N_r.

The determination of the angular position, however, is greatly improved by utilizing the information contained in the remaining $N_r - 2$ signals. This is achieved be recognizing how the signals from adjacent radiator pads must change due to the design of the disks.

Because there are slightly more than twice the number of radiator pads than modifier pads, a radiator that is well aligned with a modifier will be next to a radiator that is poorly aligned with a modifier. But, because there are not exactly twice as many radiator pads, there will be a gradual change such that a radiator that is well aligned will be π radians away from a radiator that is poorly aligned and $\pm\frac{\pi}{2}$ radians away from pads the are partially aligned (see Figure 2.2).

If there were exactly twice as many radiator pads as modifier pads, the signals could be described by:

$$V_n = A\cos(\pi n) + B$$

where n is the pad number (called the sample index)

V_n is the signal from the nth pad

A is the amplitude

B is the dc term where $B \geq A$

Also the set of N_r signals collectively is a called a sample.

If the sensor were designed with this relationship, ideally all radiator pads would produce one of two values, $A + B$ or $-A + B$. The rotor position could possibly be determined from the difference between these two values. However, with such a design A and B are not only functions of the rotor position, but also functions of the separation of the rotor and stator so a change in the rotor separation would affect the position calculations.

The vernier design can be considered as adding a modulating term which is directly related to the rotor position. This modulating term affects the oscillating component of the previous expression and produces the second geometric effect described above. A relationship which includes this effect is:

$$V_n = A\cos(\pi n)\cos\left(\frac{2\pi n}{N_r} + \theta\right) + B \tag{2.1}$$

where θ is the pattern position

In this expression A and B are still functions of the separation of the rotor and the stator but they are no longer dependent on the angular position of the rotor.

This expression can be used to interpret the angular position of the rotor because θ is a function of only the rotor position. The nature of relationship between θ and the rotor position is found by recognizing that θ must change by 2π radians whenever the rotor position is changed

by $\frac{2\pi}{N_m}$ radians. This is because such a rotation of the rotor will produce an identical alignment between the rotor and stator. Therefore:

$$\theta = N_m \gamma + \theta_o \tag{2.2}$$

Where θ is the pattern position

γ is the rotor position

θ_o is the pattern origin

and N_m is the number of modifier pads

The purpose of θ_o in equation (2.2) is to define the origin of the rotor position with respect to the stator. The choice for θ_o is arbitrary as it simply chooses what value of θ corresponds to a rotor position of 0 such that equation (2.1) holds. In practice θ_o does not play any role. Initial and final values for θ are calculated and the difference determines the net rotation of the rotor. In such a calculation θ_o drops out.

It is important to note that equation (2.2) implies that for a given value of θ the rotor position is not uniquely defined, in fact there are N_m rotor positions which produce the same value for θ. In practice this can be handled in two ways, the encoder can continuously determine the rotor position so that it can detect when the period of θ is reached or some asymmetry can be introduced into the signal which uniquely identifies the rotor position. Both approaches have been tried.

In order to report the rotor rotation directly, the sensor must use some method to determine γ, or θ given only the sample values V_n. Two possible methods of determining θ were examined, a linear solution and a solution in the frequency domain[2].

---

2 A third method tried used a non-linear curve-fitting technique called the Levenberg-Marquardt Method described in Numerical Recipes in C The Art of Scientific Computing 2nd ed., p.683. This worked well on theoretical data, however it usually failed, sometimes diverging completely, when real data was used. The algorithm was very sensitive to noise and poor rotor alignment.

2.1 A Linear Method for Calculating Angle

The first useful approach was a linear model. This can be done by recognizing that while equation (2.1) is not linear in θ, it is linear in $A\ cos(\theta)$ and $A\ sin(\theta)$.

$$A\cos(\pi\, n)\cos\left(\frac{2\pi n}{N_r}+\theta\right)$$

$$=[A\ cos(\theta)]\cos(\pi\, n)\cos\left(\frac{2\pi n}{N_r}\right)-[A\ sin(\theta)]\cos(\pi\, n)\sin\left(\frac{2\pi n}{N_r}\right)$$

$$=\Lambda\cos(\pi\, n)\cos\left(\frac{2\pi n}{N_r}\right)-\Omega\cos(\pi\, n)\sin\left(\frac{2\pi n}{N_r}\right)$$

This can be solved for Λ and Ω as linear coefficients of the basis functions $\cos(\pi\, n)\cos\left(\frac{2\pi n}{N_r}\right)$ and $\cos(\pi\, n)\sin\left(\frac{2\pi n}{N_r}\right)$ using normal linear curve-fitting techniques. Then A and θ can be determined since:

$$A^2=\Lambda^2+\Omega^2$$

$$tan(\theta)=\frac{\Omega}{\Lambda}$$

Because the method is linear, a result is guaranteed. The method gave results that were fairly insensitive to noise, but were very sensitive to poor alignment.

2.2 A Frequency Method for Determining the Angle

The frequency method comes from recognizing that the theoretical model of an ideal signal, equation (2.1), can be rewritten as

$$\frac{A}{2}\cos(\pi n+\frac{2\pi n}{N_r}+\theta)+\frac{A}{2}\cos(\pi n-\frac{2\pi n}{N_r}-\theta)+B.$$

That is, the "information" in the ideal sample is entirely contained in two frequencies, $\pi + \frac{2\pi}{N_r}$ and $\pi - \frac{2\pi}{N_r}$. This fact suggests that the angle can be determined from a noisy, real sample by filtering the sample of all but these two frequencies.

Mathematically this approach is identical to the linear method; that is, the two methods always return the same result. So the frequency method is also resistant to noise. The linear method resists noise because gaussian noise has a mean of zero, the frequency method resists noise because the noise is evenly distributed across the entire frequency spectrum. Only a very small portion of random noise in the system affects the frequencies of interest. The frequency approach improves on the linear solution because it can be made less sensitive to alignment problems. This can be achieved by using a correction factor which arises from an analysis of the frequency characteristics of the misalignment. For this reason the frequency method was used in the angular sensor.

2.3 Calculating the Angle Using the Frequency Method

The original signal, V_n, is in the time domain. What is needed with the frequency approach is to examine the frequencies of interest directly. This goal can be easily achieved by switching the signal into the frequency domain. Since the signal is discrete in the time domain, the transformation can be achieved by using the Discrete Fourier Transform, which is defined as

$$H_k = \sum_{n=0}^{N_r - 1} V_n e^{\frac{i2\pi nk}{N_r}} \quad .$$

where H_k is the kth frequency component of the signal.

This expression can be more easily evaluated by first rewritting equation (2.1).

$$\frac{A}{2}\left[cos(\pi n + \frac{2\pi n}{N_r} + \theta) + cos(\pi n - \frac{2\pi n}{N_r} - \theta)\right]$$

$$= \frac{A}{4}\left(e^{i(\pi n + \frac{2\pi n}{N_r} + \theta)} + e^{-i(\pi n + \frac{2\pi n}{N_r} + \theta)} + e^{i(\pi n - \frac{2\pi n}{N_r} - \theta)} + e^{-i(\pi n - \frac{2\pi n}{N_r} - \theta)} \right)$$

$$= \frac{A}{4} e^{-i\theta}\left(e^{-i\frac{(N_r+2)\pi n}{N_r}} + e^{i\frac{(N_r-2)\pi n}{N_r}} \right) + \frac{A}{4} e^{i\theta}\left(e^{i\frac{(N_r+2)\pi n}{N_r}} + e^{-i\frac{(N_r-2)\pi n}{N_r}} \right)$$

Therefore,

$$H_k = \frac{A}{4} e^{-i\theta} \sum_{n=0}^{N_r-1} \left(e^{-i\frac{(N_r+2)\pi n}{N_r}} e^{i\frac{2\pi nk}{N_r}} + e^{i\frac{(N_r-2)\pi n}{N_r}} e^{i\frac{2\pi nk}{N_r}} \right) +$$

$$\frac{A}{4} e^{i\theta} \sum_{n=0}^{N_r-1} \left(e^{i\frac{(N_r+2)\pi n}{N_r}} e^{i\frac{2\pi nk}{N_r}} + e^{-i\frac{(N_r-2)\pi n}{N_r}} e^{i\frac{2\pi nk}{N_r}} \right)$$

Because of the orthogonality of the exponential functions, $H_k = 0$ for all k except $k = \frac{N_r - 2}{2}$ and $k = \frac{N_r + 2}{2}$. At $k_l = \frac{N_r - 2}{2}$:

$$H_{k_l} = \frac{A}{4} e^{-i\theta} \sum_{n=0}^{N_r-1} \left(e^{-i\frac{4\pi n}{N_r}} + e^{i\frac{2(N_r-2)\pi n}{N_r}} \right) + \frac{A}{4} e^{i\theta} \sum_{n=0}^{N_R-1} \left(e^{i2\pi n} + e^{0} \right)$$

$$H_{k_l} = 0 + 0 + \frac{N_r}{4} A\, e^{i\theta} + \frac{N_r}{4} A\, e^{i\theta}$$

$$H_{k_l} = \frac{N_r}{2} A\, e^{i\theta} \tag{2.3}$$

A similar derivation gives

$$H_{k_h} = \frac{N_r}{2} A\, e^{-i\theta}$$

$$\text{for } k_h = \frac{N_r + 2}{2}$$

To summarize, analyzing an ideal sample in the frequency domain gives $H_{k_l} = \frac{N_r}{2} A\, e^{i\theta}$, where H_{k_l} is the frequency component of a Fourier transform of the sample with index $k_l = \frac{N_r - 2}{2}$. The phase of this component, $\angle H_{k_l}$, is identically θ. So θ, and γ, can be determined directly by transforming the sample into the frequency domain.

2.4 Error Anlaysis of Misalignment

While this approach reduces the effect of poor alignment on the sensor, the effect is not negligible. Fortunately the frequency analysis requires that the effect need only be characterized at the frequency of interest. This can be done by examining the type of misalignment that can occur in the sensor.

- The rotor and stator are not co-axial, so one is shifted with respect to the other.
- The rotor and stator are not parallel, so one is tilted with respect to the other.

In the case of a tilt error, the signal will be modulated by the variation in height between the rotor and stator (see Figure 2.5). The change in height of the centre of a pad is:

$$\frac{d_n}{d_o} = 1 + \frac{R}{d_o}\sin(\alpha) sin(\frac{2\pi\, n}{N_r} + \theta_t) \tag{2.4}$$

Where α is the tilt angle

and θ_t is the phase angle between the tilt axis and pad 0 on the stator.

In the approximation that the capacitance varies inversely with the distance between disks (as for a parallel plate capacitor), then the tilted signal will be:

$$V_n = \frac{d_o}{d_n} A\, cos(\pi\, n)\, cos(\frac{2\pi\, n}{N_r} + \theta) + B$$

$$V_n = \frac{A\cos(\pi n)\cos(\frac{2\pi n}{N_r} + \theta) + B}{1 + \frac{R}{d_o}\sin(\alpha)\sin(\frac{2\pi n}{N_r} + \theta_t)} \tag{2.5}$$

A tilt can have a large effect on the overall signal, but its effect on the phase of the H_{kl} is small. For sufficiently small tilt angles and for $\frac{R}{d_o} \leq 50$ the phase of H_{kl} is:

$$\angle H_{kl} \approx \theta + A_t \sin(2\theta - \theta_t).$$

Therefore provided the tilt is characterized, that is A_t and θ_t are known, it is still possible to extract the rotation from H_{kl}. Alternatively, characterizing the tilt from a series of known rotations may make it possible to measure the size and direction of the tilt.

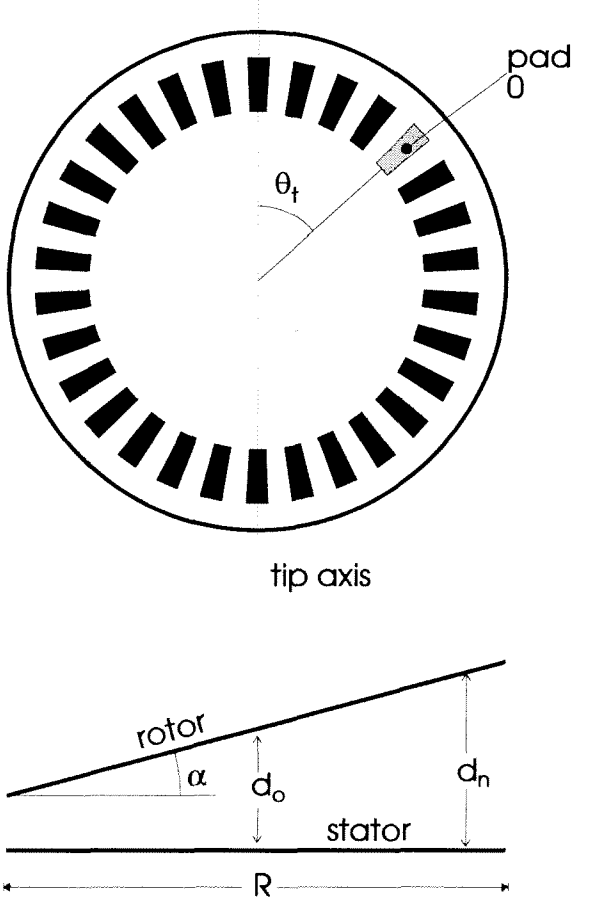

Figure 2.5
Effect of A Tilt

A shift of the centre of rotation of the rotor is more difficult to characterize than the tilt. Radiators and modifiers along the line of the shift will show virtually no change in signal. Perpendicular to the shift the signals will be maximally affected by the shift (see Figure 2.6). This gives a lengthening of one lobe of the sample envelope and a shortening of the other. The effect of a shift on the phase of H_{kl} was determined experimentally and does show this characteristic.

$$\angle H_{kl} \approx \theta + A_S \sin\left(\frac{N_r}{N_m}\theta - \theta_S\right)$$

where A_S is the amplitude of the shift error term

and θ_S is the phase of the shift error term.

As with the tilt, it should be possible to remove a shift error from the rotation measurement if the encoder is calibrated by measuring A_S and θ_S with several known rotations. This informa-

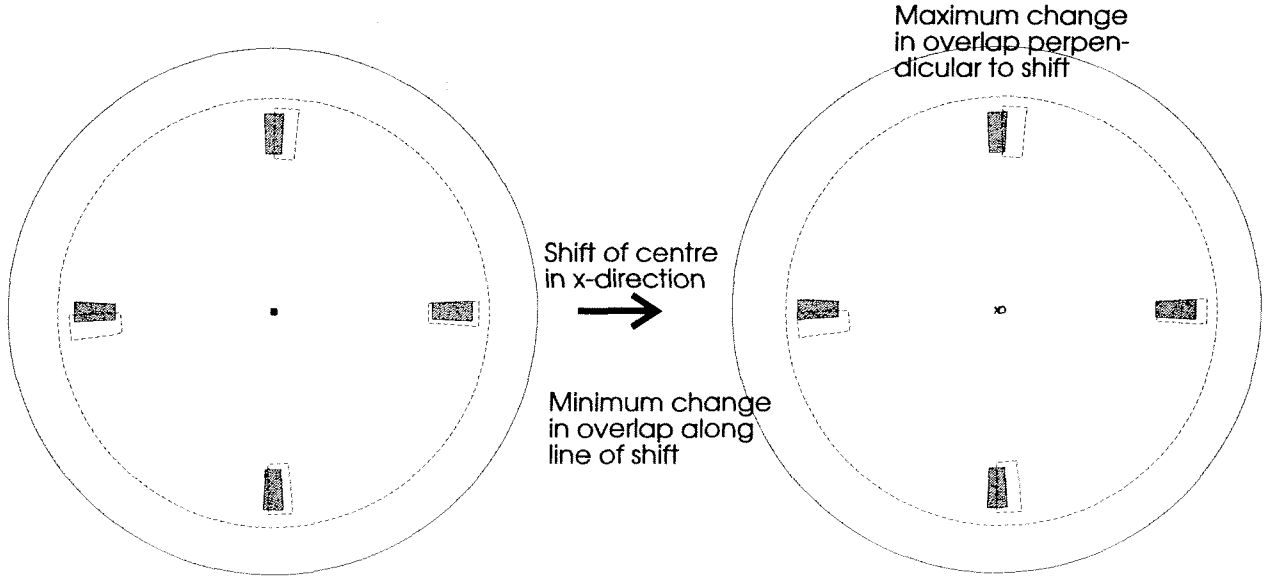

Figure 2.6
Effect of a Shift

tion may be useful not only in removing the shift error term from the rotation measurement, but may be sufficient to measure the shift.

Both a shift and a tilt have the effect of adding a sinusoidal signal to the rotation measurement for small deviations. The period of these oscillations is different for the two alignment problems.

The tilt error term has a period of one half of the periodicity of θ. That is, while θ has a period of

$$T_\theta = \frac{2\pi}{\frac{N_r}{2}+1} = \frac{2\pi}{N_m} \tag{2.6}$$

with respect to the rotor angle, the tilt error term has

$$T_t = \frac{1}{2} T_\theta$$

$$T_t = \frac{\pi}{\frac{N_r}{2}+1} = \frac{\pi}{N_m}. \tag{2.7}$$

So the period of the tilt error is dependent only on the number of pads on the rotor.

The shift error term has a period slightly greater than half of the period of θ. Specifically

$$T_s = \frac{N_m}{N_r} T_\theta.$$

$$T_s = \frac{2\pi}{N_r}. \tag{2.8}$$

The period of the shift error is dependent only on the number of pads on the stator.

Equations (2.7) and (2.8) can be used to reduce sensor errors due to a tilted or shifted rotor. This can be done when there are several known measurements which can be compared with the sensor readings.

If the angular distance between readings is $\frac{\pi}{\Delta}$ radians then the period of the tilt error term is:

$$T_t = \left(\frac{\pi}{\frac{N_r}{2} + 1} \, radians \right) \times \left(\frac{1 \, step}{\frac{\pi}{\Delta} \, radians} \right) = \frac{\Delta}{\frac{N_r}{2} + 1} \, steps.$$

The frequency of this is then:

$$f_t = \frac{\frac{N_r}{2} + 1}{\Delta} \, steps^{-1}.$$

If L sensor readings are taken at contiguous positions then the tilt error causes a frequency of:

$$f_t = L \frac{\frac{N_r}{2} + 1}{\Delta}$$

to appear within the data set.

For the stepper motor experiments, described in chapters 4 and 5, with $\Delta = 100$, $N_r = 64$, and $L = 64$ then the frequency within the data set is $f_t = 21.12$. This frequency can be seen by looking at a Fourier transform of the data set[3].

Figure 2.7 is the frequency domain representation of the first sixty-four data points from the stepper motor experiment described on page 66. This representation clearly shows that the domi-

3 This is why L=64 was chosen. Since the data set has the same number of elements as a sample, the sensor software can be used to examine the Fourier transform of the data set.

nant signal is contained at $f = 21$. There is some content at other frequencies, part of which is because the actual frequency is at 21.12 and some is due to inaccuracies in the stepper motor.

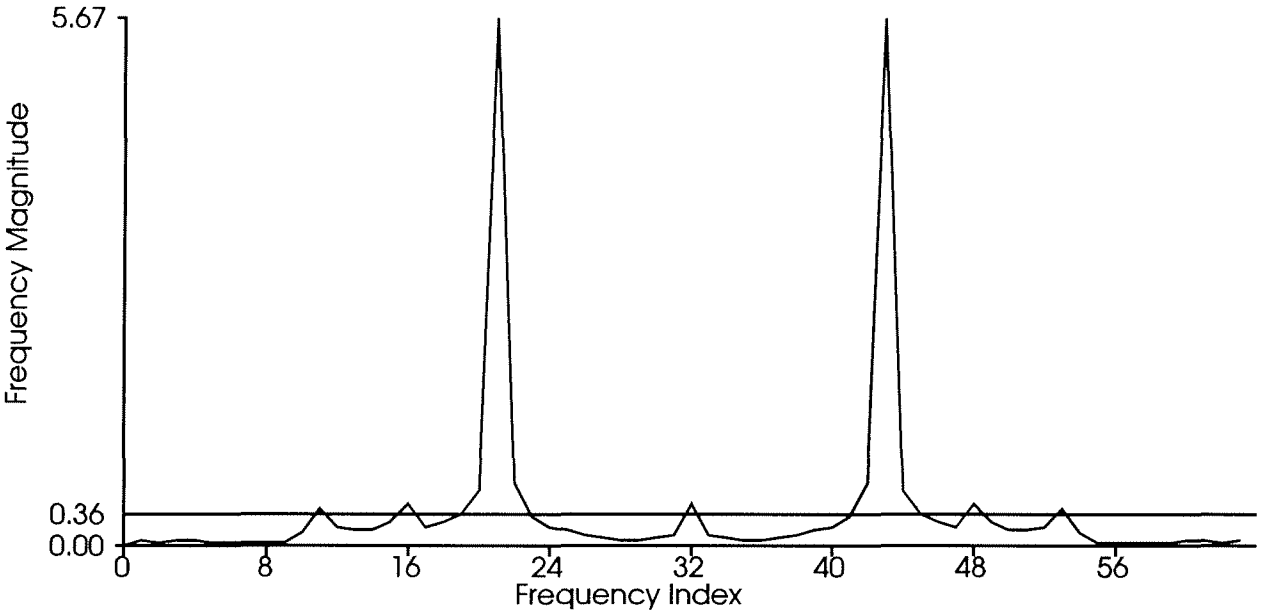

Figure 2.7
The Frequency of the Error in a Tilted Signal

This error can be partially offset by looking for the signal of the form

$$A_s \cos\left(\frac{2\pi f_t}{N_r} + \theta_t\right)$$

which best fits the data.

This best-fit curve is calculated indirectly by recognizing that this signal can be rewritten as:

$$(A_s \cos\theta)\cos\left(\frac{2\pi f}{N_r}\right) - (A_s \sin\theta)\sin\left(\frac{2\pi f}{N_r}\right)$$

$$= \Lambda \cos\left(\frac{2\pi f}{N_r}\right) - \Omega \sin\left(\frac{2\pi f}{N_r}\right)$$

which is linear in the coefficients Ω and Λ. The best-fit values for these parameters can be found through normal techniques for best-fit linear coefficients[4].

Once Ω and Λ are found, the best-fit curve is:

$$\left(\Lambda^2 + \Omega^2\right)^{\frac{1}{2}} \cos\left(\frac{2\pi f}{N_r} + atan\left(\frac{\Omega}{\Lambda}\right)\right)$$

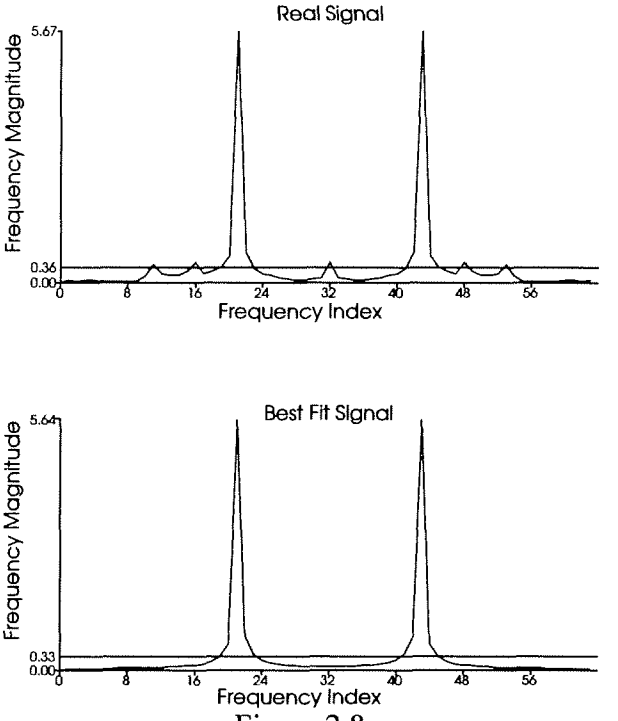

Figure 2.8
Frequency Domain Signal and the Best-Fit Signal

Figure 2.8 shows that the calculated best-fit curve agrees quite well with the original signal. This portion of the signal can then be simply removed as error due to a tilt in the rotor.

An identical analysis using (2.8) yields similar results for a shifted rotor.

2.5 Accuracy Limits

The limit on the accuracy for this sensor is determined by how accurately the ideal sample described by equation (2.1) can be measured.

---

4 William H. Press et al., Numerical Recipes in C The Art of Scientific Computing 2nd ed., p.671

Ignoring such real considerations as stray capacitance and mechanical tolerance for the moment, there are two factors which limit the accuracy of the angular measurement: the number of points at which the signals are sampled, and the amplitude of the signals with respect to the digitizing element which enables the signals to be interpreted by the computer.

An upper bound estimate on the accuracy can be considered in the following manner.

A possible continuous form of equation (2.1)

$$V(t) = A\ cos(\omega_h t) cos(\omega_l t + \theta) + B$$

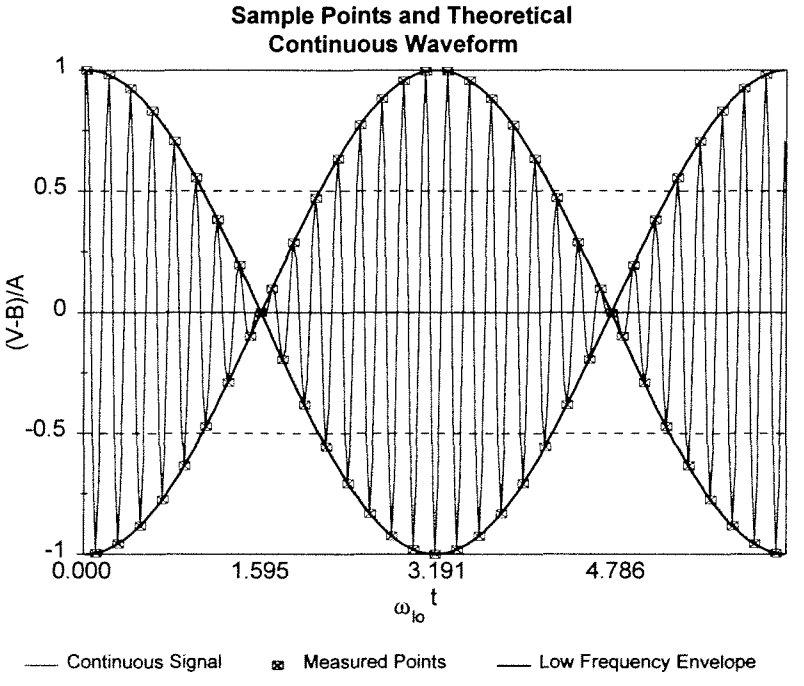

Figure 2.9
Relationship Between Measured Points and the Signal Envelope
Note that only the measured points have a physical meaning. The continuous signal and the envelope are mathematical conveniences.

Where t is a continous variable analagous to the sample index, n

ω_h is the high frequency in the signal

ω_l is the frequency of the envelope

The purpose of the sensor is to determine the phase of the envelope of this signal by sampling this waveform at points where $\omega_h t = 0,\pi,2\pi,....$ Given this, it is only necessary to consider one half of the envelope, namely

$$V_{env}(t) = -A\ cos(\omega_l t + \theta) + B$$

$$\frac{\partial V_{env}}{\partial \theta} = A sin(\omega_l t + \theta)$$

The maximum slope of the envelope is A.

If the envelope is shifted by a small angle $\Delta\theta$, then the change in the signal value at the point of maximum slope is

$$\Delta V_{env} \approx A\ \Delta\theta.$$

Let M be the minimum measurable change. This is a result of the digitization of the signal. The signal must be measurably different in order to register as a rotation.

Then taking the rotation necessary to produce a change of M in the signal then

$$A\ \Delta\theta \approx M$$

$$\Delta\theta \approx \frac{M}{A}$$

The corresponding rotor rotation is

$$\Delta\gamma \approx \frac{1}{\frac{N_r}{2}+1}\frac{M}{A}$$

$$\Delta\gamma \approx \frac{2M}{A(N_r+2)}. \tag{2.9}$$

In all likely cases, A is half of the full scale of the A/D converter and M is one unit of the full scale of the converter. Two common converters have 2^8 and 2^{12} quantization levels, so for these converters A=128 and A=2048 respectively. Because of the use of the Fourier transform, it is most convenient to have N_r as a power of 2. Three reasonable choices for N_r are 32, 64, and 128.

Table 2.1
Upper Bound On Precision for Different Sensor Configurations

	N_r=32	N_r=64	N_r=128
2^8 A/D levels	4.6×10^{-4} radians	2.4×10^{-4} radians	1.2×10^{-4} radians
2^{12} A/D levels	2.9×10^{-5} radians	1.5×10^{-5} radians	7.5×10^{-6} radians

This is an upper bound estimate because it assumes that a sample point will have to change in value by M to register. A more likely scenario is that one of the N_r sample points will be closer to the threshold for the A/D converter and so a much smaller rotation will register as a change in the sample.

One way to examine this effect is to simulate the problem numerically. This was done by programming a computer to generate signals of the type described by equation (2.1).

- An initial angle was chosen.

- A simulated signal was generated by calculating the N_r sample points described in equation (2.1).
- The simulated signal was "digitized" by truncating the sample points to integer values.
- The angle was increased by a small amount, 1×10^{-7} radians.
- A new simulated signal was generated and "digitized"
- If the new signal differed in any sample point from the original, the angle was recorded.
- The angle was increased again and the process was repeated

This simulation was carried out for 2^8 quantization levels and for 2^{12} quantization levels because these represent easily available A/D converters. The maximum rotation was the maximum change in angle that was required to cause a change in the simulated signal. Similarly the minimum rotation was the minimum change in angle to cause a change in the pattern.

As expected, the values for the maximum rotation are better than those predicted by equation (2.9). Also the average rotation when simulating 2^8 quantization levels is approximately 2^4 times larger than for 2^{12} quantization levels.

Table 2.2
Simulated Values for Precision for $N_r = 64$

Quantization Levels	Number of Test Points	Maximum Rotation	Minimum Rotation	Average Rotation
2^8	2161	7.131×10^{-5} radians	5.152×10^{-8} radians	1.164×10^{-5} radians
2^{12}	197221	5.055×10^{-6} radians	3.030×10^{-10} radians	7.265×10^{-7} radians

These anlayses suggest that the easiest way to increase the accuracy of such a sensor is to use a better analog-to-digital converter. When that is not reasonable, the number of radiator pads on the stator and the number of modifier pads on the rotor should be increased.

3 Device Description

3.1 Physical System

The physical setup used to verify the angular encoder consists of two main components: the encoder itself and the test apparatus. The encoder consists of two disks, a circuit board and a computer. The test apparatus is a rig to control the motion and position of the rotor with respect to the stator. The encoder is shown in Figure 3.1 with the rotor and stator in perspective and separated to show the geometry.

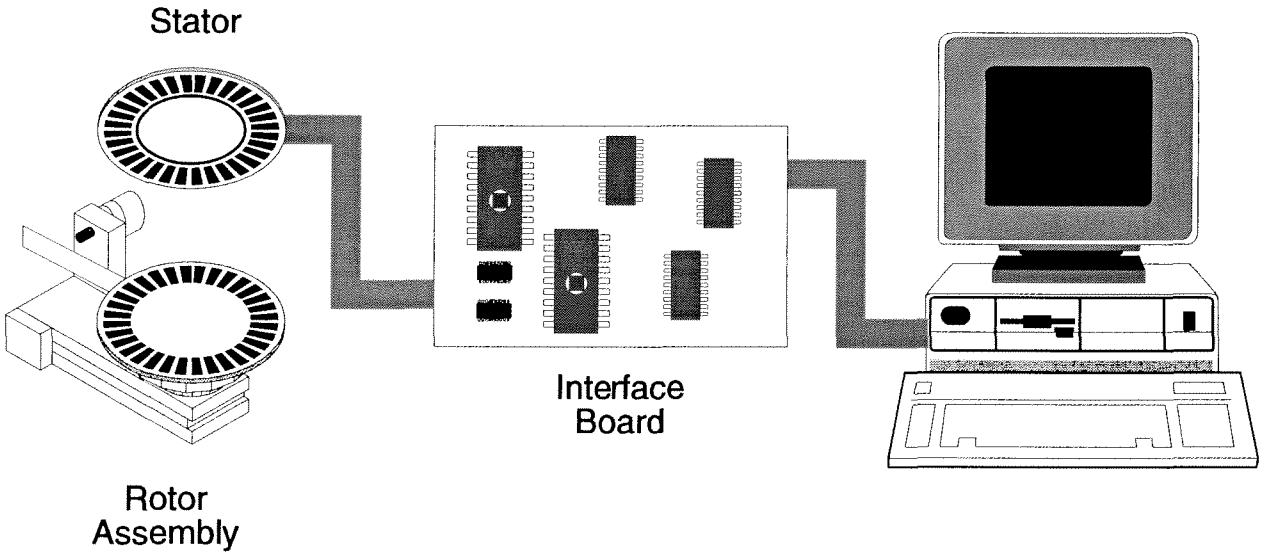

Figure 3.1
Sensor Components

The disks are the heart of the sensor because they are the implementation of the antivision concept. The disks are labeled the *stator* and the *rotor*. The stator is a circular piece of pc-board and it contains the signal generators and the signal detectors. The rotor, also a circular piece of pc-board, contains the field modifiers.

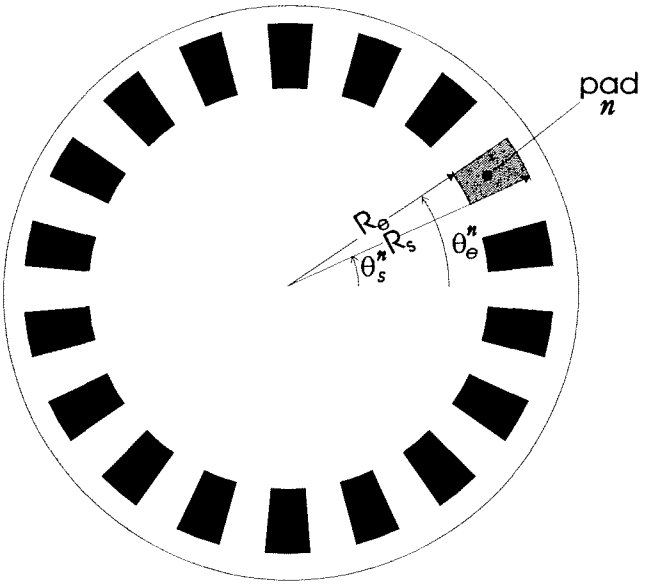

Figure 3.2
Pad Geometry

A signal generator is a bare electrode on the surface of the stator disk. Its shape is defined by inner and outer radii and start and end angles. The stator has $N_r = 64$ generators. They all have the same inner and outer radii. The start and end angles for pad n are:

$$\theta_s^n = \frac{2\,\pi\,n}{N_r} \qquad \theta_e^n = \frac{2\,\pi\,n + \pi}{N_r}$$

On the stator is a single signal detector. It is a bare conducting ring just inside the inner radius of the generators.

The stator has a radius of 2.500". The signal generators have an inner radius of 1.250" and an outer radius of 1.625". The detector ring has an inner radius of 1.125" and a width of 0.063".

A signal modifier has a similar shape, and the rotor has $N_m = \frac{N_r}{2} + 1 = 33$ pads. The rotor has a radius of 1.750". The modifiers have an inner radius of 1"and an outer radius of 1.625".

The circuit board and computer are physically connected to the stator only. The rotor has no active electrical components and no mechanical connection to the stator. It is connected to the stator only through the generated electric field. In addition the rotor modifier pads are electri-

cally isolated as opposed to being grounded. This choice makes analysis more difficult but it increases the versatility of the sensor because no connections to the rotor of any sort are needed.

The test apparatus consists of a mechanically adjustable mount for the encoder to control the alignment of the rotor. The mount has several components: a bearing, a micrometer-controlled XYZ stage, a micrometer controlled tilt stage, and holders for the rotor and stator.

The bearing allows the rotor to rotate freely with respect to the stator. The holder for the rotor is mounted on the bearing and the rotor on the holder. The XYZ stage controls the position of the rotor with respect to the stator. The XY controls position the axis of rotation of the rotor and

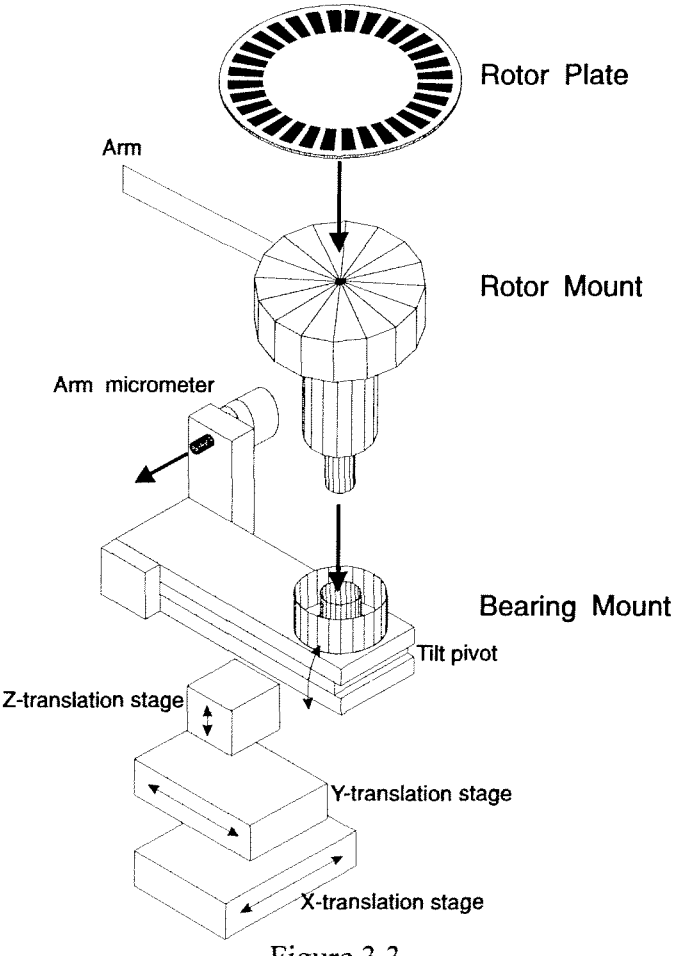

Figure 3.3
Exploded View of Rotor Mount

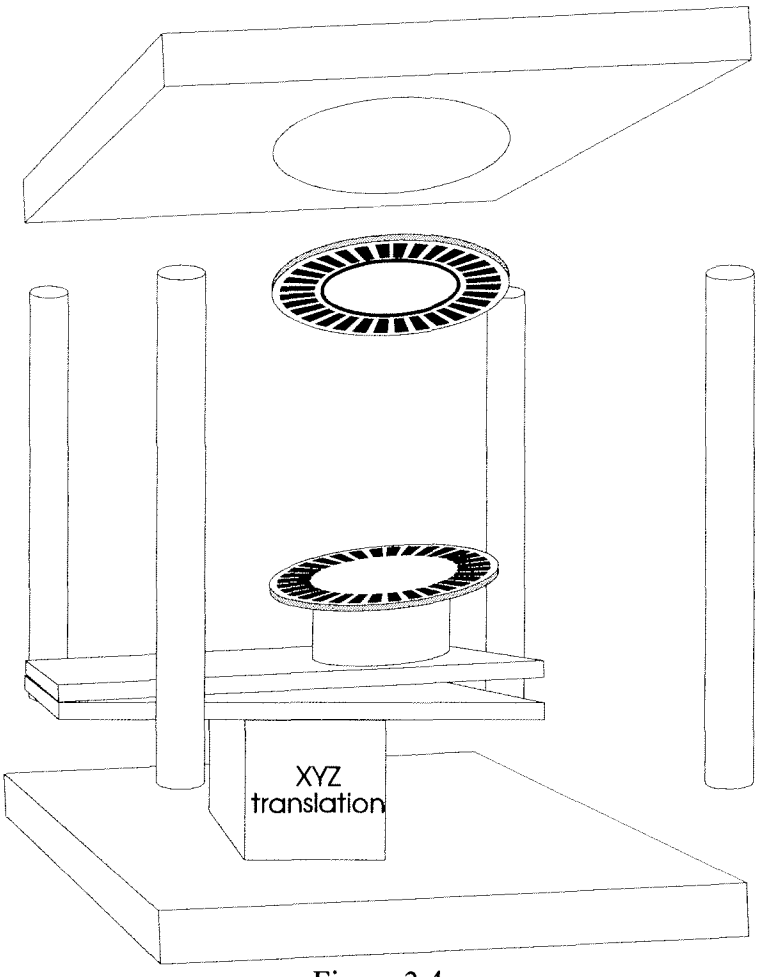

Figure 3.4
Exploded View of Stator and Rotor Stand

the Z control adjusts the spacing between the disks. The tilt stage is mounted on top of the XYZ stage and sets the tilt of the rotor. The stator holder is fixed in position and orientation above the rotor.

3.2 Electrical System

In reference to Figure 2.1, the electrical system consists of the signal generation circuits, the radiators, detectors, and the signal conditioning circuits. The nature of the radiators and the detector has already been described.

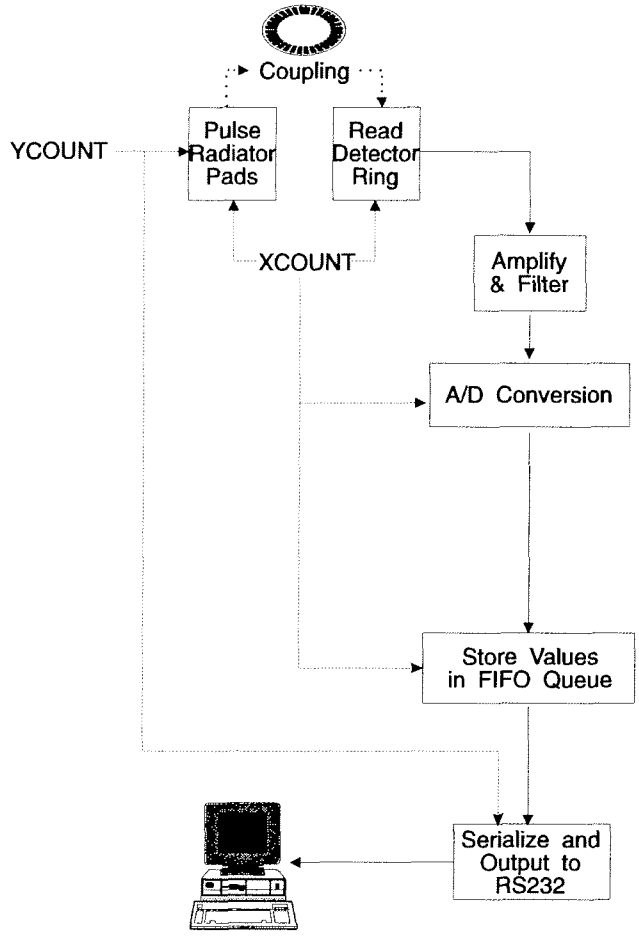

Figure 3.5
Operation of Electrical System

The signal generating circuit drives the radiators by pulsing each serially. It starts with a 6.144 MHz crystal oscillator which is the fundamental timing for the circuit. The output from this crystal is used to generate two counters, XCOUNT and YCOUNT. XCOUNT is generated by a divide-by-20 on the crystal output and has a frequency of 307.2 KHz. YCOUNT is generated by a divide-by-64 on XCOUNT and has a frequency of 4800 Hz.

The system operates by associating events with specific values of the counters.

When YCOUNT is 0 and XCOUNT is 0, a signal, DATA, is turned on. This signal is the input of a chain of eight shift registers each with eight outputs. After XCOUNT reaches 15, DATA

is turned off. The shift registers are driven by the high order bit of XCOUNT. So every time XCOUNT reaches 16, the signal introduced by DATA is shifted along the chain of shift registers.

Each output from the shift registers drives one of the radiator pads. This system drives each radiator pad sequentially for 3.25 μs. Only a single pad is active at any moment, and when the signal has propagated through the entire chain, the cycle begins again.

XCOUNT is also used to control the sampling and storage of the position signals. When XCOUNT is 1, an analog-to-digital converter samples the detector output. When XCOUNT is 5 the data from the converter is stored in a first-in first-out buffer for later transmission to the computer.

YCOUNT is used to synchronize the serial transmission of stored data to the computer.

The divide-by-20, the divide-by-64, and the control signals are implemented in a single erasable programmable logic device.

The detector output is the signal from the sense ring after it has been conditioned by several stages of amplification and filtering. The characteristic frequencies of the amplifiers and filters were chosen by recognizing that equation (2.1) could be rewritten as:

$$V_n = A\cos(\omega_h t_n)\cos(\omega_l t_n + \theta) + B \tag{3.1}$$

$$V_n = \frac{A}{2}\cos\left[\left(\omega_h + \omega_l\right)t_n + \theta\right] + \frac{A}{2}\cos\left[\left(\omega_h - \omega_l\right)t_n - \theta\right] + B$$

Where $\omega_h = 2\pi\,(307200)$

$\omega_l = 2\pi\,(4800)$

and $t_n = \dfrac{n}{2(307200)}$ is the time at which n^{th} signal is measured

Consequently the analog circuits are designed to amplify signals in the range $(\omega_h - \omega_l)$ to $(\omega_h + \omega_l)$ and attenuate other signals.

The signals directly from the detector are very weak, on the order of a millivolt, and the signal of interest is of similar magnitude to the noise picked up by the detector. Two stages of amplification and filtering are performed directly on the stator to reduce the amount of noise before directing the signal to the circuit board. The rest of the amplification and filtering, four more stages, is performed on the circuit board and gives 2.5 volts peak-to-peak signal with approximately 0.02 volts noise.

Finally the signals are digitized and temporarily stored in a buffer before being serially transmitted to the computer. The signals are digitized by an 8-bit, half-flash analog-to-digital converter set to a range of 0 - 2.5 volts.

3.3 Computer System

The computer system is a combination of hardware and software. The hardware is a 486 PC in a standard configuration. The software consists of approximately eleven thousand lines of code written in a combination of the C++ programming language and assembler. It is far more than would be needed in a final device because it provides a high-level, configurable interface to the sensor hardware. The purpose of this interface is to allow easy investigation into the properties of the samples produced by the sensor.

The software collects samples, a collection of sixty-four 8-bit values, and can then perform mathematical operations on individual or multiple samples. It can also graphically display the samples or various transformations of them. Some of the operations available are addition of samples, multiplication of samples, FFTs and inverse FFTs as well as direct manipulation of values within a sample.

The software also supports a batch programming language of its own that enables automated sample collection and manipulation without modifying the original code.

A typical sequence for measuring the position of the rotor using the software follows.

- With the rotor lowered away from the stator so that there is no significant field modification ($d \approx 20$mm), acquire a baseline sample.
- Acquire a raw position sample with the rotor raised back into position ($d \approx 1$mm).
- Subtract the baseline sample from the position sample to get an adjusted sample.

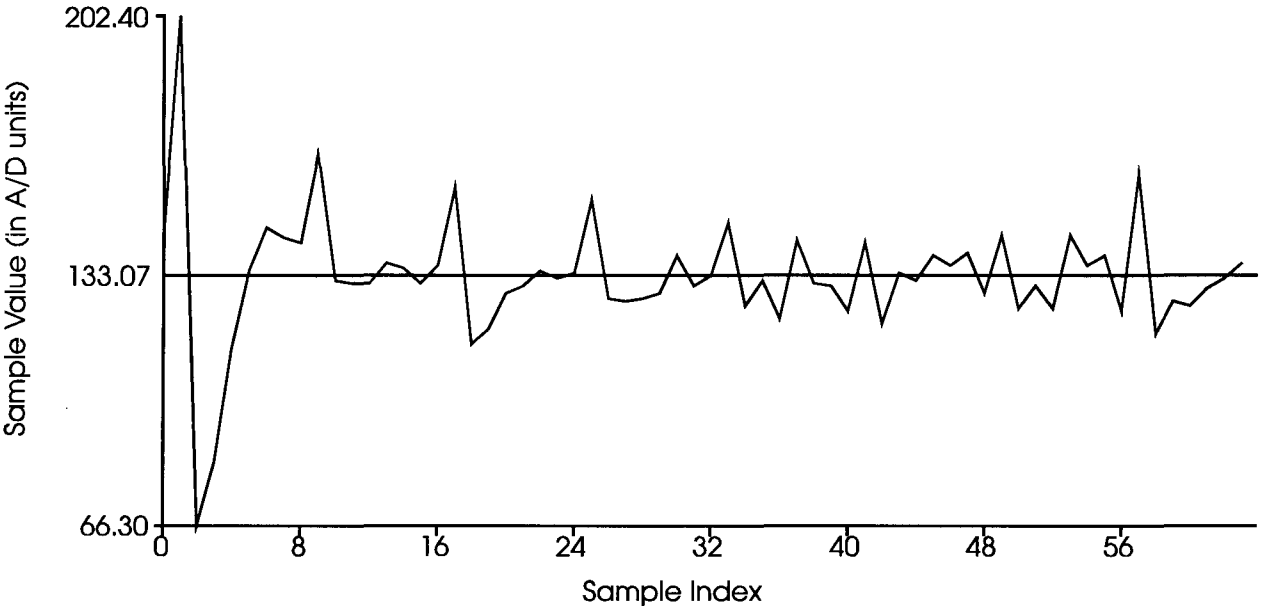

Figure 3.6
A Typical Baseline Sample

- Calculate the FFT of the resulting sample and get the phase of the thirty-first frequency component.

The baseline sample is important because the radiators are driven by eight shift registers connected serially. The detector picks up a spike when a shift register is first energized inde-

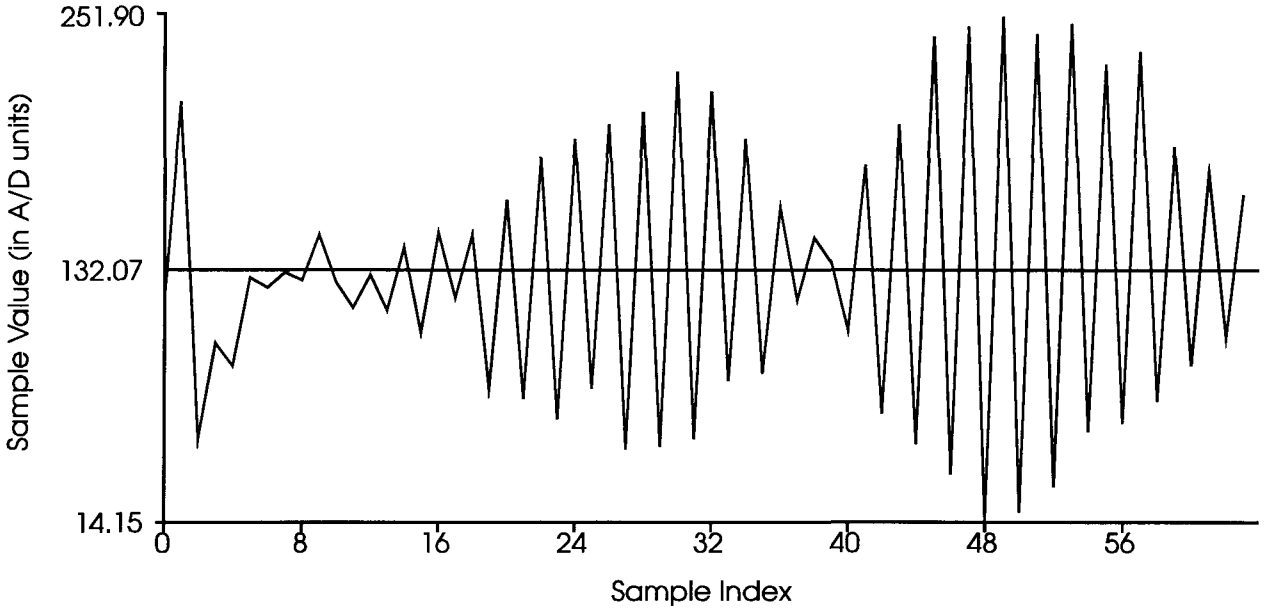

Figure 3.7
A Typical Raw Sample

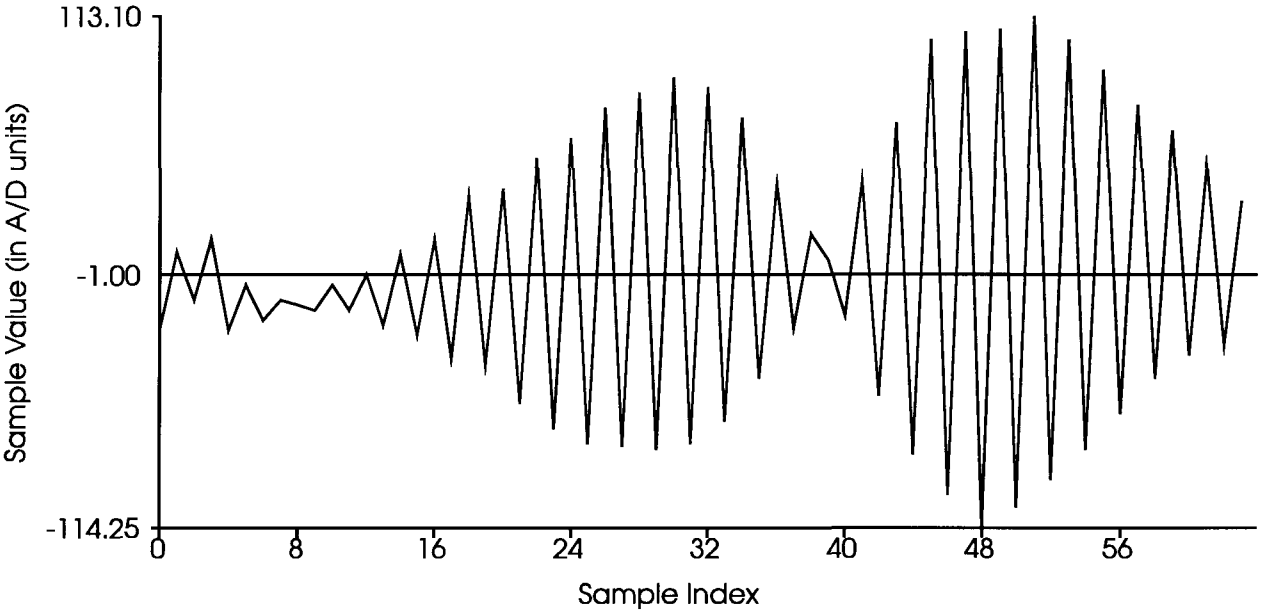

Figure 3.8
A Typical Sample with the Baseline Removed

pendent of the rotor position. Subtracting this baseline sample from all position samples removes this, and any other steady-state effect from the position calculations.

See Appendix B for a detailed description of sample graphs.

A second software component is used to simulate the encoder signals. The simulator models the system as a collection of parallel-plate capacitors whose signal output is proportional to the overlapping area and separation of any radiator-modifier pair.

The simulator models a tilt in the encoder as a change in the separation of the pair and a shift of the axes as a change in the area of overlap.

The simulator allows easy modification of the simulation parameters, such as the number of radiators and modifiers or the size and direction of tips and shifts. It shows good qualitative agreement with signals from the actual device. These characteristics make the simulator a useful tool for planning future designs before incurring the cost of building a new device.

This describes the device and the basic test apparatus. A detailed description of the test methods used with the sensor follows in chapter 4. Experiments conducted with the sensor are described in chapter 5.

4 Test Setup

The preceeding chapters have outlined a theoretical model for a high precision angular sensor and a possible implementation for such a sensor. This chapter describes how this implementation was tested to determine its capabilites under various conditions.

Three test strategies were used in investigating the encoder design. Each was intended to examine the sensor design in a different way. The first strategy used the computer simulator. The simulator output was compared to real signals from the sensor. The simulator was then used qualitatively to investigate signals from the sensor under various conditions not easily achievable in the lab and to give clues as to the effect of different sources of error.

The second test method was to attach a small, front-surface mirror on the rotor bearing. The deflection of a laser beam reflected by this mirror was used to measure the rotor rotation independently of the sensor reading. This method provided readings with an accuracy of 2×10^{-6} radians but only over a very short range of rotation, typically 1×10^{-3} radians.

The final test method replaced the rotor bearing with a stepper motor. The stepper motor had 1.8° steps with an accuracy of five percent, or 0.09°. While this resolution is not as accurate as the desired resolution of the sensor, it does provide a rough idea of the sensor capabilities over a complete revolution. In addition, while the accuracy between steps is only plus or minus five percent, the repeatability of a given step is of the same order as the derived sensitivity of the encoder, typically 10^{-5} radians.

4.1 Simulator

The simulator uses several models to approximate the rotor and stator. The lowest level model is called a pad. A pad can represent both a generator and a modifier. A pad is defined by four parameters: a start radius, an end radius, a start angle and an end angle (see Figure 3.2 on page 30). So a pad has an area of

$$A^n = \frac{\theta_e^n - \theta_s^n}{2}\left[\left(R_e^n\right)^2 - \left(R_s^n\right)^2\right]$$

Where n is the pad number

A^n is the area of pad n

θ_s^n is the start angle of pad n

θ_e^n is the end angle of pad n

R_s^n is the start radius of pad n

and R_e^n is the end radius of pad n

The second model in the simulation is the model of a disk. A disk is a collection of equally sized pads spaced around a circle of given size with the size of blank space between each pad equal to the size of a pad. The parameters for a disk include the number of pads, the radius of the circle, the rotation of the disk from its initial position, the tilt of the disk from planar and the shift of the centre of the disk.

The rotor is modeled as a disk with thirty-three pads and the stator is modeled as a disk with sixty-four pads.

A disk rotation by an amount θ simply adds θ to the start and end angles for each pad on the disk. When neither disk is tilted or shifted, the signal output associated with each stator pad is simply the proportion of its area that overlaps any rotor pad. The area of overlap of a pad on the rotor and a pad on the stator has the same wedge shape as a pad and its area is calculated by defining

$$R_s^{overlap} = \max\left\{R_s^{rotor}, R_s^{stator}\right\}$$

$$R_e^{overlap} = \min\{R_e^{rotor}, R_e^{stator}\}$$

$$\theta_s^{overlap} = \max\{\theta_s^{rotor}, \theta_s^{stator}\}$$

$$\theta_e^{overlap} = \min\{\theta_e^{rotor}, \theta_e^{stator}\}.$$

Then

$$A^{overlap} = \frac{\theta_e^{overlap} - \theta_s^{overlap}}{2}\left[\left(R_e^{overlap}\right)^2 - \left(R_s^{overlap}\right)^2\right]$$

A tilt is parameterized by a tilt angle α. For convenience the simulation only models tips about the x-axis. The circular symmetry of the sensor makes this a general model of a tilt about any axis through the centre of the disk.

The tilt causes three effects. The height of the centre of a pad is changed according to equation (2.4). The effective area is reduced due to cosine foreshortening so that $A^{pad,tilt} = A^{pad}\cos(\alpha)$. Finally there is a very slight shift of each pad towards the tilt axis.

If a shift is to be accurately modeled then the area of overlap of two pads will no longer be the same wedge shape. This would make the overlap calculation very cumbersome. Consequently a general shift is approximated as a shift along the radial direction followed by a rotation. For sufficiently small shifts this approximation is a good one and it does not alter the overlap calculation.

Given these models, the simulator mimics a device which consists of ideal parallel plate capacitors, that is, the voltage signal is linearly related to the overlap between the stator and rotor pads. The simulator should provide a good approximation of the real device as long as this assumption holds true. A design which used much smaller rotor and stator pads or had a larger

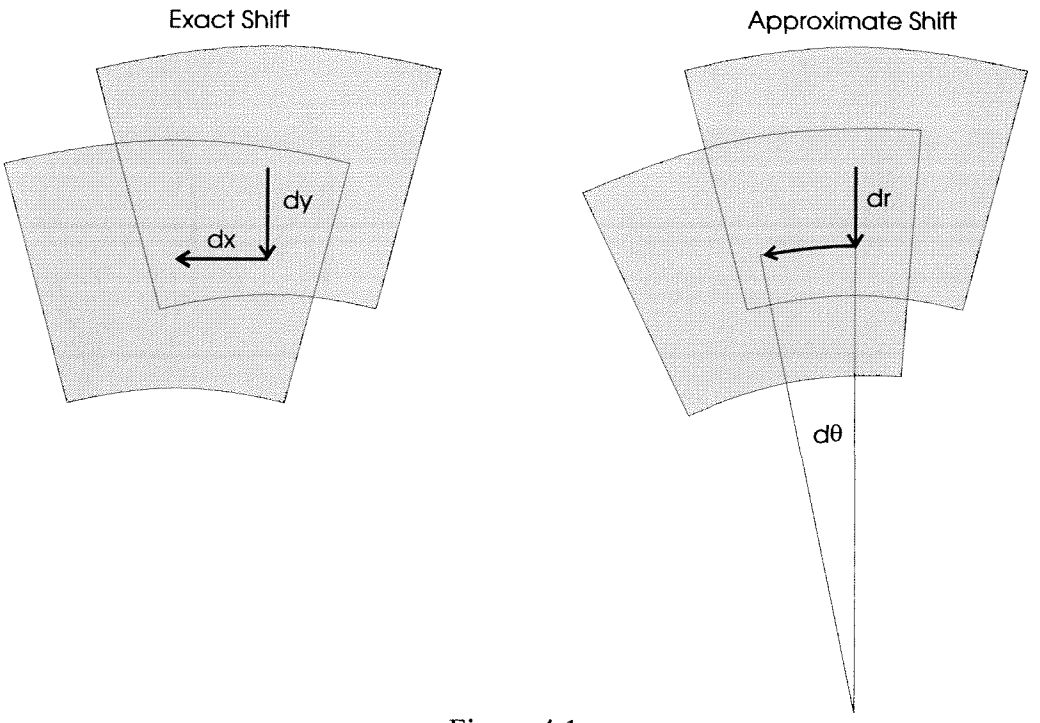

Figure 4.1
Simulating a Shifted Pad

separation between the rotor and stator might violate this since fringe fields could become the dominant effect.

In order to be useful the simulator must provide results that approximate those from the real device. The models used were not designed to provide numerically identical results because the models are strictly geometric. That is, they do not include physical scaling relationships such as the effect of the permittivity on the capacitance, and they do not include nonlinear effects such as the effect of fringe fields. So the most that the simulator can deliver is results that are qualitatively similar to results from the sensor when the sensor is operating under the conditions described. Certain signal characteristics that appear in both the real signals and the simulated signals indicate that the simulator does provide this level of similarity.

The real signal (on the left of Figure 4.2) and the simulated signal both have the expected frequency spikes at $f = 31$. The simulated signal is much more symmetric than the real signal because the real device can not be perfectly aligned and is subject to noise.

The real and simulated tilted signals (see Figure 4.3) also show several similarities. Both show a significant frequency spike appearing at $f = 1$. At $f = 32$ both signals show an increased signal content over the ideal signals. Also this frequency oscillates in both real and simulated signals as the rotor is rotated. In the time domain, both signals show that the envelope of the signal is skewed, making one lobe larger than the other. Varying the tilt angle indicates that the amount of skewing is proportional to the tilt angle.

It is important to note that no attempt was made in preparing these figures to produce identical tilt or shift conditions in the real device and the simulator because the simulator is only capable of qualitative results in any case.

The real and simulated signals from a shifted rotor also show similar characteristics. One lobe of the pattern is elongated while the other is shortened.

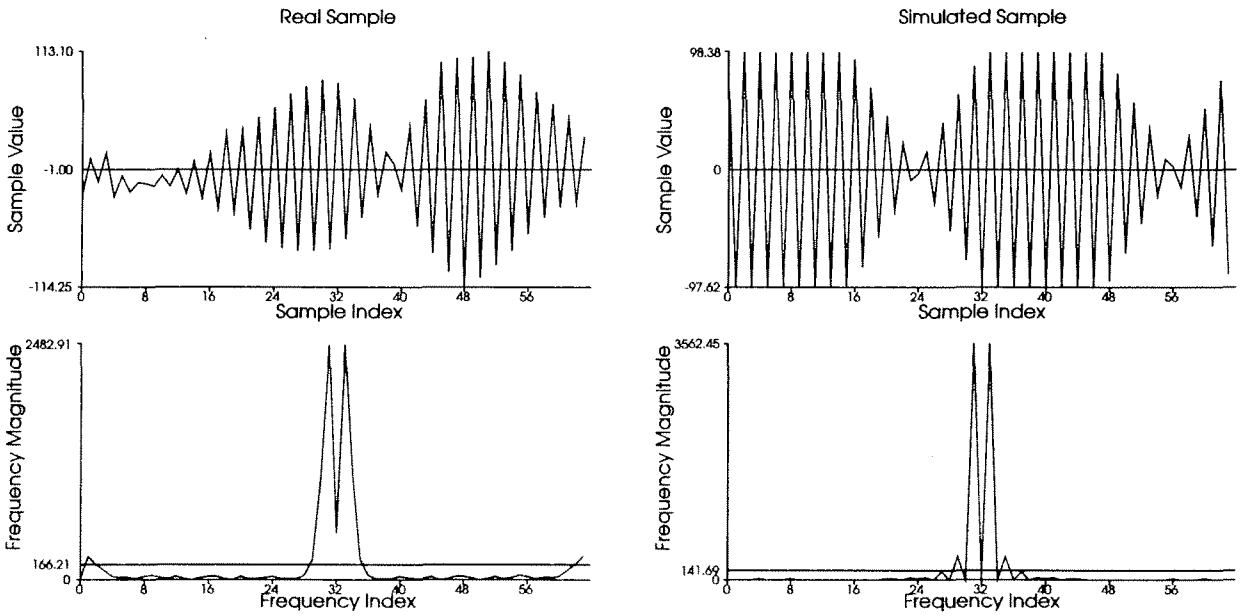

Figure 4.2
Real and Simulated Signals in the Time and Frequency Domains

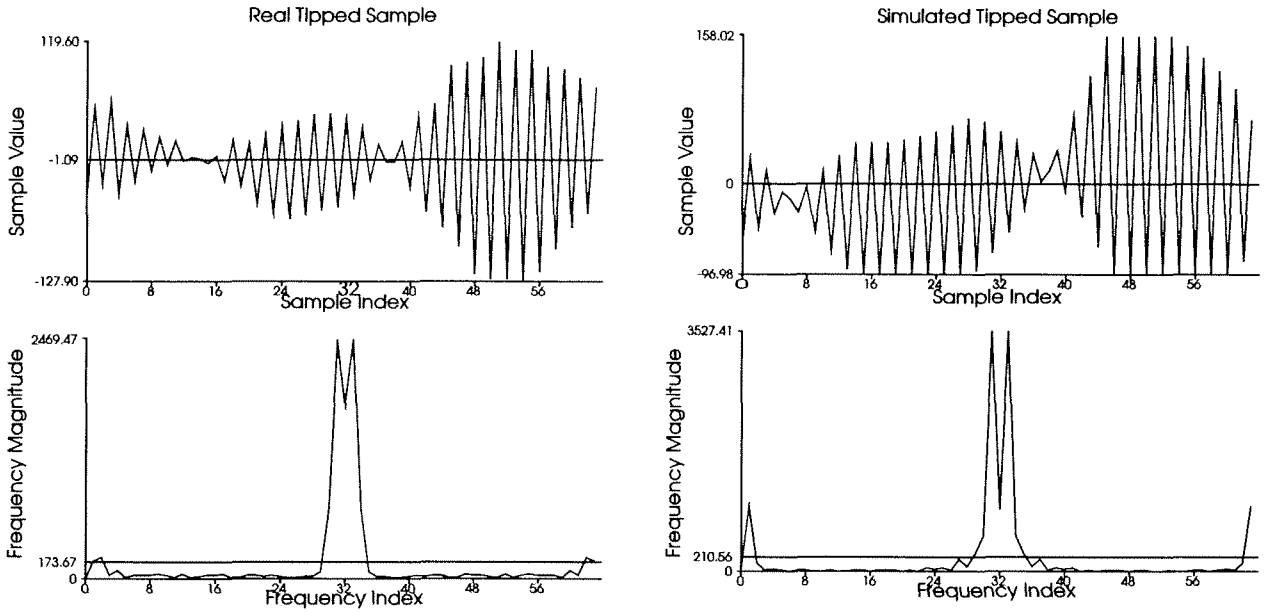

Figure 4.3
Real and Simulated Tilted Signals

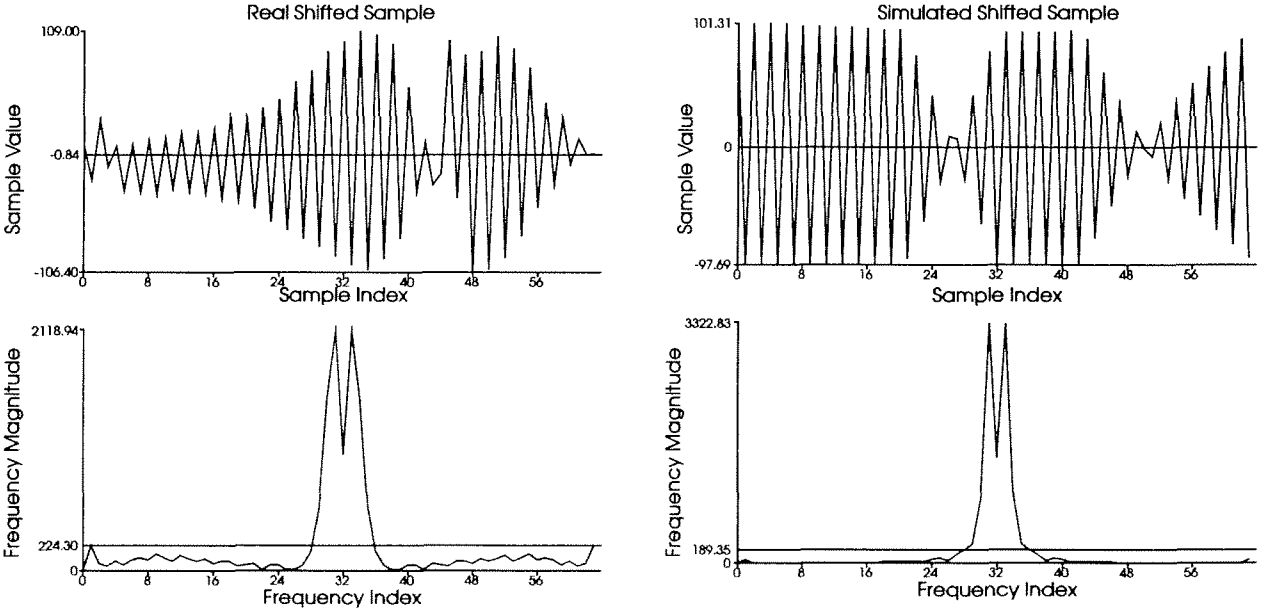

Figure 4.4
Real and Simulated Shifted Signals

4.2 Mirror and Laser

This setup is designed to produce a very accurately determined rotation to test the sensor but only under a very limited range. A front-surface mirror is attached on the section of the rotor mount that extends beneath the bearing mount (see Figure 3.3). The section of the rotor mount is faced off so that the axis of rotation of the rotor is in the plane of the reflecting surface.

The beam from a laser approximately ten meters away is reflected from the mirror at almost perpendicular incidence. When the rotor is turned, the beam is deflected through an angle twice the size of the rotation. This angle is determined by measuring the sides of the associated triangle.

The long measurement, D, is taken using a steel surveyor's tape. Over a distance of approximately ten meters, given thermal effects and bending, its reading is accurate to not more than five millimetres. As is shown below, this error has very little effect on the accuracy of the measurement even when ten times larger.

The short measurement, X, is determined by using a laser spot detector mounted on a micrometer slide that travels perpendicular to the outgoing beam. The detector consists of two photodiodes approximately two centimeters apart. The reflected beam, which is approximately three centimeters in diameter after the twenty meter round trip, is detected by adjusting the slide position until the current in the two photodiodes balances. Manufacturing differences in the diodes make it unlikely that the centre of the beam is detected with this method, but it should consistently find the same point within the beam. This measurement has a repeatability of five micrometers.

The beam deflection, φ, is calculated as:

$$h^2 = X^2 + D^2 - 2XDcos\ \beta$$

$$X^2 = h^2 + D^2 - 2hDcos\ \varphi$$

$$\therefore X^2 = \left(X^2 + D^2 - 2XD\cos\beta\right) + D^2 - 2hD\cos\varphi$$

$$\therefore 0 = 2D^2 - 2XD\cos\beta - 2hD\cos\varphi$$

$$\therefore \cos\varphi = \frac{D - X\cos\beta}{h}$$

$$\therefore \varphi = \cos^{-1}\left(\frac{D - X\cos\beta}{\sqrt{X^2 + D^2 - 2XD\cos\beta}}\right). \tag{4.1}$$

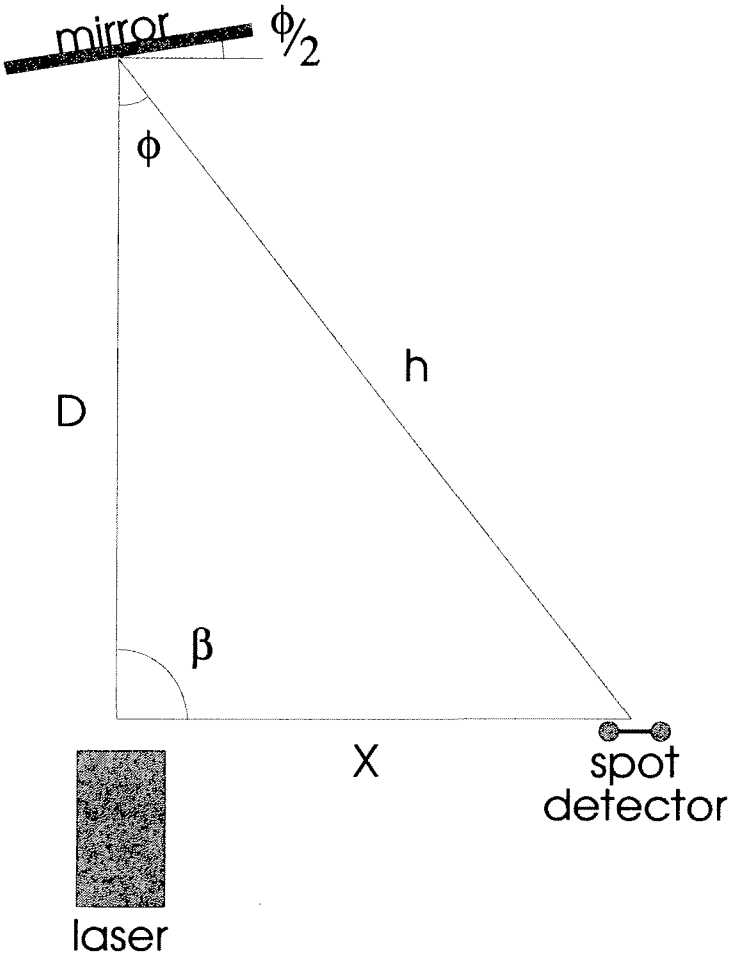

Figure 4.5
Laser Test Setup

Ideally the angle β is ninety degrees. The accuracy of this angle is at least within one degree of this ideal from using the laser mounted on an optical bench to align two sides of the triangle.

In measuring the deflection angle, it would be best to take as the starting position $\varphi = 0$. Then rotate the rotor, measure X and D and calculate φ directly. Unfortunately the spot detector is one-sided so it can not detect the position of the outgoing beam, only the reflected beam. Also the outgoing beam has a radius of about half of a centimetre so the spot detector would not work in any case.

The effect on the measurement of not starting from $\varphi = 0$ is determined as follows:

$$\varphi_{ideal} = \tan^{-1}\left(\frac{X}{D}\right)$$

$$\varphi_{actual} = \tan^{-1}\left(\frac{X + X_o}{D}\right) - \tan^{-1}\left(\frac{X_o}{D}\right).$$

Since the situation is assumed ideal, the error is:

$$\varphi_e = \varphi_{ideal} - \varphi_{actual}.$$

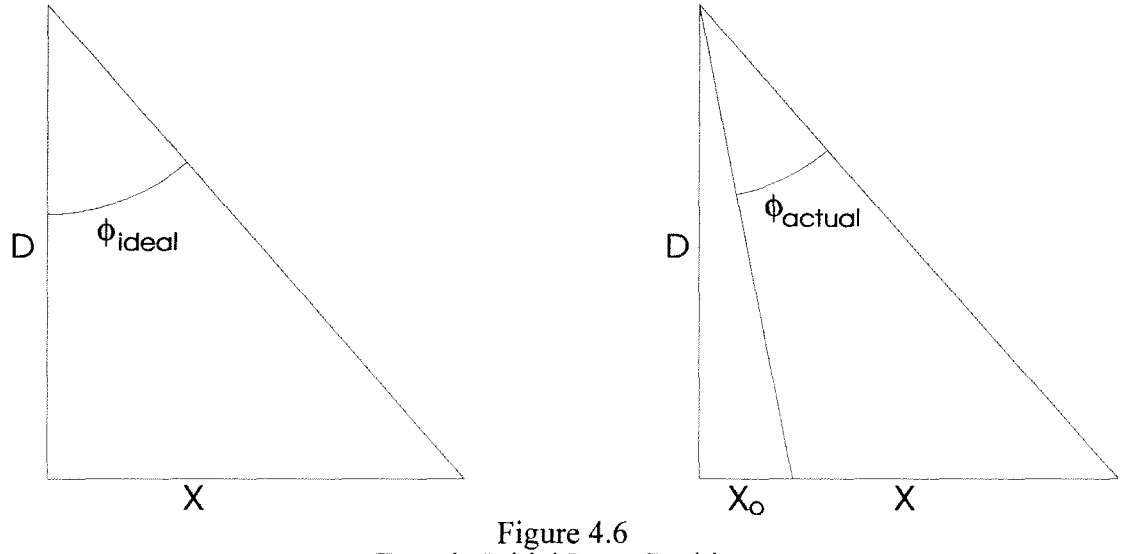

Figure 4.6
Error in Initial Laser Position

The long measurement, D, is constant at around ten metres and X is around the maximum travel of the micrometer slide, one inch. The error associated with assuming the ideal starting position is shown as a graph in Figure 4.7.

The graph shows that even when the displacement from the ideal starting position is the same size as the measurement of X itself, the typical error is on the order of 10^{-8} radians. This error is approximately two orders of magnitude smaller than the desired resolution of the sensor so it does not significantly impair the results.

To compare results from the laser and from the sensor, the accuracy of the laser setup must be determined. If the measurement errors for D, X, β are dD, dX, $d\beta$ respectively, then the true

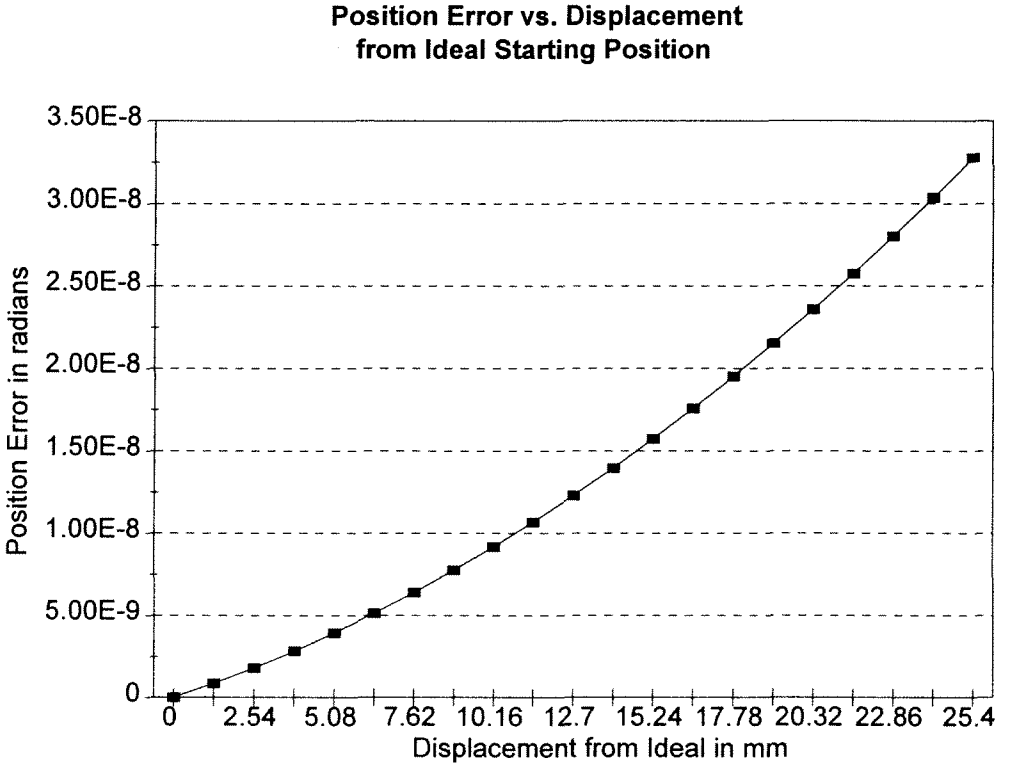

Figure 4.7
Effect of Error in Initial Laser Position

value for D is in the range $[D-dD,D+dD]$, the true value for X is in $[X-dX,X+dX]$, and the true value for β is in the range $[\beta-d\beta,\beta+d\beta]$.

Considering φ as a density function, then there is a cube defined by the measurement errors, dD, dX, $d\beta$. The true value for φ must be inside this cube, so the true value of φ must be in the range of $\varphi_{min} \leq \varphi \leq \varphi_{max}$.

These two values can be determined in the following way from equation (4.1):

$$\cos\varphi = \frac{D - X\cos\beta}{h}$$

$$-\sin\varphi \frac{\partial\varphi}{\partial D} = \frac{h - (D - X\cos\beta)\dfrac{\partial h}{\partial D}}{h^2}$$

$$\frac{\partial\varphi}{\partial D} = \frac{-1}{\sqrt{1-\cos^2\varphi}} \frac{h - \dfrac{(D - X\cos\beta)^2}{h}}{h^2}$$

$$\frac{\partial\varphi}{\partial D} = \frac{-h}{\sqrt{h^2 - (D - X\cos\beta)^2}} \frac{h - \dfrac{(D - X\cos\beta)^2}{h}}{h^2}$$

$$\frac{\partial\varphi}{\partial D} = \frac{-1}{\sqrt{1 - \left(\dfrac{D - X\cos\beta}{h}\right)^2}} \frac{1 - \left(\dfrac{D - X\cos\beta}{h}\right)^2}{h}$$

$$\frac{\partial\varphi}{\partial D} = \frac{-1}{h^2}\sqrt{h^2 - D^2 + 2XD\cos\beta - X^2\cos^2\beta}$$

$$\frac{\partial \varphi}{\partial D} = \frac{-X}{h^2}\sqrt{1-\cos^2\beta}$$

Using similar derivations:

$$\frac{\partial \varphi}{\partial X} = \frac{D}{h^2}\sqrt{1-\cos^2\beta}$$

$$\frac{\partial \varphi}{\partial \beta} = \frac{X\sin\beta}{h^2}\,\frac{D\cos\beta - X}{\sqrt{1-\cos^2\beta}}.$$

For this experiment *D*–*dD* and β–*d*β are strictly positive. Using the property previously described, it is safe to set X-dX positive also. The cube defined above does not contain the origin and $\nabla\varphi \neq 0$ everywhere inside the cube. The maximum and minimum values of φ must occur on the boundary planes of the cube.

A similar analysis of each of the boundary planes shows that the maximum and minimum must occur on the edges of the cube. Analyzing the edges shows that the maximum and minimum for φ must occur either at one of the eight corners of the cube or at one of four points on the edges defined by $\cos\beta = \frac{X}{D}$ provided these points are on the cube.

To find the measurement error of φ given the measurement errors in *D*, *X*, and β it is sufficient to calculate φ at each of these eight or twelve points and take the maximum and minimum from the set. Then:

$$\varphi_{measured} = \frac{\varphi_{max} + \varphi_{min}}{2} \pm \frac{\varphi_{max} - \varphi_{min}}{2}$$

Typical experiments have:

$$D = 10 \pm 0.005\ m$$

$$X = 2 \pm 0.0005\ cm$$

$$\beta = \frac{\pi}{2} \pm 0.017\ radians$$

Which yield an experimental error in φ of $\pm 2\times10^{-6}$ *radians*.

Finally φ is related to the rotation of the rotor by:

$$\varphi = 2\gamma$$

And to the pattern rotation by:

$$\varphi = \frac{2}{33}\theta.$$

So this experiment measures the rotor rotation to an accuracy of $\pm 1\times10^{-6}$ *radians* and the pattern rotation to an accuracy of $\pm 3\times10^{-5}$ *radians*.

Even if the error in D is ten times greater, that is $D = 10 \pm 0.05m$ still yields an accuracy in the rotor rotation of 5×10^{-6} *radians.*

4.3 Stepper Motor

The stepper motor setup replaces the rotor mount and rotor bearing in Figure 3.3 with a stepper motor. The rotor disk is attached directly to the motor drive shaft. The stepper motor is controlled by the computer through a power circuit that is capable of delivering half of an amp of current to each of the two motor windings at twelve volts.

The stepper motor has a full step size of $\frac{2\pi}{200}$ radians, or 1.8°. These positions are used to check the results from the sensor. The control circuitry also allows half-stepping the motor, that is, 0.9°steps, but this capability is not used because half-step positions have alternately one motor winding energized or two windings energized. This oscillation introduces a further source of

error into the accuracy of the motor. When the motor is full-stepped both windings are energized in all positions.

The rated accuracy of the stepper motor is ±5%. This is not very accurate when compared to the desired accuracy of the sensor, however it does provide a complete cycle of rotation for comparison with the sensor. In addition, the rating applies to the precision of the angle between different steps. The stepper motor can return to the identical position with much greater accuracy. This capability is dependent on the amount of current in the windings which is precisely controlled by the power circuit.

This capability, the return accuracy, can be used to test the sensor by taking an initial reading, rotating the rotor through a known number of steps, then rotating it back the same number of steps. The reading at the final position can then be compared with the initial reading. This method also has the advantage of reducing the effect of tilt and shift errors because both readings are taken at almost the same position.

5 Experimental Results

Experiments were conducted with each of the setups previously described. The simulator was used first to get qualitative results on the signal characteristics. These simulated signals were compared to signals from the sensor under conditions of ideal alignment and controlled misalignment. The simulator was also used to get an idea of noise response of the system and to examine some possibilities that would have been awkward to examine with the physical apparatus.

The laser and mirror test was used in a straight-forward comparison of rotation measurements under conditions of no tilt and no shift. The short range of the test setup made it incapable of testing the sensor when tilted or shifted. The periods of the associated error terms for these conditions are too large to measure A_t, θ_t, A_s, and θ_s using the laser.

The stepper motor was also used to compare rotation measurements but also to further examine the errors associated with tips and shifts.

5.1 Simulator Results

The first experiment with the simulator was to verify equation (2.3):

$$H_{31} = 32A\,e^{j\theta}$$

which suggests that the angular position can be determined from the Fourier transform of the sample.

Simulated samples were generated and the Fourier transform of each was calculated. The simulator was programmed to rotate through a full pattern rotation in sixty-four steps. At each step the simulated rotor position was calculated using the Fourier transform method. The calculated position was then compared to the known, programmed position at each point and both were recorded.

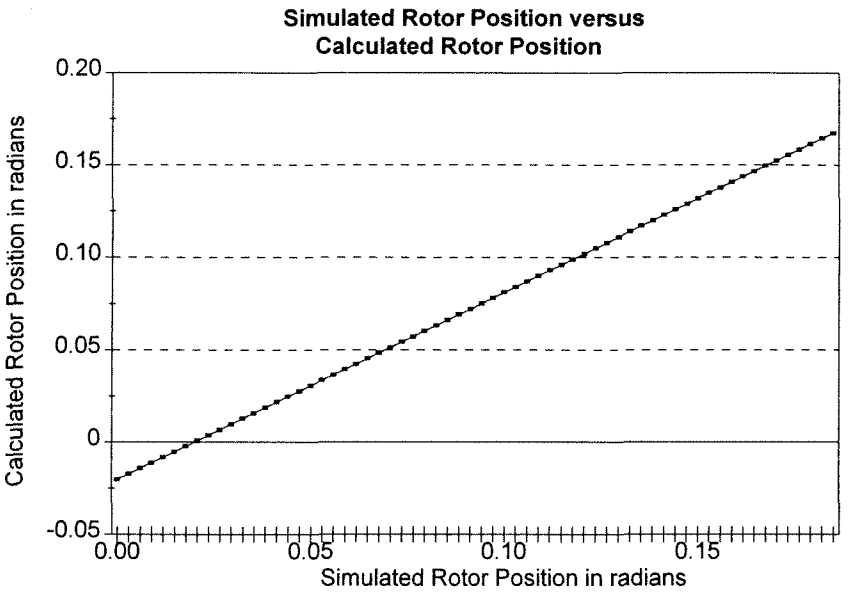

Figure 5.1
Simulated Rotation versus Measured Rotation

For a perfect angular sensor the experiment would return $\gamma_{calc} = \gamma_{sim}$. For the real and the simulated sensors, the expected relationship was $\gamma_{calc} = (1 - \mu)\,\gamma_{sim}$ for the best-fit line through the data, where μ is the slope error of the sensor.

The best fit line for the data gives $\gamma_{calc} = (1 - 4.5\times10^{-5})\gamma_{sim} - 0.02006$. The y-intercept of this line is unimportant as it only signifies that the simulator did not start off in the zero position. The slope error of this line, $\mu = 4.5\times10^{-6}$, indicates that the rotor rotation can be determined from the Fourier transform of the sample to an accuracy of at least five parts in a hundred thousand.

The next two experiments with the simulator examine the effects from tipping or shifting the simulated rotor. The rotor was rotated through sixty-four positions with a pattern rotation of $\frac{2\pi}{64}\ radians$ between each position.

In the first of the two experiments the simulator was programmed to have a tilt angle of $\alpha = 0.08 radians$. At each point the position was calculated using the Fourier transform method. The error in this calculation was determined from the known, programmed position of the simulated rotor. The error for each of the measurement points is shown in Figure 5.2 against the position index.

Figure 5.2 shows that the tilt does significantly decrease the accuracy of the measurement. However, equation (2.7) suggests that this error can be removed by subtracting a best fit curve with the period specified in the equation from the error. The resulting adjusted position error shown in Figure 5.3 was an order of magnitude better than the original.

The second experiment in this series was very similar to the first except the rotor was shifted 0.8mm instead of tilted. Again the results, Figure 5.4, show a considerable error associ-

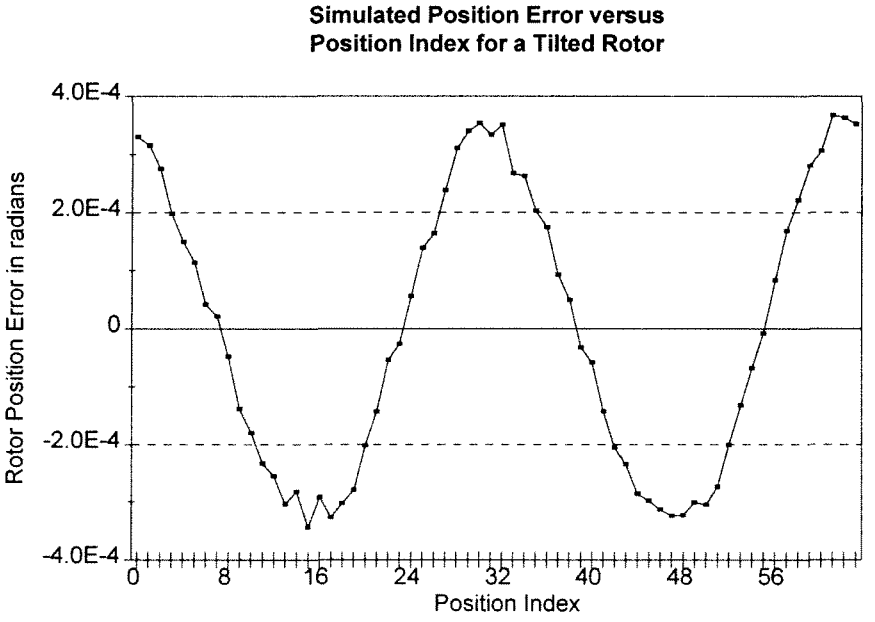

Figure 5.2
Simulated Error for a Tilted Rotor

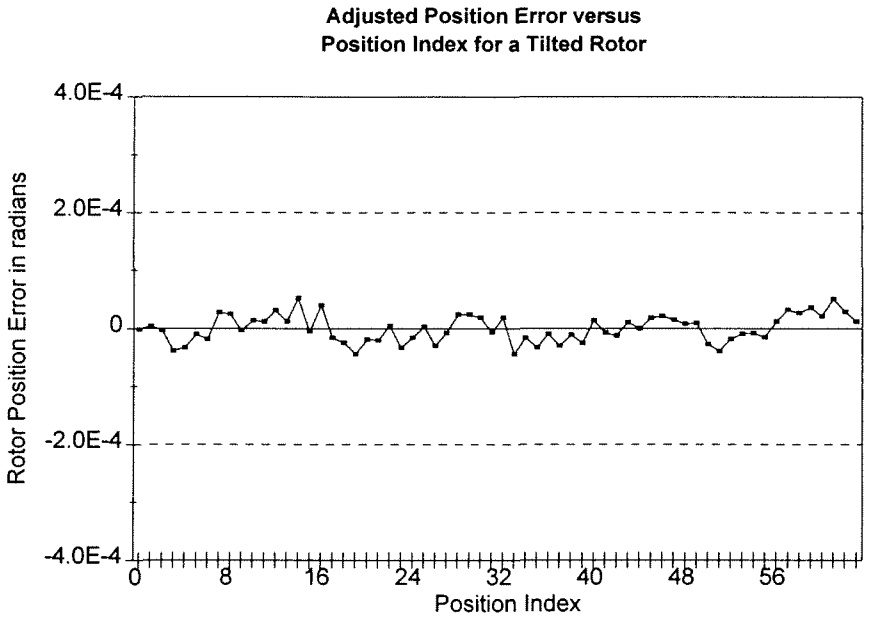

Figure 5.3
Simulated Error for a Tilted Rotor After Adjustment

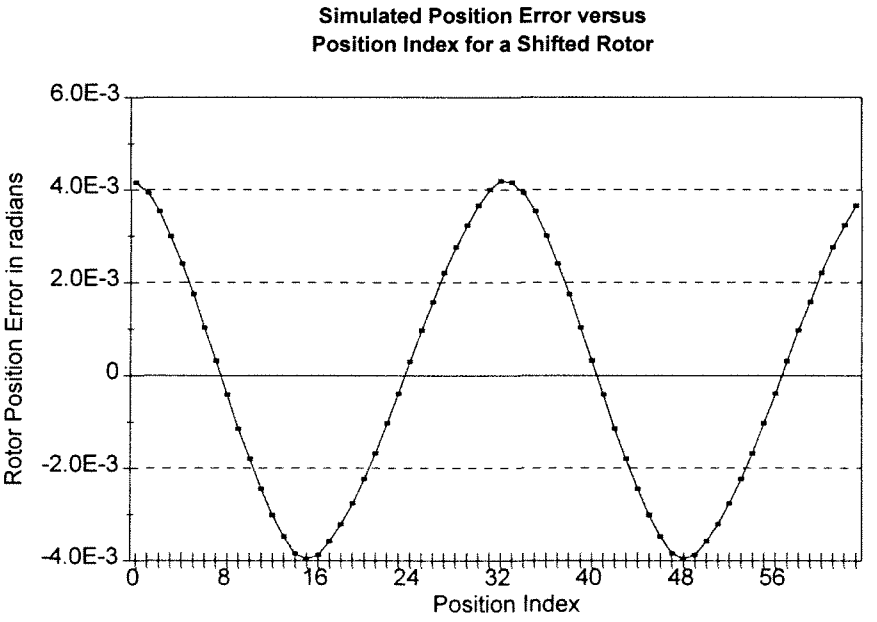

Figure 5.4
Simulated Error for Shifted Rotor

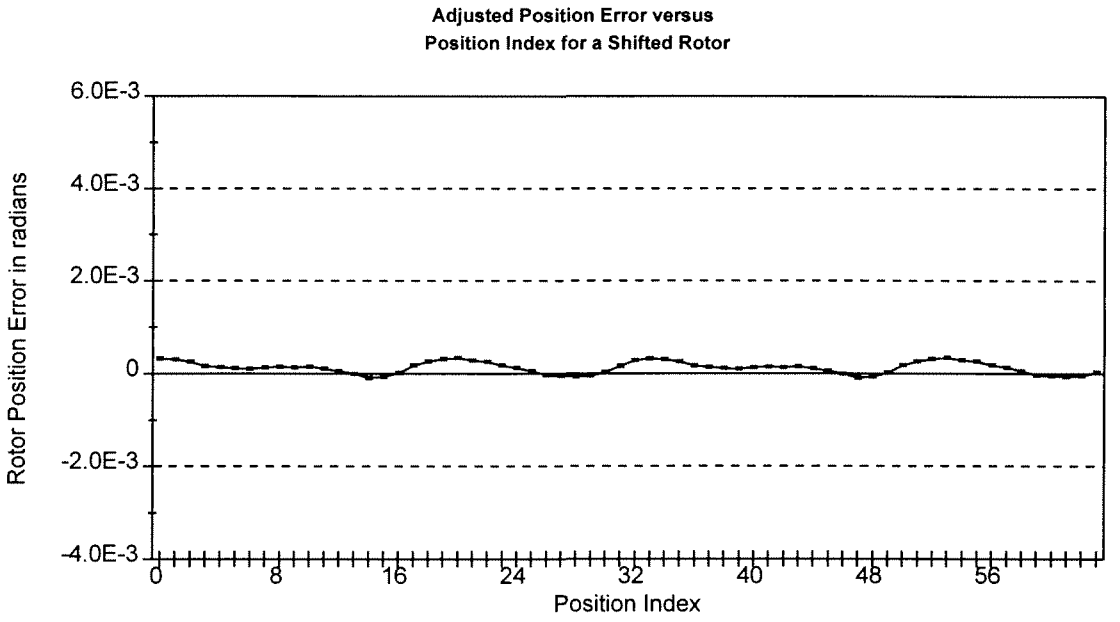

Figure 5.5
Simulated Error for Shifted Rotor After Adjustment

ated with the shift. Using equation (2.8) this time to remove the error, the accuracy improved to within 2×10^{-4}*radians*, as seen in Figure 5.5.

The next set of experiments conducted with the simulator was intended to check further that the periods of the error terms associated with a tilt or a shift are as expressed in equations (2.7) and (2.8).

The simulator was programmed to simulate $N_m = \frac{N_r}{2} - 1$ pads on the rotor instead of $N_m = \frac{N_r}{2} + 1$. The resulting pattern had the same basic shape as with $\frac{N_r}{2} + 1$ pads but it rotated in the opposite direction with respect to the rotor. According to equations (2.7) and (2.8), only the tilt error period should change to reflect the different number of rotor pads. The shift error period should remain unchanged because it depends on N_r, not N_m. The tilt and shift experiments were repeated except the best fit curve calculation for the tilt was adjusted to reflect the new period. The results are shown in Figure 5.6 through Figure 5.9.

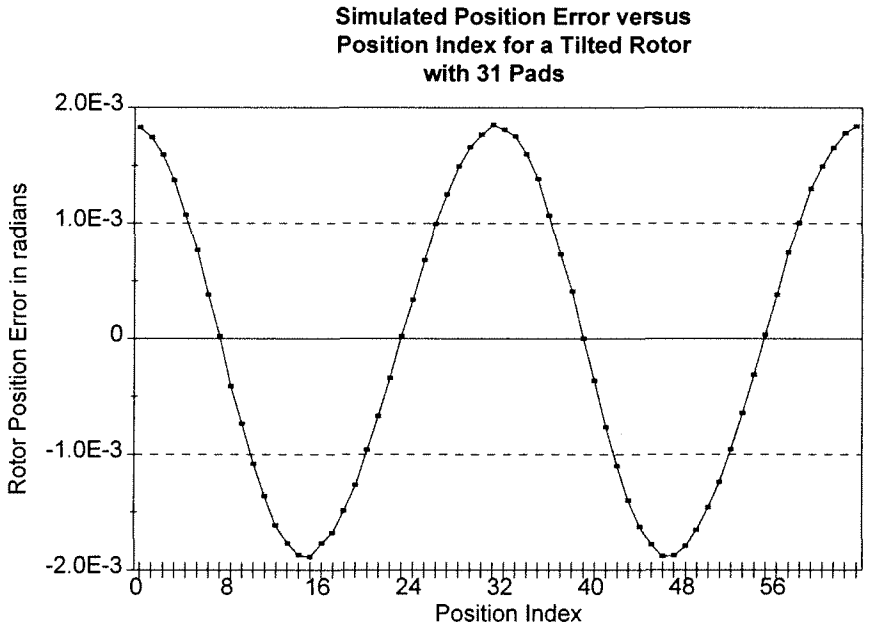

Figure 5.6
Simulated Error for a Tilted Rotor with 31 Modifier Pads

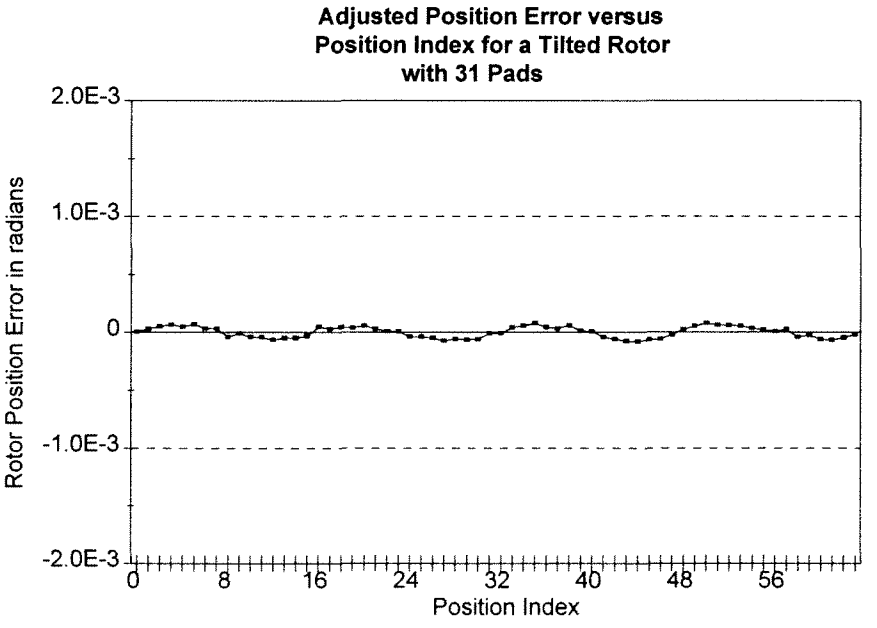

Figure 5.7
Adjusted Error for a Tilted 31 Pad Rotor

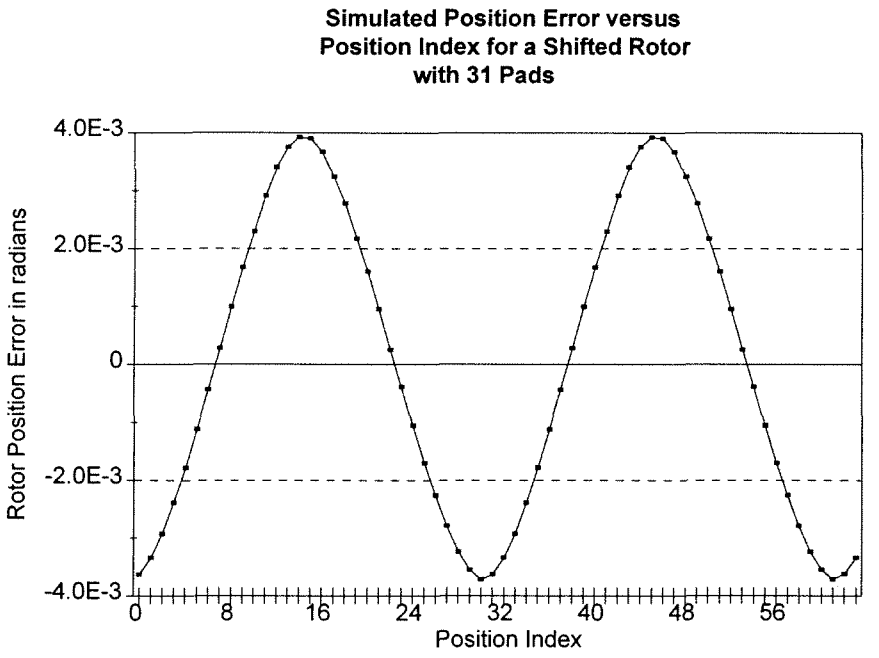

Figure 5.8
Simulated Error for a Shifted Rotor with 31 Modifier Pads

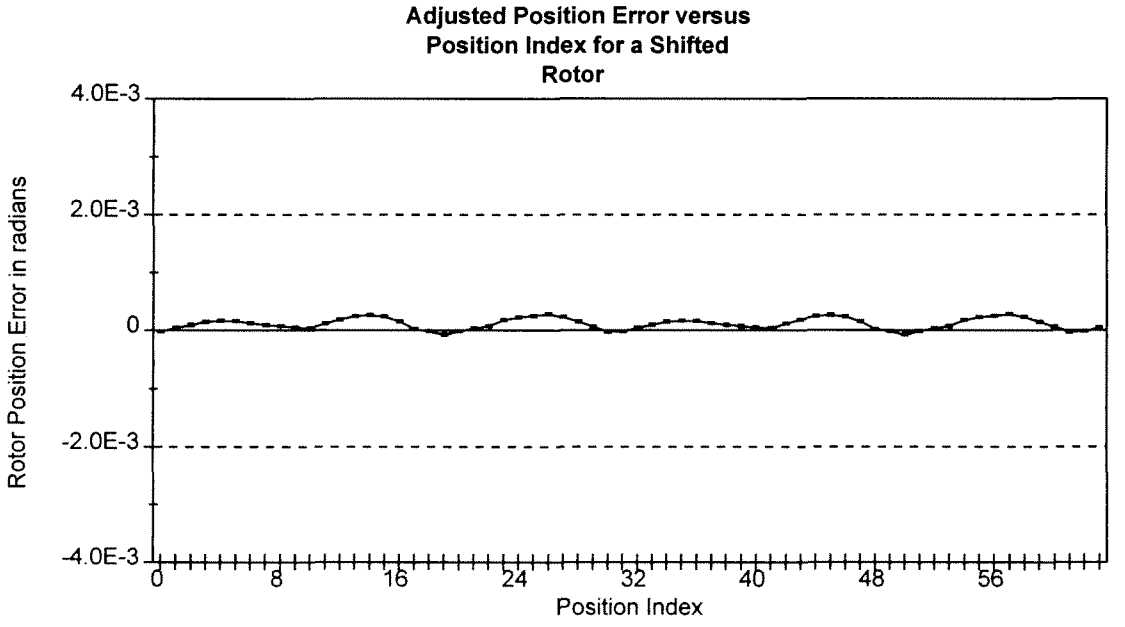

Figure 5.9
Adjusted Error for a Shifted 31 Pad Rotor

For both sets of experiments, removing the best fit error terms with the periods given by equations (2.7) and (2.8) increased the precision of the simulated measurements by an order of magnitude. The error terms specified do appear to be the dominant errors when the sensor is misaligned through tipping or shifting.

Another important characteristic of this sensor design is the relationship between the number of stator pads, N_r, and the sensor precision. The simulator provided an effective way to examine this relationship. The first experiment compared the programmed position for the simulated sensor and the calculated position. This experiment was repeated for simulated sensors with $N_r = 32$ stator pads and $N_r = 128$ pads. For each simulated sensor the number of rotor pads was set to $\frac{N_r}{2} + 1$.

The best-fit line through the position data:

$$\gamma_{calc} = (1 - \mu)\gamma_{sim} - \gamma_{start}$$

where γ_{calc} is the calculated rotor position

γ_{sim} is the rotor position programmed into the simulator

γ_{start} is the initial position of the simulated rotor

μ is the slope error of the simulated sensor.

is summarized in Table 5.1.

As expected the sensor accuracy does appear to increase with pad number. This result must be treated with caution because the data is entirely simulated with no backup from real data. In addition, while the sensor pad number was altered, no other disk geometry was changed. In a real device with 128 pads the fringe fields could become a significant proportion of the total field so the simulator approximation might break down.

Table 5.1
Simulated Encoder Error for Different Generator Pad Numbers

Number of Generator Pads	μ
32	1.1×10^{-3}
64	4.5×10^{-5}
128	3.6×10^{-6}

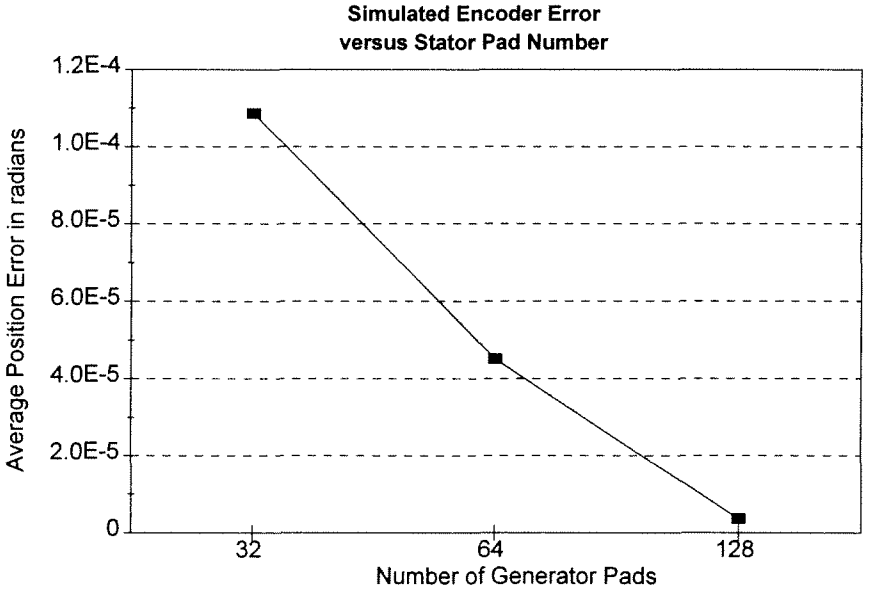

Figure 5.10
Sensor Accuracy versus Number of Generator Pads

The simulator was also used to explore the effect of gaussian, white noise on the position calculation. The experiment consisted of the following steps.

1. A "pure" signal was acquired from the simulator and the position calculation was performed on it to get a "perfect" position. A noise standard deviation was chosen.

2. One thousand and twenty-four gaussian noise signals with the given standard deviation and a mean of zero were generated, where a noise signal is a collection of N_r values each randomly selected from a gaussian distribution with standard deviation σ_{noise}, and zero mean. The units of σ_{noise} were chosen to correspond with the resolution of the analog-to-digital convertor. So in for this sensor, $\sigma_{noise} = 1$ corresponds to $(1\ {}^{A}/_{D}unit)\times(2.5\ volts)\times(256\ {}^{A}/_{D}units)^{-1} \approx 1\times10^{-2}\ volts.$

3. Each noise signal was independently added to the pure signal.

4. For each noise signal, j, the position calculation was repeated and the difference with the "perfect" position, ε_j, was recorded.

5. For each standard deviation the average rms-error was calculated as:

$$error_{rms} = \left(\frac{\sum_{j=1}^{1024} \varepsilon_j}{1024}\right)^{\frac{1}{2}}$$

6. This procedure was repeated sixteen times for each noise standard deviation and for fifty different standard deviations.

The calculated best-fit line, shown in (5.1), was:

$$Error_{rotor} = 4.9\times10^{-5}\ \sigma_{noise} \tag{5.1}$$

This result must be suspect as it does come from entirely simulated data, however, if it is accepted for the moment, it suggests that the standard deviation of the electrical noise in the sensor should be kept down to around one unit of the analog-to-digital convertor in order to maintain precision in the microradian range.

Real noise data from the sensor was collected by taking ten samples with no position change between the samples. Let

$V_{p,n}$ be the nth value in sample p.

$$\overline{V}_n = \frac{\sum_{p=0}^{9} V_{p,n}}{10}$$

$$\sigma_n = \left(\frac{\sum_{n=0}^{10} (V_{p,n} - \overline{V}_n)^2}{9} \right)^{\frac{1}{2}}$$

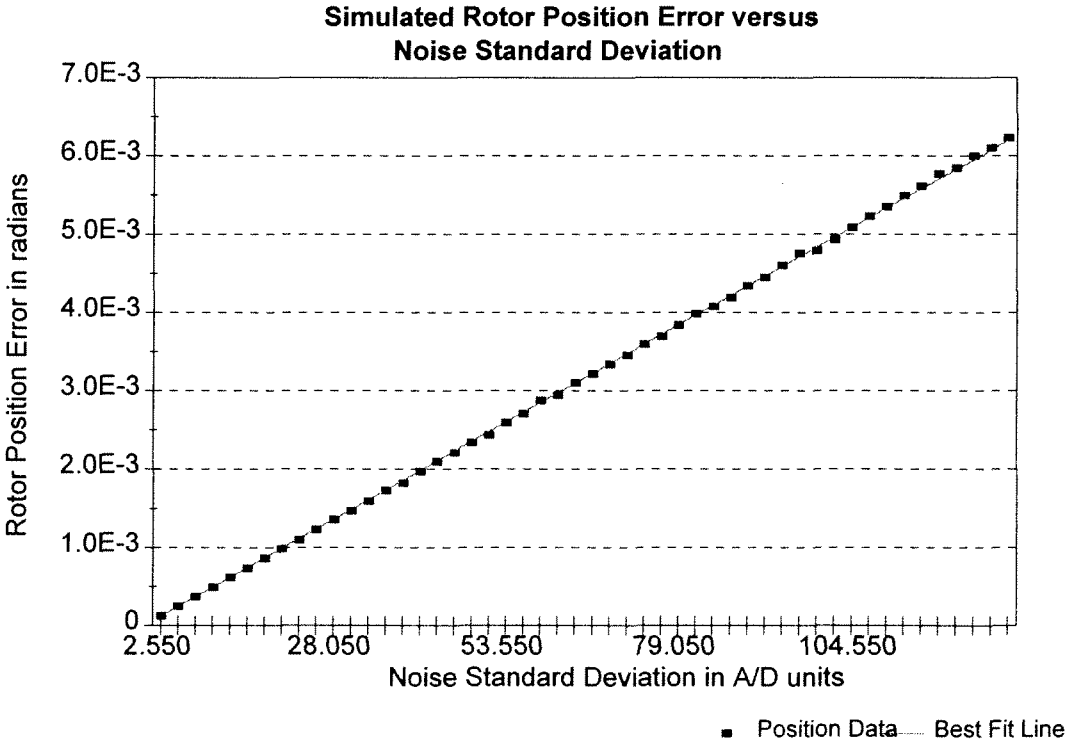

Figure 5.11
Position Error Due To Gaussian Noise

$$\sigma_{noise} = \frac{\sum_{n=0}^{63} \sigma_n}{64}$$

The value for σ_{noise} calculated from the experiment was 1.3, putting this value in equation (5.1) suggests that electrical noise limits the accuracy of this sensor to around 6×10^{-5} radians. This precision limit is probably quite variable however, as it is a result of several factors most of which are uncontrollable. For example, recall that the sensor circuitry amplifies electrical signals in the frequency range of 302.4 kHz to 312.0 kHz. If the other equipment is generating fields containing these frequencies, then these spurious fields could be a source of electrical noise.

5.2 Laser and Mirror Results

The laser and mirror setup previously described was the first to test results from the real sensor. It tested sensor accuracy in the range of very small rotations (thousandths of a radian).

The experimental procedure used for this setup was as follows.

1. The rotor was lowered using the Z-translation stage away from the stator and a baseline sample was acquired as the average of twenty samples from the sensor.

2. The rotor was raised back into a position where the signal filled the full range of the A/D convertor.

3. The distance from the spot detector to the reflecting mirror was measured using the surveyor's tape.

4. The fluorescent lights were turned off to reduce the effect of flicker and stray light on the spot detector.

5. The rotor was rotated to a reasonable starting position such that the reflected beam was slightly to the side of the outgoing beam from the laser.

6. The computer calculated the rotor position from the average position from twenty samples with the baseline removed.

7. The reflected spot position was measured by moving the spot detector from the position of the outgoing beam into the reflected beam until the currents in the photodiodes balanced. The average of five measurements at each position was taken as the position and the standard deviation was taken as the measurement error.

8. The rotor was rotated by hand a small amount from the starting position.

9. The measurements were repeated for the new position.

The experiment was conducted three times with the results shown in table 5.2.

The results suggest that the sensor can measure rotations at least to within $\pm 5.6\times10^{-5}$ radians and possibly to within $\pm 3.2\times10^{-5}$ radians. Unfortunately the short range of the laser apparatus prevented measuring for a tilt or a shift in the rotor position. These results are around the expected precision of the device given the amount of electrical noise in the system which sug-

Table 5.2
Rotation Measurements for Laser Setup

ΔX in metres	D in metres	γ_{laser} in radians	γ_{calc} in radians
0.01377±0.000096	10.36±0.005	$(6.65\pm0.05)\times10^{-4}$	6.65×10^{-4}
0.0187±0.00019	10.36±0.005	$(9.03\pm0.10)\times10^{-4}$	8.57×10^{-4}
0.0157±0.0002	10.36±0.005	$(7.58\pm0.10)\times10^{-4}$	8.00×10^{-4}

gests that the rotor and stator were actually aligned quite well. If, however, they were slighlty misaligned then measuring the tilt and shift would have increased the accuracy of the measurements further.

5.3 Stepper Motor Results

The stepper motor setup provided the means to examine the sensor over much larger ranges than the laser did. In addition, it enabled testing some of the results obtained with the simulator.

The first experiment with the stepper motor was very straight-forward. The following procedure describes the experiment.

1. The rotor was lowered away from the stator and a baseline sample was calculated as the average of twenty samples from the sensor.

2. With the rotor raised back into position, the motor was energized to hold the rotor in a fixed position.

3. An initial position was calculated from the average of twenty samples with the baseline removed.

4. The motor was driven one full step forward to the next position.

5. The sensor position was calculated from the average of twenty samples with the baseline removed and the rotation from the previous position was recorded.

The calculations were performed for one hundred and ninety-two step positions. The results are shown in the three following graphs, each showing sixty-four of the positions. Also shown in each graph are two types of adjusted results, after the tilt error term is removed and after the tilt and shift error terms are removed using the technique described in chapter 2.

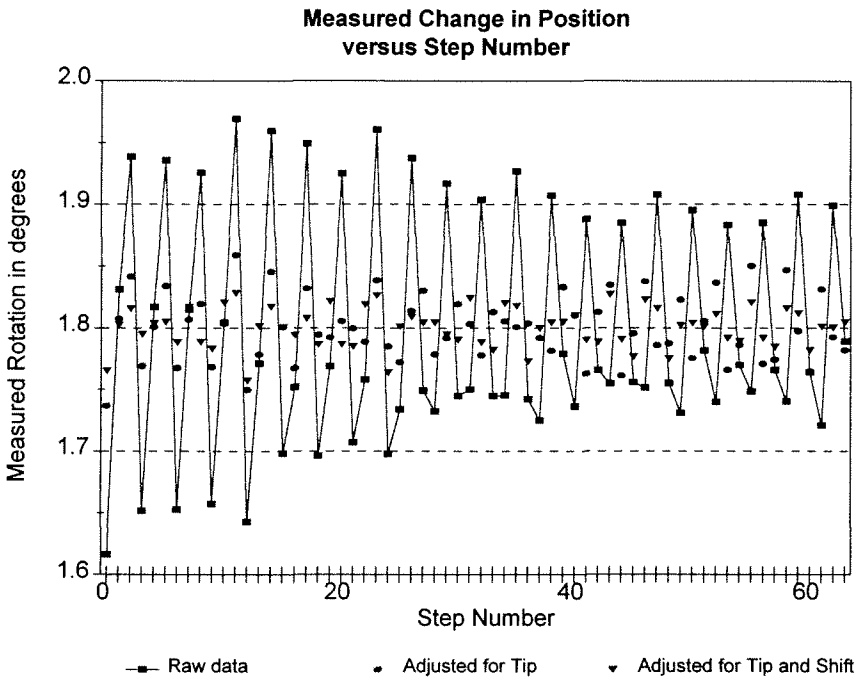

Figure 5.12
Measuring Full Steps for Step Positions 0 to 63

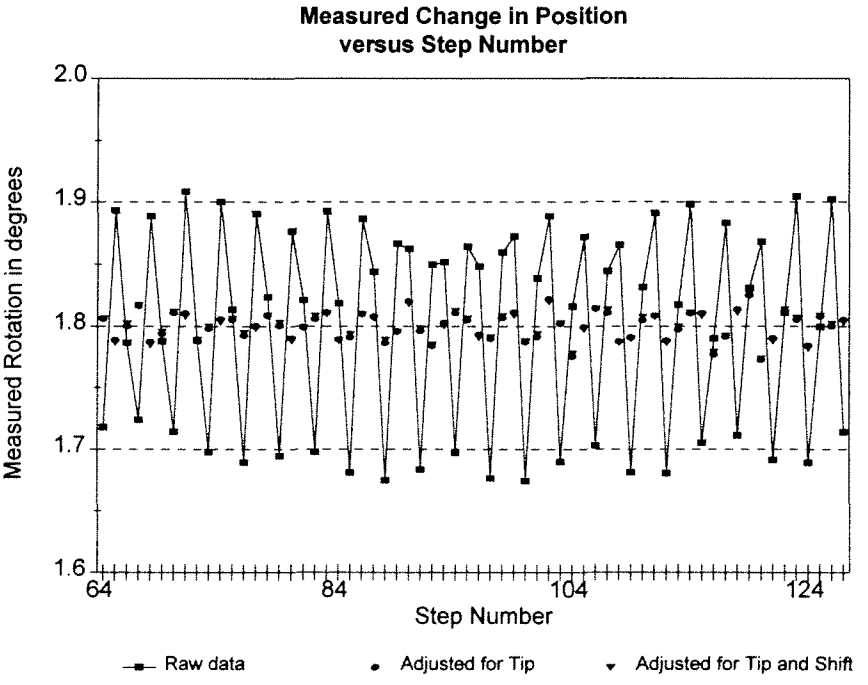

Figure 5.13
Measuring Full Steps for Step Positions 64 to 127

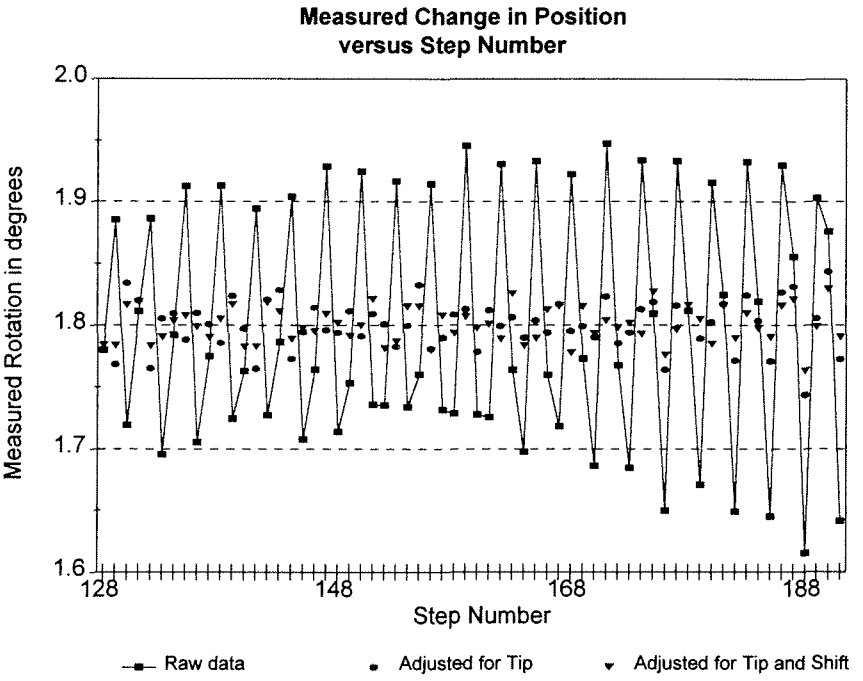

Figure 5.14
Measuring Full Steps for Step Positions 128 to 191

The raw signals appear to show that the sensor was not producing readings within even the five percent accuracy of the motor since the maximum calculated deviation from the 1.8° step size was 0.17°. The five percent motor specification only allows for a maximum deviation of 0.09°. However, when equations (2.7) and (2.8) were used to remove the best-fit tilt and shift error terms, the maximum calculated deviation was 0.04°, which is well within the motor specification. Consequently this experiment shows that the sensor is returning results at least as accurately as the stepper motor.

This property was further tested with another experiment. Single stepping the motor may have introduced some error because the motor has to overcome the stiction holding it in place. The previous experiment was modified so that the motor was programmed to take six full steps forward in radpid succession and five full steps backward between measurements.

The results shown in Figure 5.15, with tilt and shift errors already removed, for the sixty-four positions measured show the same range of readings as the previous experiments.

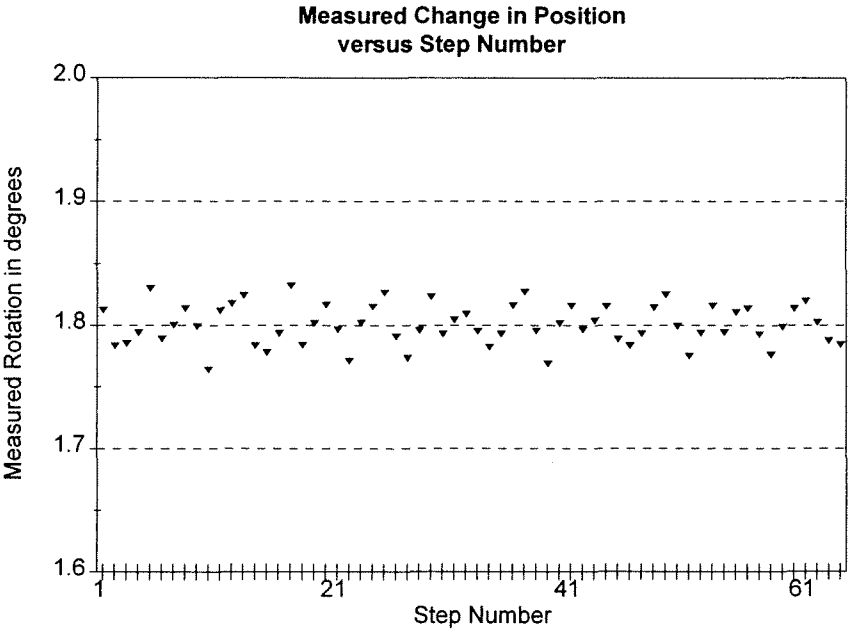

Figure 5.15
Measuring Step Size by Taking Multiple Steps Out and Back

Both of these experiments showed poor results before the tilt and shift errors were removed. As can be seen from the graphs for the first experiment, most of the error was actually due to a tilt of the rotor. This is a consequence of the rotor mount (see Figure 3.3).

The mount has three linear directions of control so that a shift error in any direction can be removed. The mount has only one degree of tilt control, so only one direction of tilt error can be corrected with the mount. Care was taken in the assembly of the stand (see Figure 3.4), but small inaccuracies are present which appear as a tilt in the rotor.

The next experiment tested the sensor against the ability of the stepper motor to return to the identical position. The steps in the experiment were the following.

1. A baseline sample was acquired as for previous experiments and the motor was energized.

2. An initial position was calculated.

3. The motor was driven five full steps forward then five full steps backward followed by a two second pause to allow the rotor position to settle.

4. The sensor position was calculated from the average of twenty samples with the baseline removed and the changes from the previous and initial positions were recorded.

Sixty-four samples were taken by repeating the last two steps of the procedure. The results are presented in the following graph.

The results show that the sensor is very sensitive for determining deviation from the initial position with a maximum recorded deviation of 2.5×10^{-5} radians and an average of 6.0×10^{-6} radians. The stepper motor did not have a rating for stability of a given step position, but it is unlikely that an error in the sensor and an error in the stepper motor would cancel out to such a high degree.

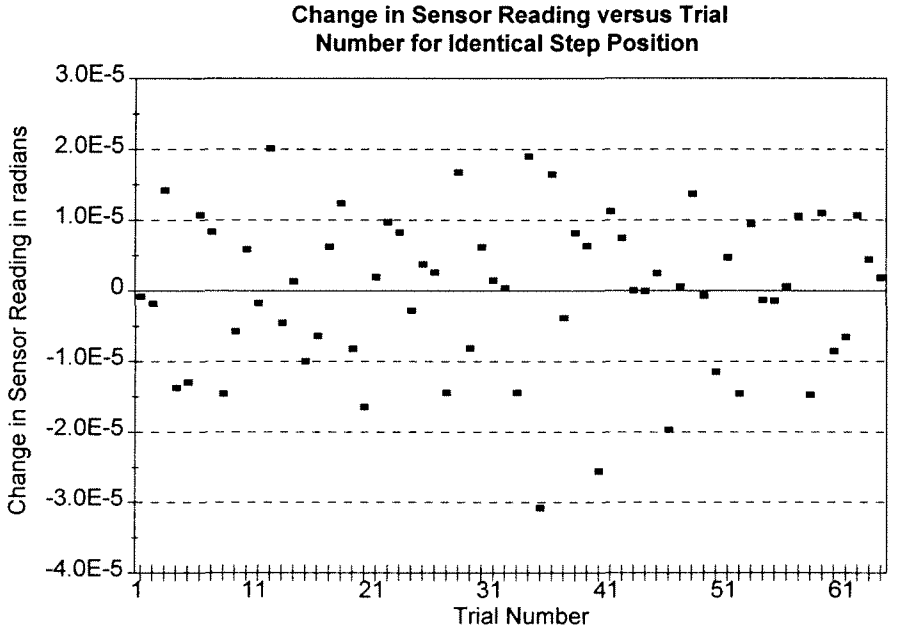

Figure 5.16
Measuring Sensor Ability to Return to Identical Position

Some of the accuracy should be attributed to the fact that for returning to an identical position, alignment problems do not have as much of an effect.

The previous results needed to be verified for several different positions in the range of rotation of the sensor. This was done in the next two experiments, the first of which used the following procedure.

1. A baseline sample was acquired and the motor was energized.
2. The motor was driven six full steps forward then five full steps backward followed by a two second pause to allow the rotor position to settle.
3. An initial position was calculated.
4. The motor was driven five full steps forward then five full steps backward.
5. The sensor position was calculated from the average of twenty samples with the baseline removed and the change from the previous position was recorded.

The last two steps were repeated fifteen more times for the inner loop, then the entire sequence returned to step 2. This outer loop was performed sixteen times. So repeatability was tested at sixteen locations with sixteen measurements at each location. Each location was separated by one step, or 1.8°.

As seen in Figure 5.17, the results at each location are essentially identical with a maximum change in sensor reading of 4.8×10^{-5} radians and an average change of 2.3×10^{-6} radians.

A different method of displaying this same information is to calculate the standard deviation of the sixteen absolute position readings at each of the sixteen positions. This value was then plotted against position number. This value is representative of the repeatability of the sen-

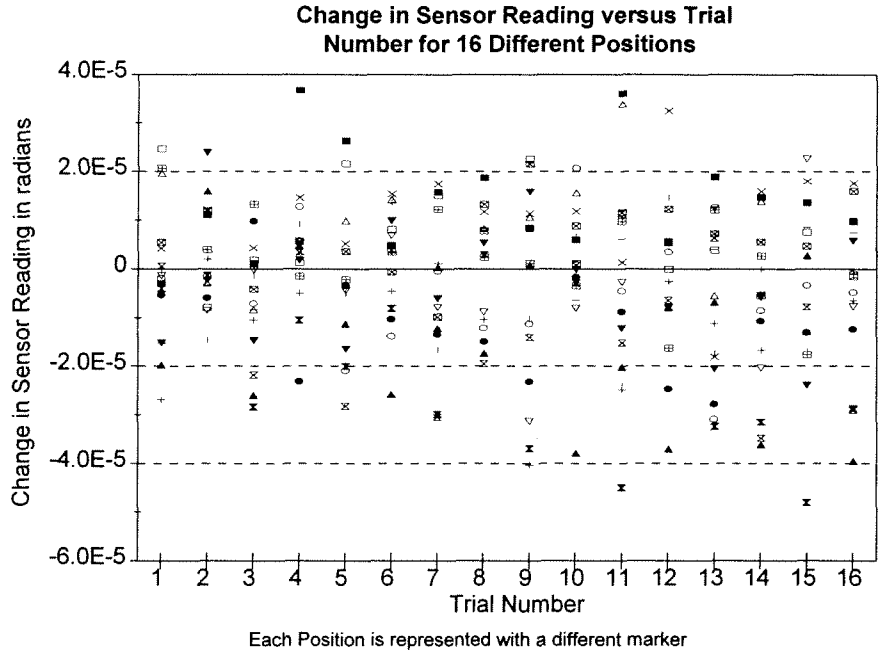

Figure 5.17
Repeatability of Sensor at 16 Points One Step Apart

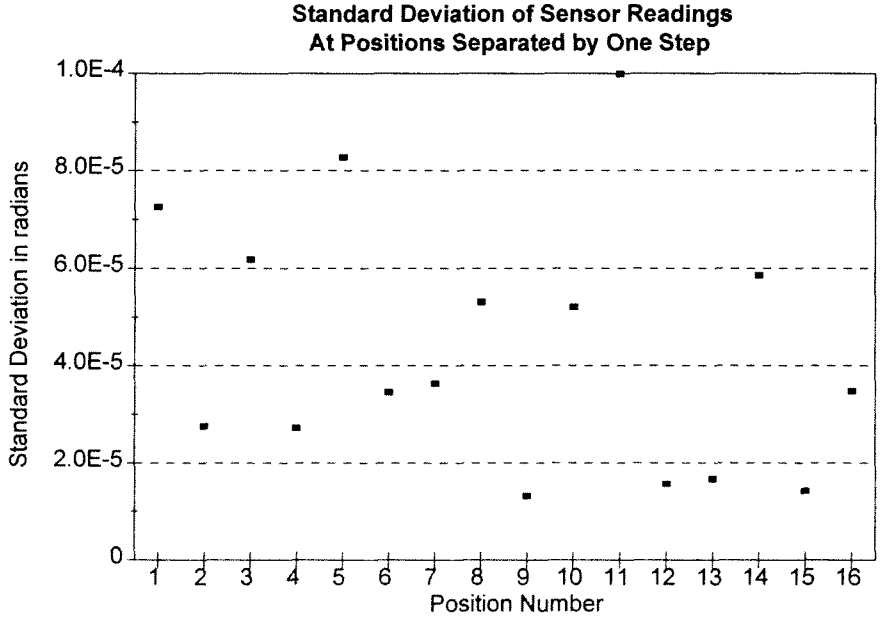

Figure 5.18
Standard Deviation of Repeatability at 16 Points

sor when it is returned to the same position. Of course, some of this error can be attributed to the stepper motor, so using this value provides an upper limit on the accuracy of the sensor.

Using this measure of repeatability, the maximum standard deviation was 1.0×10^{-4} radians and the average was 4.4×10^{-5} radians.

The next experiment was to test further the repeatability of the sensor over a full rotation of the sensor.

1. A baseline sample was acquired and the motor was energized.

2. The motor was driven ten full steps forward.

3. The position was calculated and recorded.

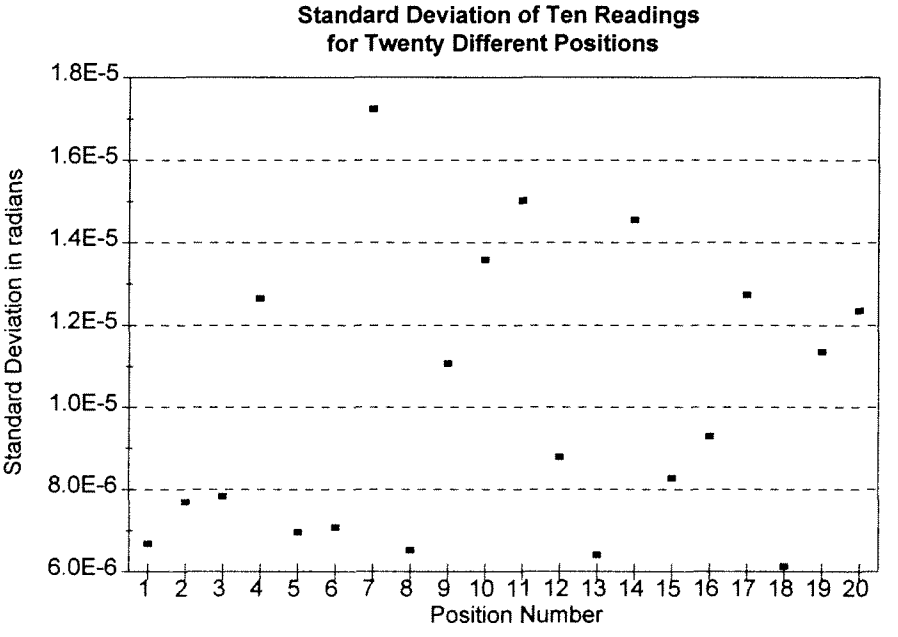

Figure 5.19
Standard Deviation of Repeatability After a Full Rotation

The final two steps were repeated two hundred times. Since there were two hundred steps in a full revolution of the stepper motor, this experiment gave ten readings for each of twenty positions. Subsequent readings for a given position were separated by a full rotation of the sensor.

For each of the twenty positions the standard deviation of the ten readings was calculated and is shown. The maximum of these is 1.7×10^{-5} radians and the average is 1.0×10^{-5}. This indicates that the sensor is equally sensitive at any position in its range.

These experiments with the stepper motor indicate that the angular sensor is operating correctly over the entire range of the sensor. When returning to the initial position, the results obtained with the stepper motor give a sensor accuracy that is as good or better as the results obtained with the laser and mirror. Measuring between stepper motor positions at first appears very inaccurate but using the methods described in chapter 2 to remove tilt and shift errors, these results show that the sensor is consistent through its entire range.

5.4 Summary of Results

Several experiments were described in this chapter, all with the goal of determining the resolving capabilities of this angular sensor. Each gave a possible value for this parameter.

Recall that in chapter 2 a model was developed to express an upper bound on the precision of the sensor. This model for the current sensor configuration (see page 27) suggests that the sensor has an average accuracy of approximately $20\mu rad$ in the absence of noise.

The results from the laser and mirror experiment described on page 64 measured a sensor accuracy in the range of $32\mu rad$ to $56\mu rad$ for very small rotations.

The stepper motor experiments described starting on page 66 which measured the sensor readings when the sensor was returned to its starting position indicate that the sensor accuracy was $25\mu rad$ or better for this sort of measurement.

These numbers agree quite well. The discrepancies most likely result from the different conditions for each: the model of course does not account for system noise or incorrect alignment, the stepper motor experiments were subject to noise, but not misalignment because there was no net rotation between the starting and ending positions, and the laser experiment was subject to both sources of error.

The stepper motor experiments which measured angular differences between adjacent steps provided a convenient way to measure the effect of misalignment on the sensor. These experiments show that even a small tilt or shift in the sensor can seriously effect the signals.

Fortunately, the frequency domain analysis of these sources of error described in chapter 2 provided a means of drastically reducing their effects. The use of this analysis reduced the error in these experiments by at least a factor of four. The stepper motor could not be used to test the limits of this analysis because the experiments exceeded the accuracy of the stepper motor. Experiments conducted using the simulator to test this analysis suggest that the improvement may be as high as a factor of ten.

5.5 Comparison with Existing Designs

The design presented is for a non-contact angular sensor with infinite range. There are similar products available commercially[1] and under development. The technologies used cover a fairly large spectrum, so the focus here is on sensors which use either optical or capacitive techniques.

Optical angular sensors are typically available as incremental or absolute encoders[2]. They are fundamentally discrete devices. They operate by directing light at a slotted disk and counting

---

1 Instrument Society of America, ISA Transducer Compendium, vol. II. 2nd ed.

the light pulses as the disk is rotated (or some variation on this general scheme). Being discrete devices, the resolution of these sensors is often described in terms of bits of resolution. A device with B bits of resolution can resolve an angle of $\frac{2\pi}{2^B}$ *radians.*

Devices with B ranging from eight to twelve are easily available commercially. Also available but much less common (and much more expensive) are devices with B as high as seventeen. A device with $B = 17$ has a resolution of 4.8×10^{-5}*radians*.

Such optical angular sensors are available with infinite range. They are contact devices.

High precision capacitive angular sensors are not available as commercial products. A few designs have been presented in journals. A design presented by Jankauskas and others[3] uses a rotating drum. They report a resolution on the order of 5 arc minutes, or 1.4×10^{-3}*radians*.

A design presented by R.D. Peters[4] is similar to the design presented here in that it uses coplanar, coaxial disks, but the arrangement of electrodes is quite different and his design uses two stator disks and one rotor disk between them. He reports accuracy in the microradian range. His sensor is a non-contact sensor.

A design very similar to the one presented here was presented by Gerben W. de Jong and others.[5] This design uses two static disk, one is the signal generator and the other is the detector. A third disk which can freely rotate is placed between the two static disks. The group reports a repeatability of 4.4×10^{-5} radians.

---

2 Hermann Karl Paul Neubert, Instrument Transducers: An Introduction to Their Performance and Design, 2nd ed.

3 G.T Jankauskas, J.R. LaCourse and D.E. Limbert, "Optimization and Analysis of a Capacitive Contactless Angular Transducer," IEEE Transactions on Instrumentation and Measurement, XLI (April 1992), 311-315.

4 R.D. Peters, "Capacitive angle sensor with infinite range," Review of Scientific Instruments, LXIV (March 1993), 810-813.

5 Gerben W. de Jong et. al., "A smart capacitive absolute angular-position sensor," Sensors and Actuators A, XLI (1994), 212-216.

A tilt transducer designed by F.D. Stacey and others[6] uses a ratio transformer bridge to compare the capacitances in a differential capacitance transducer. They report tilt sensitivity on the order of nanoradians but with a range of ten millradians. This is also a contact sensor.

The sensor presented here has sensitivity on the order of tens of microradians making it as sensitive as most commercial optical devices and similar to the devices reported by Peters and de Jong. The primary advantages of this sensor are that it has infinite range and is a non-contact design. The rotor and stator are completely separated and the rotor is only a part of the circuit through its capacitive coupling with the stator. The designs from Peters and de Jong, while also non-contact and infinite range, are limited by the placement of the rotor between two stators.

5.6 Future Experiments

The experiments conducted so far provide a good picture of the sensor capabilities. There are a few factors that could still be investigated.

The stepper motor experiments which measured the angle between adjacent step positions provided only a rough idea of the capabilities of the sensor under large rotations. This regime could be tested further by using a test setup which could accurately measure large rotations. Probably the simplest method would be to couple a high-precision optical angular sensor to this sensor and directly compare the results. This approach has the added advantage of directly checking the sensor capabilities with those of an existing sensor.

Another parameter that was not examined was the capability of the sensor for measuring rotational velocity as opposed to just static position. There are two factors which are relevant to this question.

---

6 F.D. Stacey, et. al., "Displacement and tilt transducers of 140dB range," Journal of Scientific Instruments II (Series 2), 945-949.

From the engineering point-of-view, the limit on this capability is the speed of data acquisition from the sensor. Sixty-four signals have to be generated, measured, sampled, and recorded serially for each position measurement. If the rotor is rotated significantly between the first and last stage, then the data will be skewed.

For the current system, the time between the first and last signals is determined by the YCOUNT described in section 3.2 which has a period of $2.083\times10^{-4} seconds$. This is the amount of time to collect all sixty-four components of the sample. The experiments suggest that the resolution of the encoder is not better than $20\mu rad$. Imposing the limit that the rotor rotate at most one half of this amount over the time taken in acquiring the signals gives a maximum measurable velocity of $4.8\times10^{-2} {}^{rad}/_{sec}$ or $7.6\times10^{-3} Hz$. Measuring velocities greater than this will introduce a new source of error into the measurement. Thus this sensor is very limited in its ability to measure rotational velocities.

One simple solution to this problem is to decrease the period of the YCOUNT. While this will increase the measurable frequency of rotation, it does impose the second factor which limits velocity measurement. As the clock period gets smaller and smaller, the fields measured become increasingly less static. At some point, the assumption that the sensor is a collection of ideal parallel capacitors at constant voltage will break down and the time-varying nature of the signals will have to be taken into account. Future experiments could be performed to determine the optimal YCOUNT period for velocity measurements.

Another area that could be examined is the nature of the electric field generators. In the current design the generators are driven to five volts in order to create the field. Five volts was used primarily for convenience because most electronics use this level. If the design of the generating circuits was changed to use CMOS parts, then a higher voltage could be used. A higher generating voltage would be analagous to using a brighter light in the optical case. It would allow

greater resolution or the stator and rotor could be farther apart. So a future experiment could examine the relationship between field strength and resolution.

6 Conclusions

The original premise for designing an angular encoder based on electric field modification was to build a sensor capable of measuring angles in the microradian range that would be inexpensive to manufacture. Both more and less has been achieved. The current device is capable of measuring angles in the range of tens of microradians. This is not quite as accurate as was desired. However, the analyses did suggest some avenues for improving the accuracy. The sensor also appeared at first to be very sensitive to poor alignment. Further investigation uncovered a means to reduce significantly the impact of poor alignment on the sensor accuracy.

The real strength of this device comes from the design which keeps the stator and rotor physically separate. All of the electronics reside with the stator and the rotor is part of the device only through its capacitive coupling with the stator. Position information is carried entirely in the electric field that exists between the stator and the rotor.

This trait can be used particularily where attaching the rotor to an object would be difficult or impossible. For example, the position of a rotating shaft could be measusured by redesigning

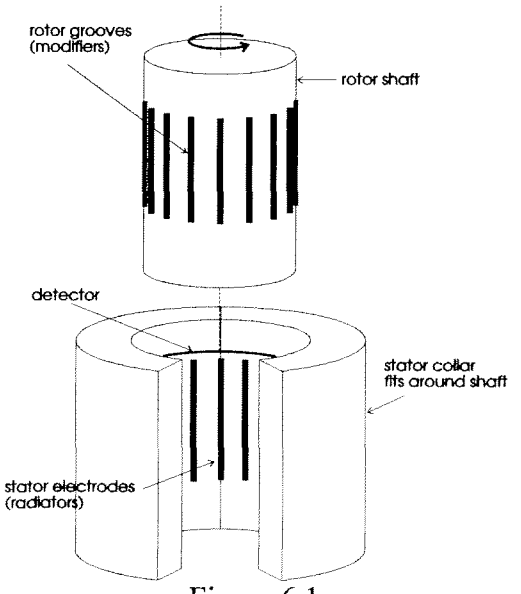

Figure 6.1
Shaft Position Sensor

the stator as a collar that fits around the shaft. The shaft itself could be the rotor by cutting a series of grooves longitudinally into it. This design removes the need for a mechanical linkage between the sensor and the shaft as the shaft is integrated into the sensor itself.

As mentioned previously, this design can correct for some of the error associated with incorrect alignment of the stator and rotor. An alternative approach would be to use the sensor as a device for measuring tilt and shift of the rotor with respect to the stator by measuring the signals at known angular positions. The error terms introduced into the measurement are sufficient to characterize the tilt or shift in magnitude and direction. This sensor, then, can be used for more than just angular position measurement. Preliminary measurements show that the sensor output is sensitive to shifts as small as a few microns although an detailed analysis has not yet been performed.

Returning to the shaft example, a shift in the shaft with respect to the collar would introduce a sinusoidal term into the position measurement assuming that the shaft is rotating at a constant velocity. The sensor could then be used to detect when the shaft is subject to some deflecting torque which could be a sign of impending failure. A sensor which was mechanically linked to the shaft might be able to detect the torque but might also be ruined itself from shift.

The angular sensor investigated here provides results that are on par with most commercial devices. It is also similar in capability to designs currently under research. The advantage of this design over these others is its ability to sense more than just angular position. It can detect lateral shift and tilt. This added information can be used to improve the angular precision or on its own. In addition, this design, which keeps the rotor and stator mechanically separate, is useful in some environments where other designs are not.

Bibliography

Bastion, Joseph. "Electrosensory Organisms," *Physics Today*, XLVII (February 1994), 30-37.

de Jong, Gerben W. et. al. "A smart capacitive absolute angular-position sensor," *Sensors and Actuators A*, XLI (1994), 212-16.

Dower, Roger. "Electrostatic Imaging Apparatus," Patent Application.

Faraday, Michael. *Experimental Researches in Electricity*. vol. I. New York: Dover Publications, Inc., 1965.

Guralnik, David B. ed. *Webster's New World Dictionary of the American Language*. 2nd College Ed. New York: Simon & Schuster. Inc., 1984.

Instrument Society of America. *ISA Transducer Compendium*. vol. II. 2nd ed. Pittsburgh, Pa.: Instrument Soc.of America, 1970.

Jankauskas, G.T., J.R. LaCourseand D.E. Limbert. "Optimization and analysis of a capacitive contactless angular transducer," *IEEE Transactions on Instrumentation and Measurement*, XLI (April 1992), 311-15.

Meeks, E.L., R.D. Peters and R.T. Arnold. "Capacitance Microphones for Measurement of Ultrasonic Properties of Solids," *Review of Scientific Instruments*, XLII (October 1971), 1446-1449.

Neubert, Hermann Karl Paul. *Instrument Transducers: An Introduction to Their Performance and Design*. 2nd ed. Oxford: Oxford Clarendon Press, 1975.

Peters, R.D. "Capacitive angle sensor with infinite range," *Review of Scientific Instruments*, LXIV (March 1993), 810-813.

-----. "Linear rotary differential capacitance transducer," *Review of Scientific Instruments*, LX (August 1989), 2789-2793.

Press, William H., Saul A. Teukolsky, William T. Vetterling, Brian P. Flannery, *Numerical Recipes in C: The Art of Scientific Computing*. 2nd ed. Cambridge: Cambridge University Press, 1992.

Stacey, F.D., J.W.M. Rynn, E.C. Little, and C. Croskell. "Displacement and tilt transducers of 140dB range," *Journal of Scientific Instruments (Journal of Physics E)*. Series 2. II (1969), 945-949.

A Commonly Used Variables

Several variables are used throughout the document. Each is defined when it is first used, but for convenience they are all collected here together with their meanings.

Variable Name	Definition
N_r	Number of radiator pads on the stator disk
N_m	Number of modifier pads on the rotor disk
n	The index of a given reading within a sample (between 0 and 63)
V_n	The sensor reading within a sample that corresponds to the index
A	Amplitude of a sample
B	DC offset of a sample
θ	Phase of a sample
γ	Rotor position that corresponds to θ through $\gamma = \frac{\theta}{33}$
H_n	The nth frequency component of a sample converted to the frequency domain
$\lvert H_n \rvert$	The magnitude of the nth frequency component
$\angle H_n$	The phase of the nth frequency component
d_o	Average separation between stator disk and rotor disk
d_n	Separation of pad n on the stator and the rotor
α	Tilt angle of rotor disk
R	Distance from the centre of the stator to the centre of a radiator pad
θ_t	Phase of tilt error term
A_t	Amplitude of tilt error term
θ_s	Phase of shift error term
A_s	Amplitude of shift error term
T_θ	Period of θ compared with rotor period of 2π radians
T_t	Period of tilt error term compared with rotor period of 2π radians

T_S	Period of shift error term compared with rotor period of 2π radians
ω_{hi}	Frequency of rapid oscillation in a sample
ω_{lo}	Frequency of envelope in a sample
t_n	Time that corresponds to index n in a sample
D	Distance from the laser to the reflecting mirror
X	Deflection of the reflected beam from the outgoing laser beam
φ	Angle of deflection of the reflected beam which is related to γ by $\varphi = 2\gamma$
β	Angle between outgoing laser beam and direction of deflection measurement
h	Distance from the mirror to the laser spot detector
μ	Deviation of the calculation of θ from the true angle

B Sensor Samples and Graphs

The sensor presents data about the angular position to the computer in the form of a sequence of sixty-four bytes of data each eight bits in length. The collection of data is collectively referred to as a *sample*. The individual bytes of data within a sample are indexed by a sample index which can be any integer value between zero and sixty-three. This index is usually given the name n. The corresponding data value is V_n

Internally the computer translates these unsigned bytes of data into a floating point format. This allows two samples to be added, subtracted, or otherwise transformed without loss of precision. This is important because, usually, a sensor reading is taken as the average of ten or twenty samples with a baseline sample subtracted.

Sensor samples are displayed graphically in two ways. The first way is in the index domain. The index domain loosely corresponds to the time domain but the basic unit is the index number of the sample, n. The relationship between index number and time is given by $t_n = \frac{n}{2(307200)}\,seconds$(see equation (3.1) for a further explanation). The sample index is given on the x-axis of the graph. The corresponding sample data value is graphed on the y-axis. This sample data value is in units determined by the analog-to-digital convertor used to digitize the signals. For this device, the convertor had 256 digitization levels and the corresponding voltage range was set to 2.5 volts. So one unit one the graph corresponds to $\frac{2.5}{256} \approx 0.01 \text{volts}$.

The second way of presenting sample data is in the frequency domain. The Fourier transform of a sample can be considered as an operator that returns two new samples. The first is the magnitude sample and the second is the phase sample.

Since the original sample contains only real values, the magnitude sample values, M_n are symmetric about $n = 32$, that is $M_n = M_{63-n}$. The phase sample values, P_n, are antisymmetric so $P_n = -P_{63-n}$.

As can be seen in the example graphs, the samples from the sensor are strongly peaked in the frequency domain at frequency index 31 as expected from equation (2.1).

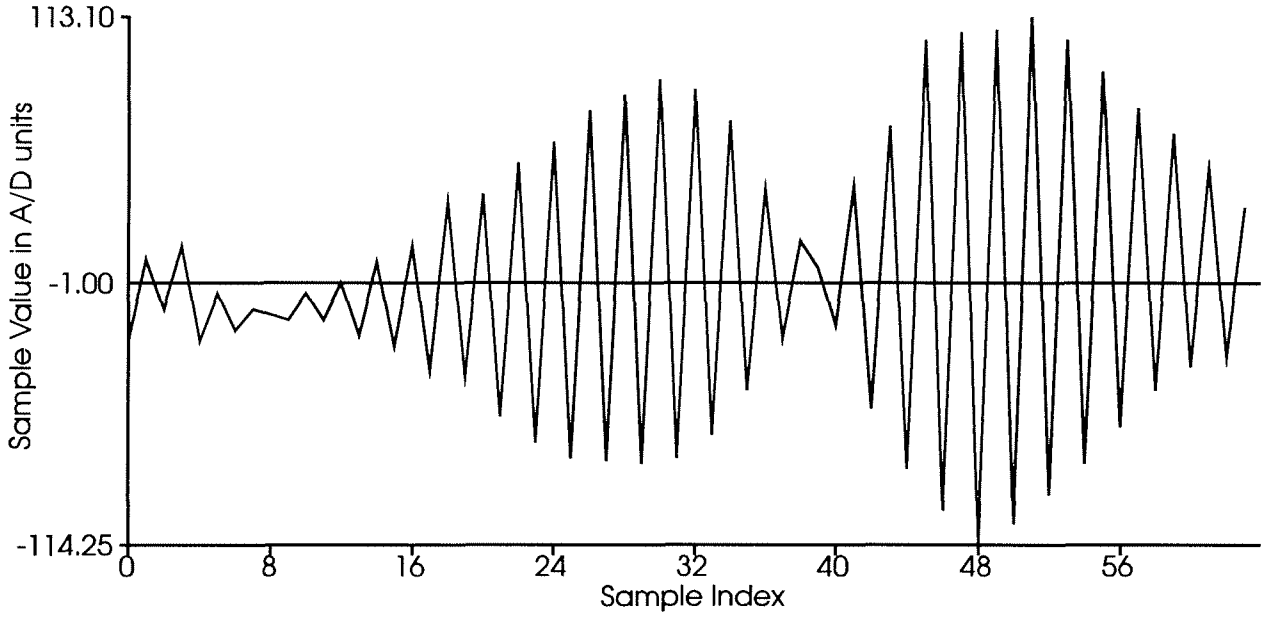

Figure B.1
Sample in Index Domain

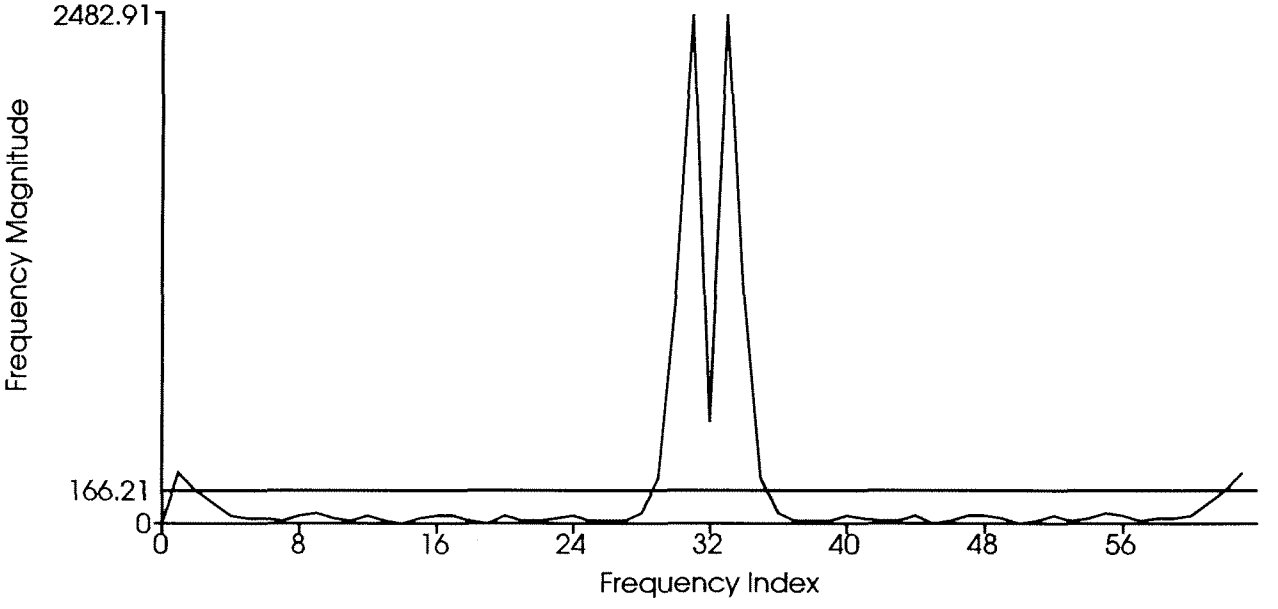

Figure B.2
Magnitude of Sample in Frequency Domain

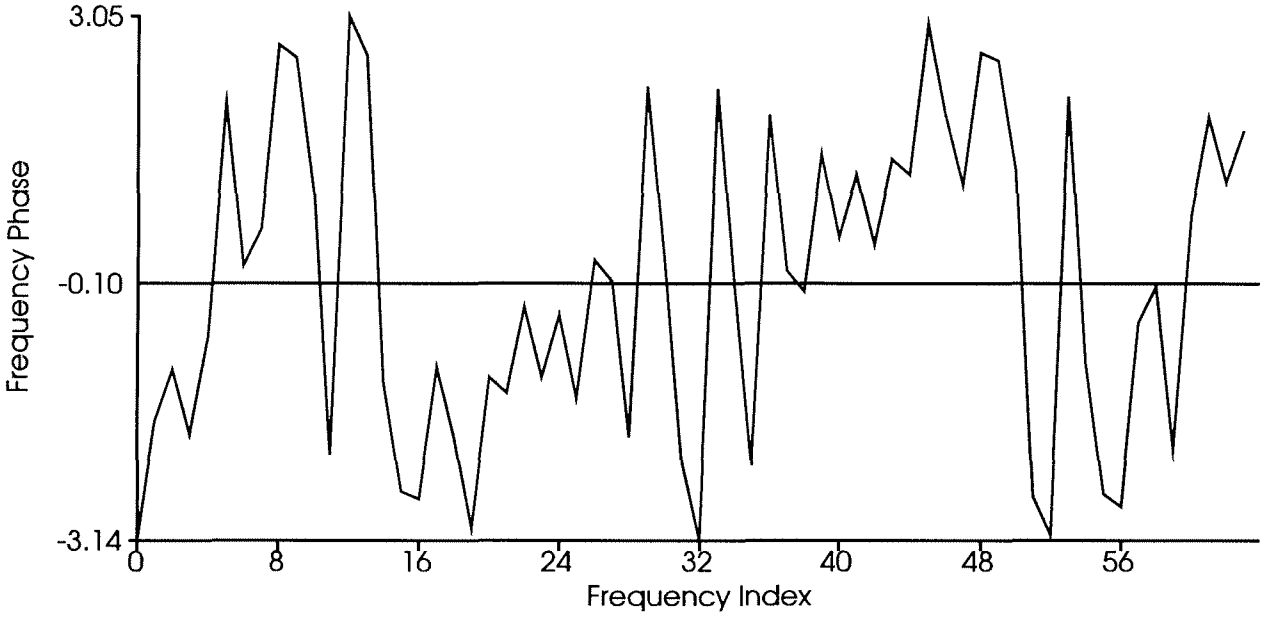

Figure B.3
Phase of Sample in Frequency Domain

C Circuit Diagram for Interface Board

The circuit diagram for the interface board is shown on the following pages. The diagram is broken into six pieces which resolve into the original diagram according to the table.

Page 89	Page 92	Page 95	Page 98
Page 90	Page 93	Page 96	Page 99
Page 91	Page 94	Page 97	Page 100

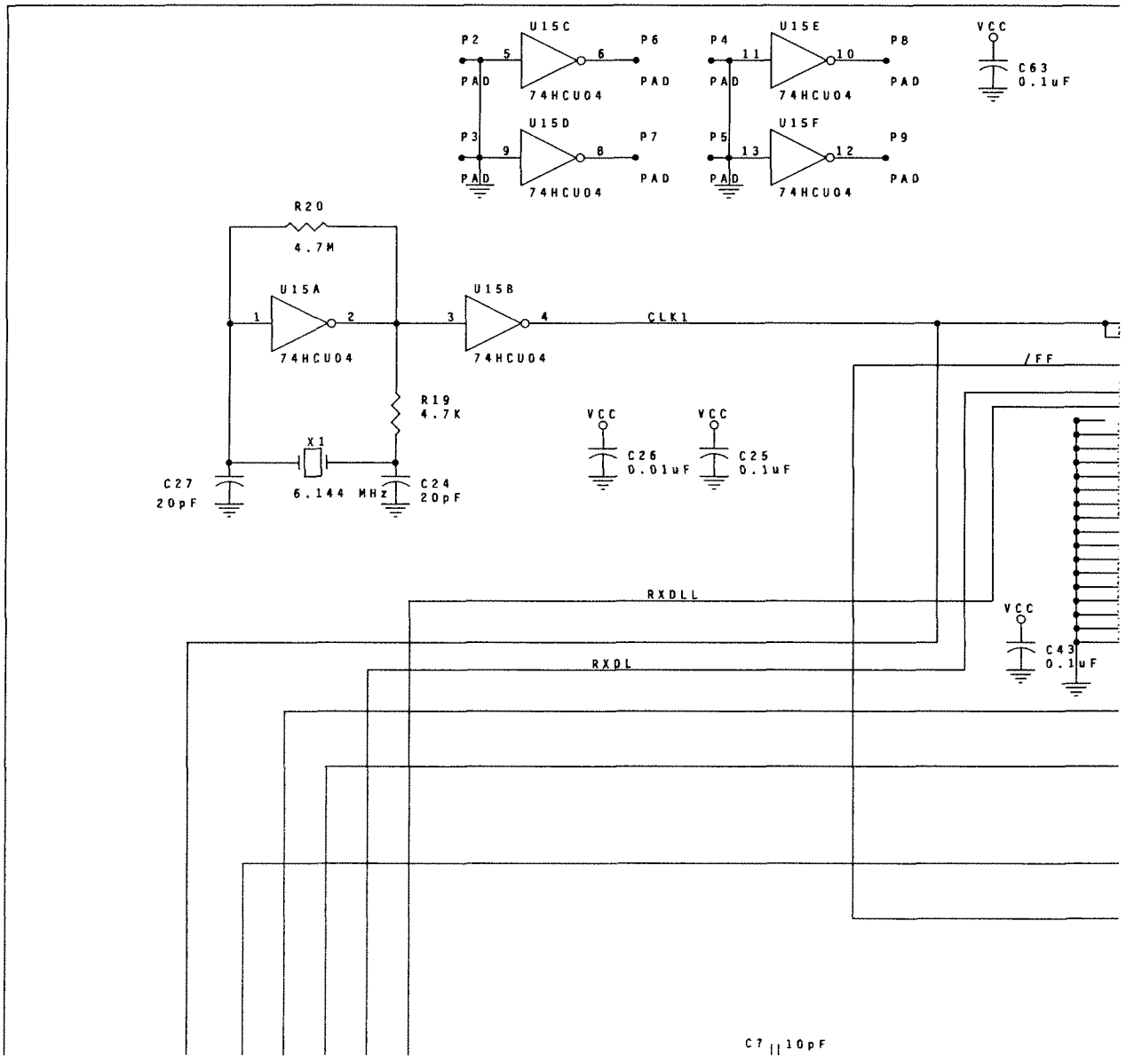
U15C
P2
5
6
P6
PAD
PAD
74HCU04
U15E
P4
11
10
P8
PAD
PAD
74HCU04
VCC
C63
0.1uF
U15D
P3
9
8
P7
PAD
PAD
74HCU04
U15F
P5
13
12
P9
PAD
PAD
74HCU04
R20
4.7M
U15A
1
2
74HCU04
U15B
3
4
74HCU04
CLK1
/FF
R19
4.7K
X1
C27
20pF
6.144 MHz
C24
20pF
VCC
C26
0.01uF
VCC
C25
0.1uF
RXDLL
RXDL
VCC
C43
0.1uF
C7
10pF

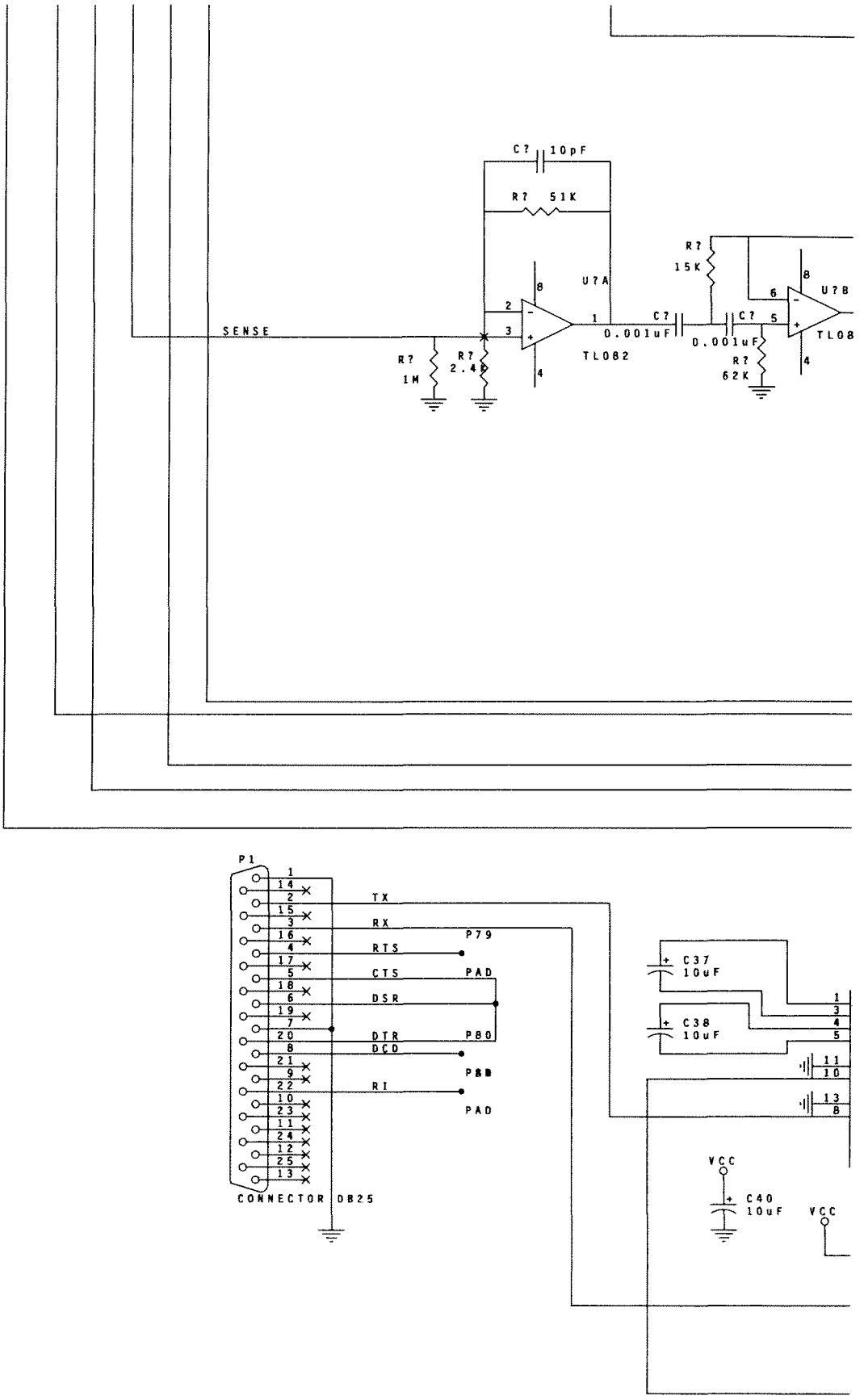
C? 10pF
R? 51K
R? 15K
U?A
U?B
SENSE
C?
0.001uF
C?
0.001uF
R? 1M
R? 2.4K
TL082
R? 62K
TL08
P1
TX
RX
RTS
CTS
DSR
DTR
DCD
RI
P79
PAD
P80
P&B
PAD
CONNECTOR DB25
C37 10uF
C38 10uF
VCC
C40 10uF
VCC

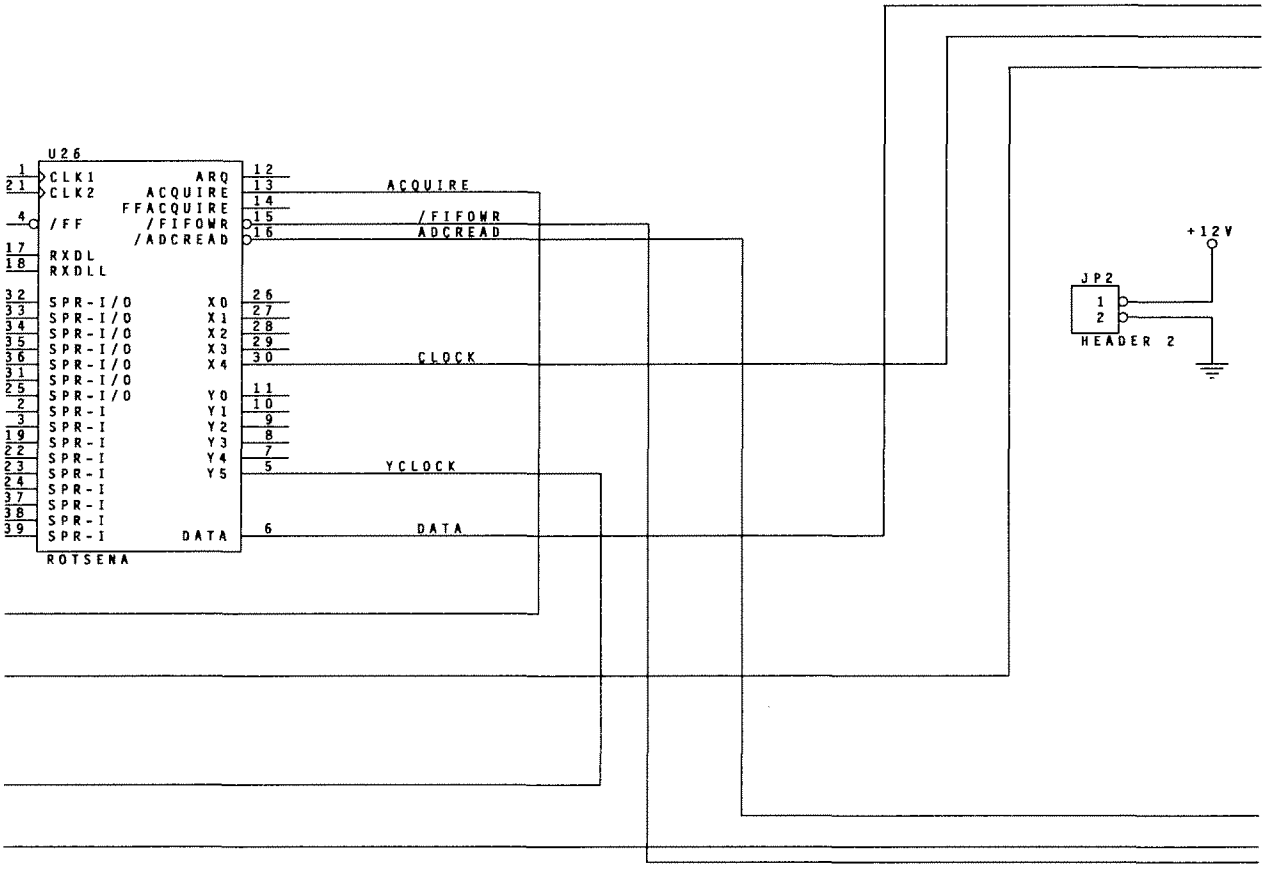
U26
CLK1
CLK2
/FF
RXDL
RXDLL
SPR-I/O
SPR-I
ARQ
ACQUIRE
FFACQUIRE
/FIFOWR
/ADCREAD
X0
X1
X2
X3
X4
Y0
Y1
Y2
Y3
Y4
Y5
DATA
ROTSENA
ACQUIRE
/FIFOWR
ADCREAD
CLOCK
YCLOCK
DATA
+12V
JP2
HEADER 2

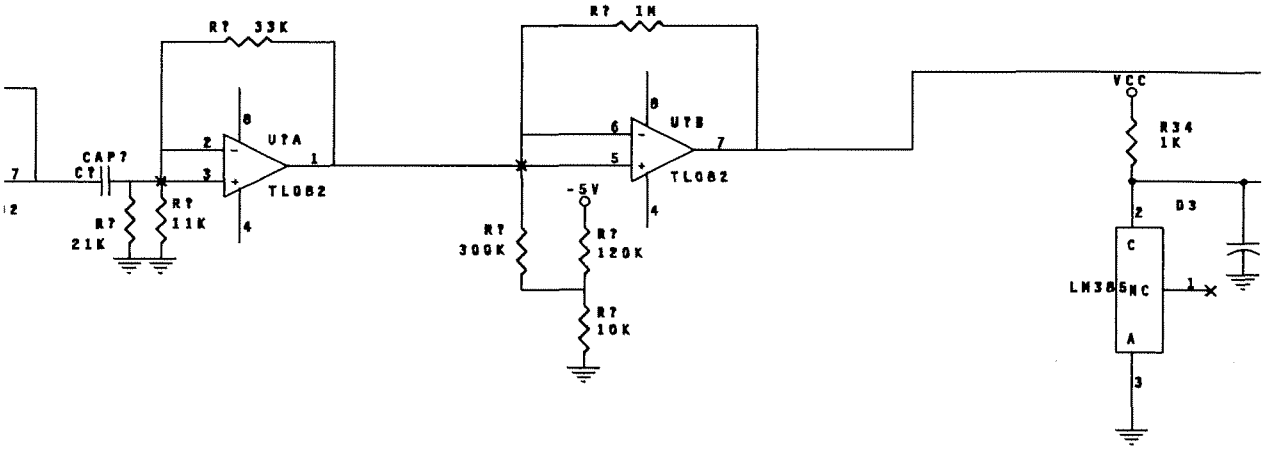
R? 33K
R? 1M
CAP?
C?
R?
21K
R?
11K
U?A
TL082
U?B
TL082
-5V
R?
300K
R?
120K
R?
10K
VCC
R34
1K
D3
LM385
C
NC
A
1
2
3

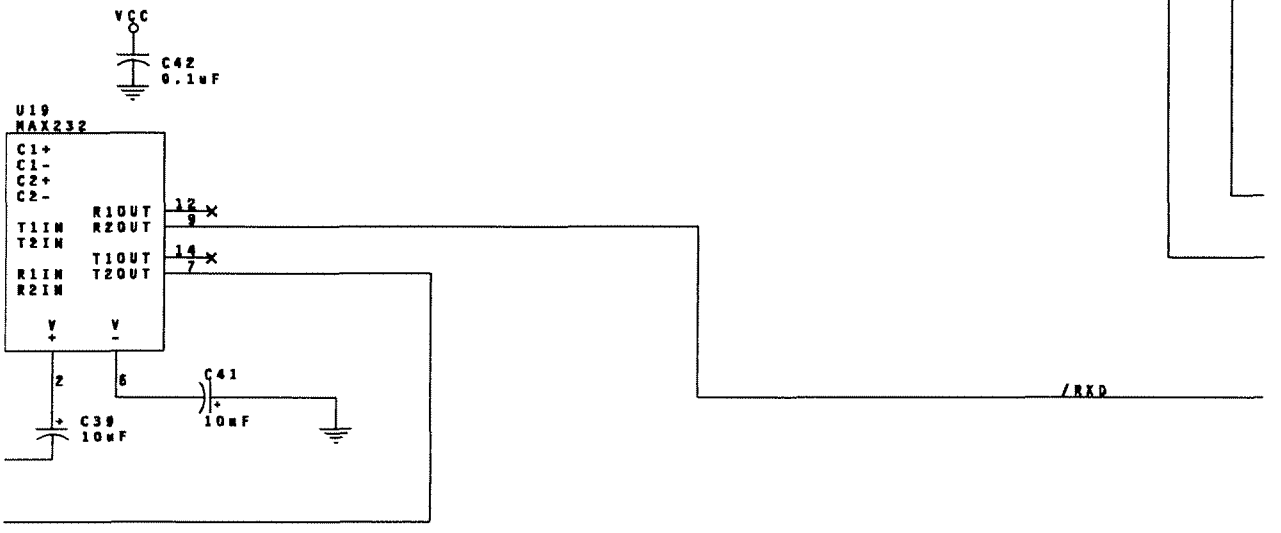
VCC
C42
0.1uF
U19
MAX232
C1+
C1-
C2+
C2-
T1IN
T2IN
R1IN
R2IN
R1OUT
R2OUT
T1OUT
T2OUT
V+
V-
C39
10uF
C41
10uF
/RXD

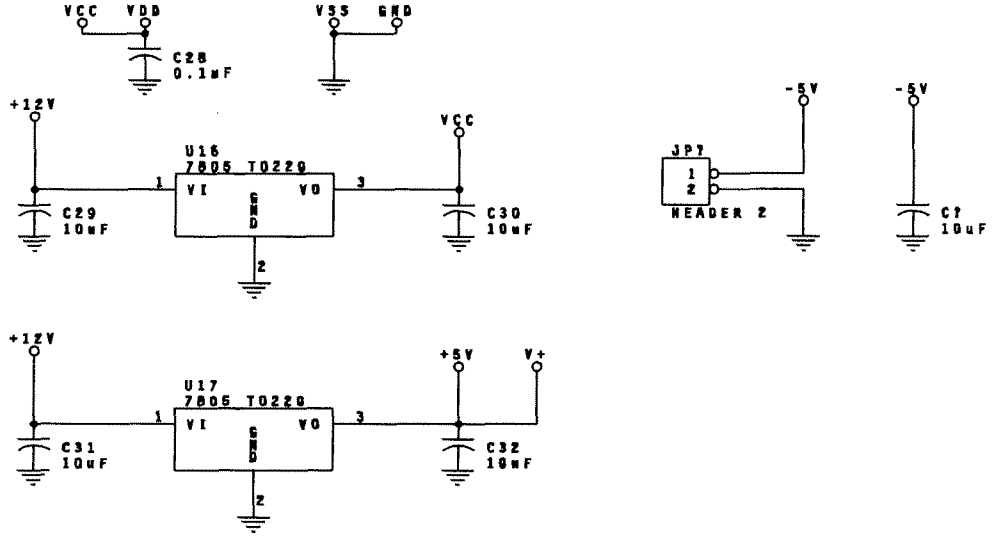
VCC
VDD
C28
0.1uF
VSS
GND
+12V
U16
7805 TO220
VI
GND
VO
C29
10uF
C30
10uF
VCC
+12V
U17
7805 TO220
VI
GND
VO
C31
10uF
C32
10uF
+5V
V+
-5V
JP?
HEADER 2
-5V
C?
10uF

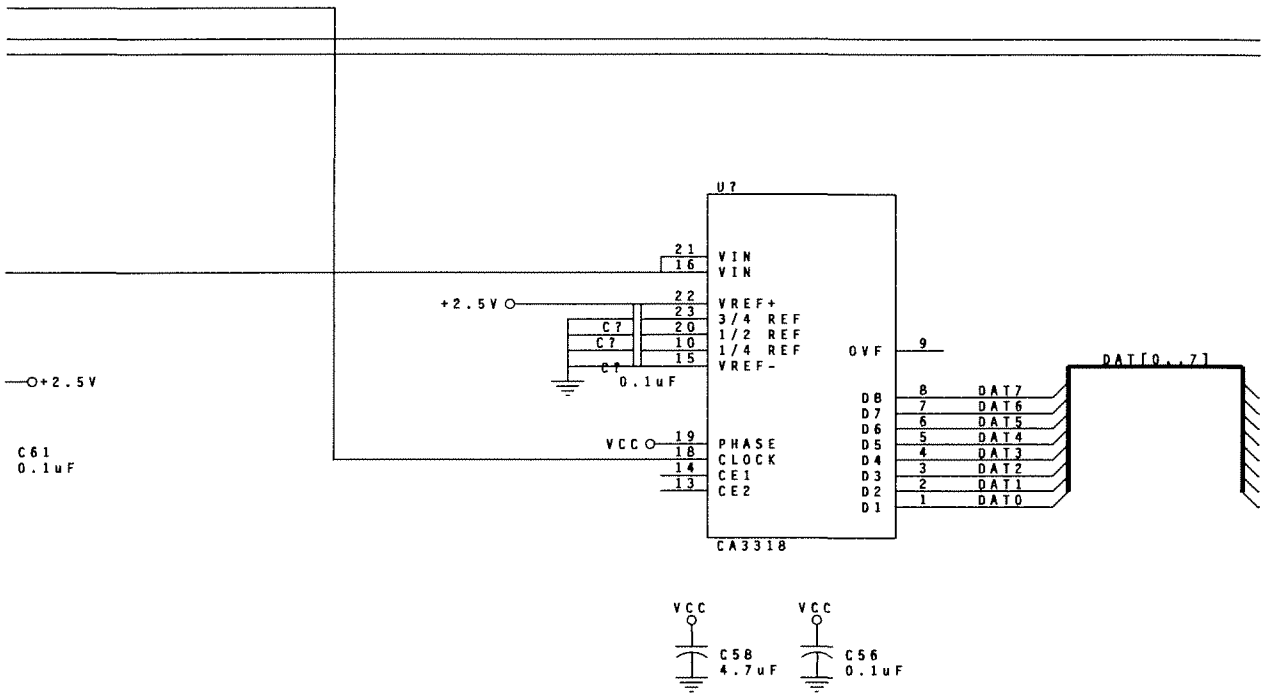
U7
VIN
VIN
+2.5V
VREF+
3/4 REF
1/2 REF
1/4 REF
VREF-
C7
C7
C7
0.1uF
+2.5V
C61
0.1uF
VCC
PHASE
CLOCK
CE1
CE2
OVF
D8
D7
D6
D5
D4
D3
D2
D1
DAT7
DAT6
DAT5
DAT4
DAT3
DAT2
DAT1
DAT0
DAT[0..7]
CA3318
VCC
C58
4.7uF
VCC
C56
0.1uF

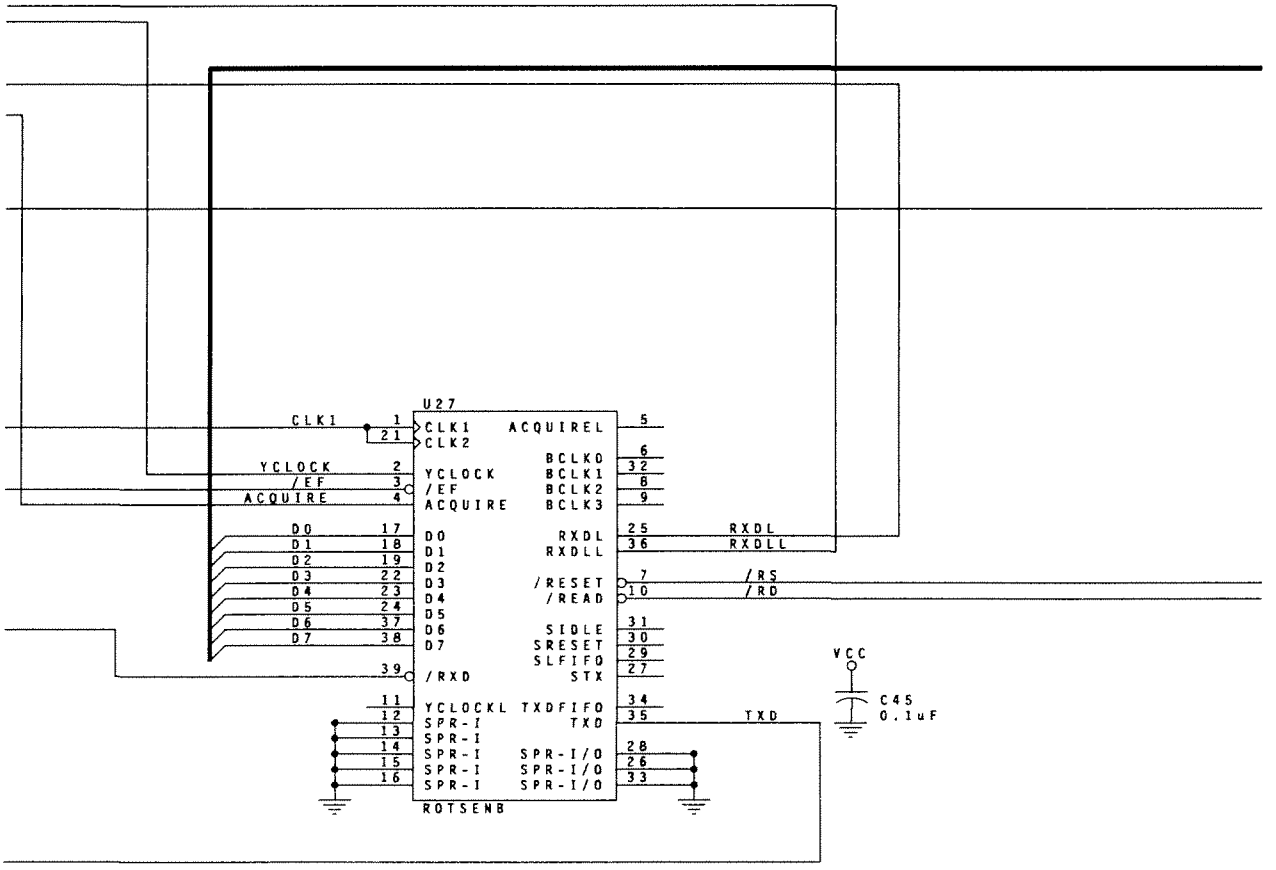
U27
CLK1
CLK2
ACQUIREL
BCLK0
BCLK1
BCLK2
BCLK3
YCLOCK
/EF
ACQUIRE
D0
D1
D2
D3
D4
D5
D6
D7
RXDL
RXDLL
/RESET
/READ
SIDLE
SRESET
SLFIFO
STX
/RXD
YCLOCKL
TXDFIFO
TXD
SPR-I
SPR-I/O
ROTSENB
RXDL
RXDLL
/RS
/RD
TXD
VCC
C45
0.1uF

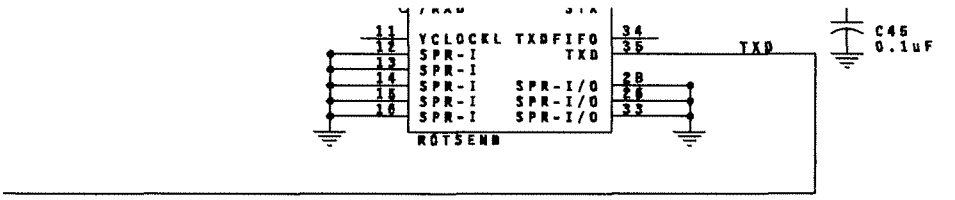
11
12
13
14
15
16
YCLOCKL
SPR-I
SPR-I
SPR-I
SPR-I
SPR-I
TXBFIFO
TXD
SPR-I/O
SPR-I/O
SPR-I/O
34
35
28
26
33
TXD
C45
0.1uF
ROTSEND

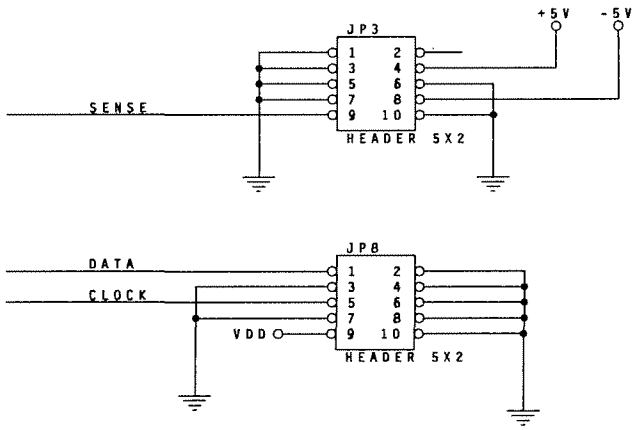
JP3
+5V
-5V
SENSE
1 2
3 4
5 6
7 8
9 10
HEADER 5X2
JP8
DATA
CLOCK
VDD
1 2
3 4
5 6
7 8
9 10
HEADER 5X2

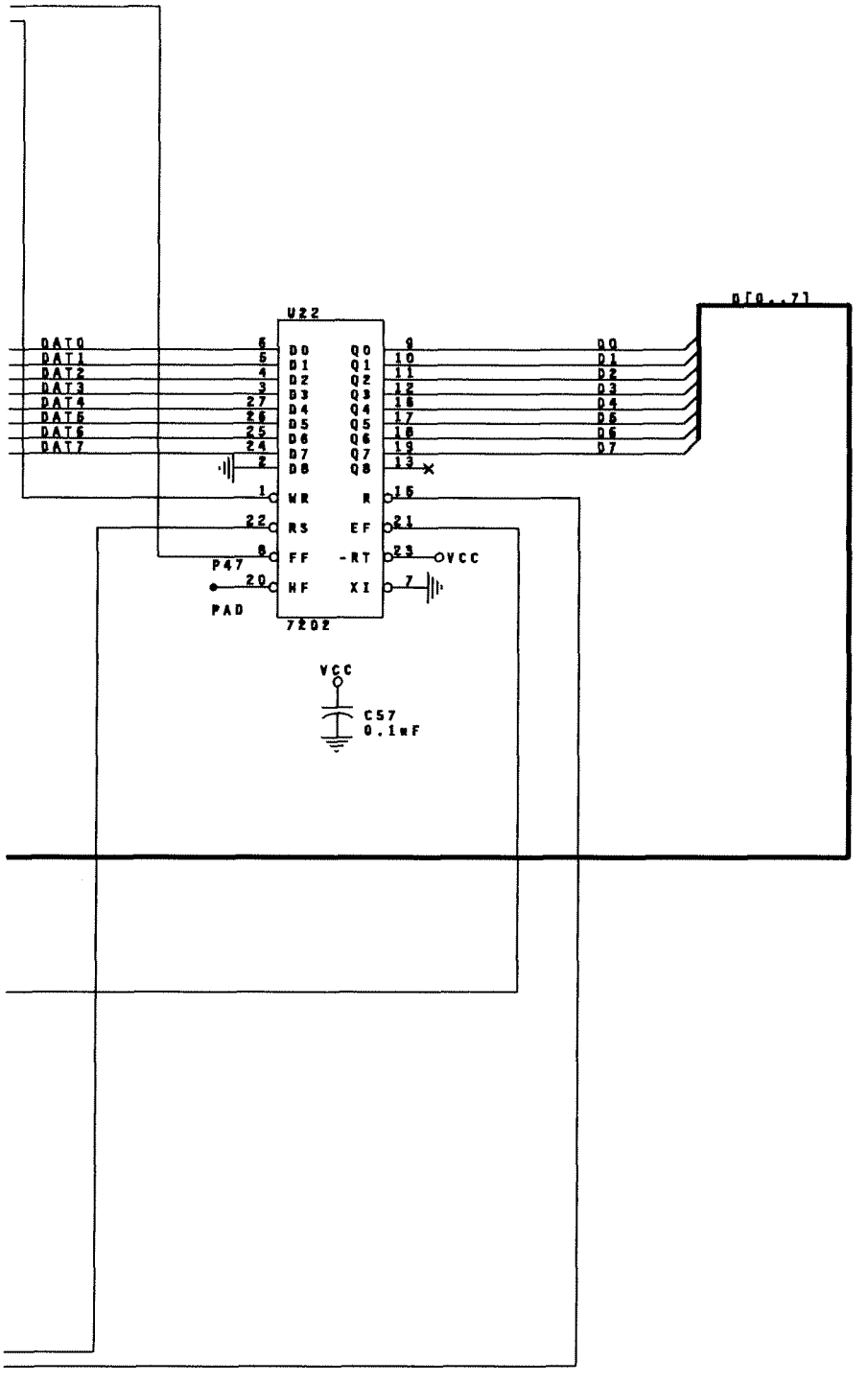
U22
DAT0
DAT1
DAT2
DAT3
DAT4
DAT5
DAT6
DAT7
D0
D1
D2
D3
D4
D5
D6
D7
D8
WR
RS
FF
HF
Q0
Q1
Q2
Q3
Q4
Q5
Q6
Q7
Q8
R
EF
-RT
XI
VCC
P47
PAD
7202
VCC
C57
0.1uF
Q[0..7]

Title	ROTORY SENSOR INTERFACE	
Size D	Document Number SENINT1.SCH	REV C
Date: February 16, 1994	Sheet of	

D Circuit Diagram for Stator Board

The circuit diagram for the stator board is shown on the following pages. The diagram is broken into two pieces which resolve into the original diagram according to the table.

Page 102	Page 103

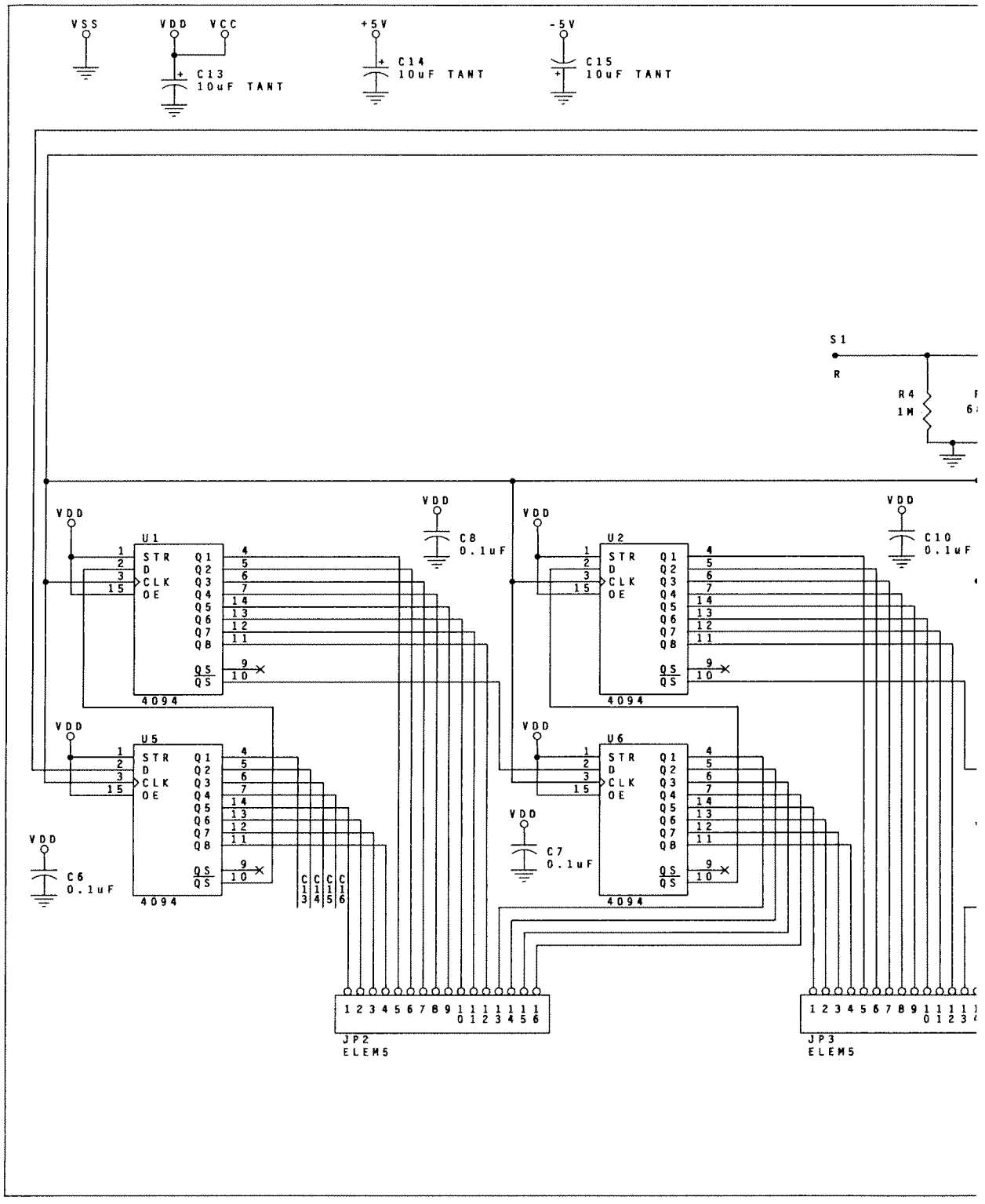
VSS
VDD
VCC
C13
10uF TANT
+5V
C14
10uF TANT
-5V
C15
10uF TANT
S1
R
R4
1M
U1
U2
U5
U6
4094
STR
D
CLK
OE
Q1
Q2
Q3
Q4
Q5
Q6
Q7
Q8
QS
QS
C8
0.1uF
C10
0.1uF
C6
0.1uF
C7
0.1uF
JP2
ELEM5
JP3
ELEM5

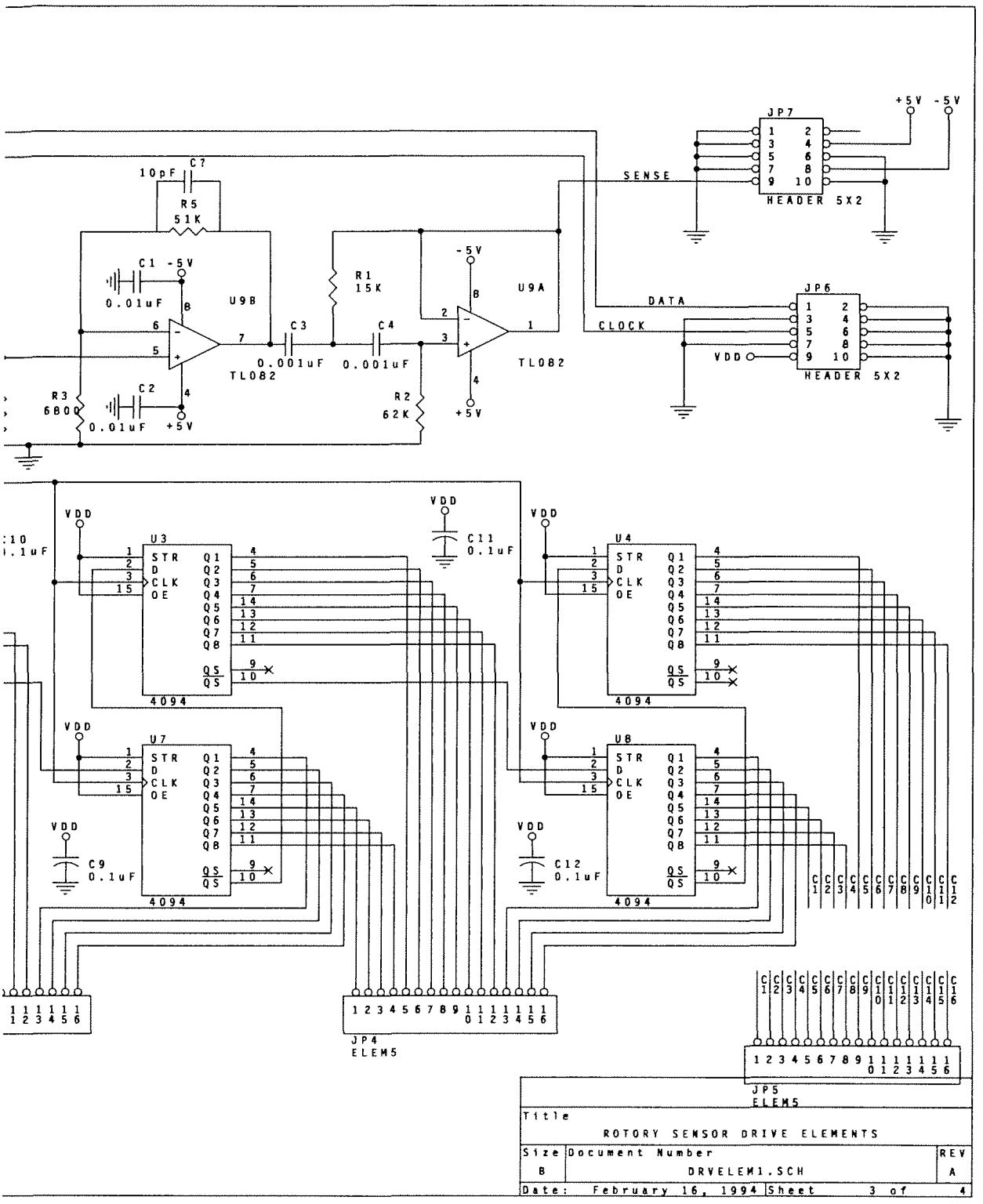
JP7
HEADER 5X2
+5V
-5V
SENSE
C7
10pF
R5
51K
C1
0.01uF
U9B
TL082
R1
15K
U9A
TL082
C3
0.001uF
C4
0.001uF
JP6
HEADER 5X2
DATA
CLOCK
VDD
R3
680
C2
0.01uF
R2
62K
U3
U4
U7
U8
4094
C9
0.1uF
C11
0.1uF
C12
0.1uF
JP4
ELEM5
JP5
ELEM5
Title
ROTORY SENSOR DRIVE ELEMENTS
Size
B
Document Number
DRVELEM1.SCH
REV
A
Date: February 16, 1994
Sheet 3 of 4

E Laser Spot Detector

The laser spot detector determines the position of the reflected laser beam in the experiment described in section 4.2.

The total length of the beam described in the experiment is approximately twenty metres. Over this distance, the laser beam expands to a half-power width of three centimetres. The two phototransistors in the laser detector circuit are physically mounted two centimetres apart on a micrometre slide. The laser and detector are both mounted on an optical bench and aligned so that the direction of travel of the slide is perpendicular to the bench.

The output of the circuit is a voltage. This voltage is positive or negative if the currents through the phototransistors do not balance and zero if they do balance. The point at which the currents balance is used as the reference point.

When the rotor is turned, the slide is adjusted to find the new balance point. The change in position is read directly off the micrometre.

The one Hertz low-pass filter in the circuit removes noise from the signal which results from flicker in the room lights or in the laser beam.

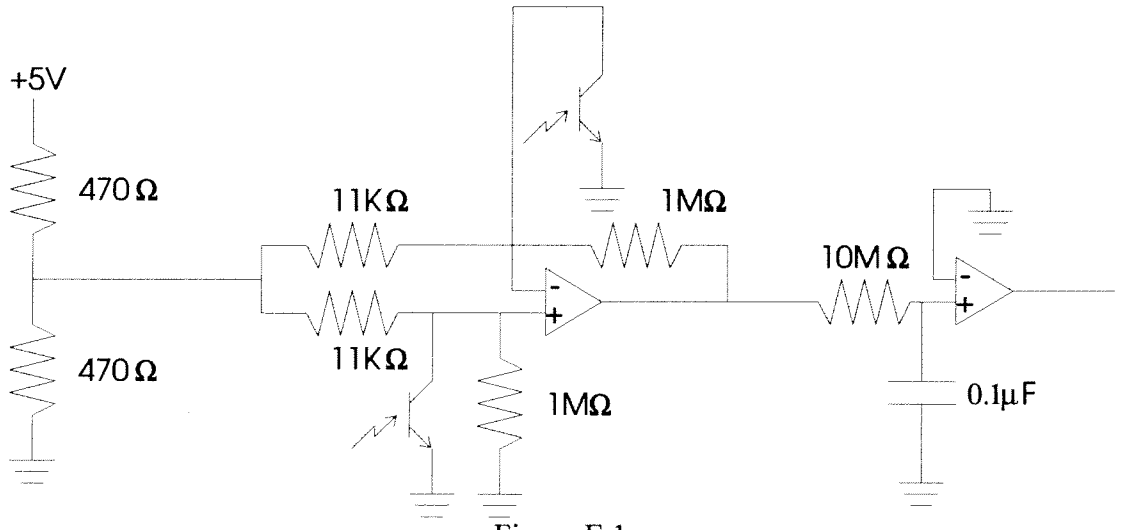

Figure E.1
Laser Spot Detector Circuit

F Stepper Motor Driver

The stepper motor driver circuit is used to control the stepper motor described in section 4.3 from a personal computer with a twenty-five pin parallel port.

The circuit shown below is half of the total driver circuit. The stepper motor used has two coils, so an identical circuit is used to drive the second coil.

All of the parts used were standard parts except the power MOSFETs. A part, MPM3004, from Motorola was used for each coil. This part contains the two p-channel and two n-channel FETs needed and includes diode protection for the inductive load.

The points A,B,C, and D connect to the indicated pins on the parallel port of the computer. The circuit driving the second coil connects to pins indicated by A',B',C', and D'.

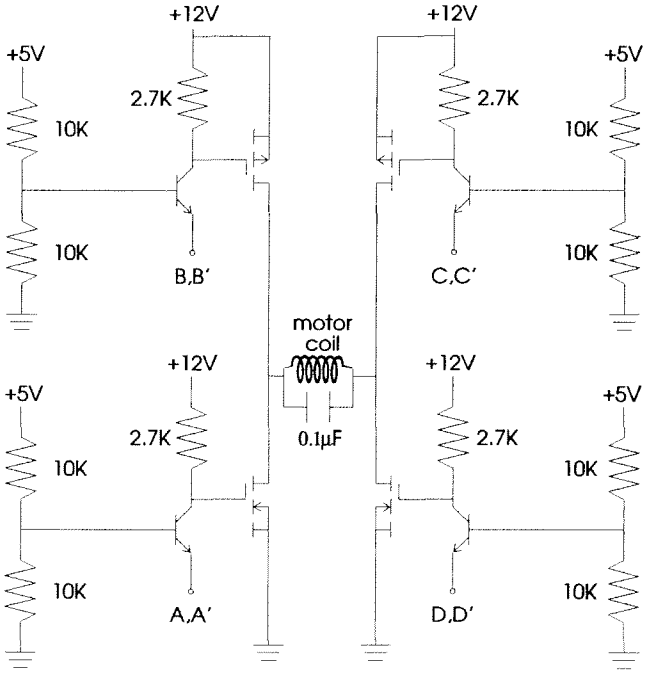

A connects to pin 2 on the computer parallel port
B connects to pin 3
C connects to pin 4
D connects to pin 5

A' connects to pin 6 on the computer parallel port
B' connects to pin 7
C' connects to pin 8
D' connects to pin 9

Figure F.1
Stepper Motor Controller Circuit

G Analog Filters

As mentioned in section 3.2 there are two stages of amplification and filtering performed on the stator board directly in order to strenthen the relevant signals to the point where they can be safely transmitted to the interface board. The signals are further conditioned by another four stages on the interface board so that the signals use the full range of the analog-to-digital convertor.

The first stage on the stator board is a low-pass amplifer with a single pole at $f = \frac{1}{2\pi CR_1} = 310kHz$ and a single zero at $f = \frac{1}{2\pi}\left(\frac{1}{CR_2} + \frac{1}{CR_1}\right) = 3.0MHz$. The gain of the amplifer at unity is 19dB.

The transfer function of the filter is:

$$T(s) = \frac{(R_1 + R_2) + sCR_1R_2}{R_2 + sCR_1R_2}$$

where:

$$C = 10pF$$

$$R_1 = 51K\Omega$$

$$R_2 = 6.8K\Omega$$

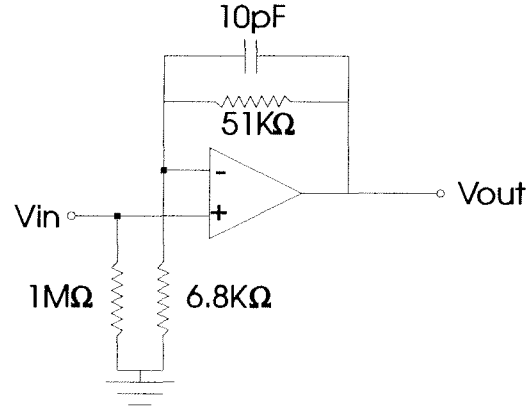

Figure G.1
Stator Amplifer Stage 1

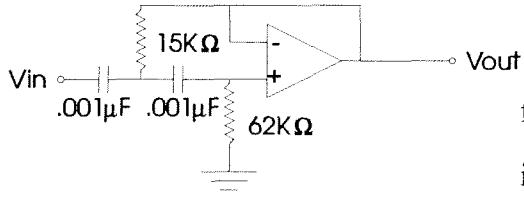

The second stator stage is designed to filter out low frequency noise. It is a high pass filter with unity gain in its pass band. The transfer function for the filter is:

Figure G.2
Stator Amplifer Stage 2

$$T(s) = R_1R_2C_1C_2 \frac{s^2(R_2C_1s + 1)}{(R_1R_2^2C_1^2C_2)s^3 + (2R_1R_2C_1C_2 + R_1^2C_1^2)s^2 + (R_1C_1 + R_1C_2 + R_2C_1)s + 1}$$

where:

$$C_1 = 0.001\mu F$$

$$C_2 = 0.001\mu F$$

$$R_1 = 15K\Omega$$

$$R_2 = 62K\Omega$$

The filter has three zeroes, two at $f = 0$ and one at $f = 2.6kHz$. There is a simple pole at $f = 2.1kHz$ and a quadratic pole at $f = 5.7kHz$.

The next four stages of amplification and filtering are on the interface board. The first two of these are identical configurations to the two on the stator board except that $R_2 = 2.4K\Omega$ in the first stage. This change moves the zero further away from the pole so that there is greater attenuation of high frequency noise.

The third stage on the interface board is another high pass filter with:

$$T(s) = CR_3(1 + \frac{R_1}{R_2})\frac{s}{sCR_3 + 1}$$

where:

$$C = 22pF$$

$$R_1 = 33K\Omega$$

$$R_2 = 11K\Omega$$

$$R_3 = 21K\Omega$$

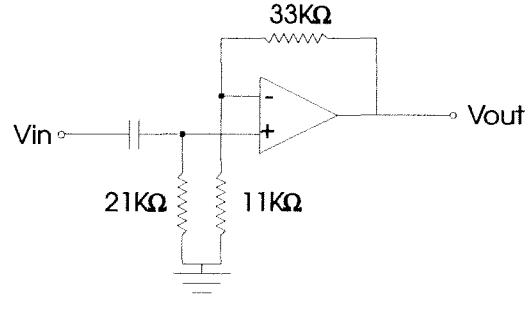

Figure G.3
Board Amplifier Stage 3

The amplifier has a zero at the origin and a pole at $f = \frac{1}{2\pi CR_3} = 340kHz.$

The final amplifier does not filter the signal (except in the bandwidth limit of the op-amp) and is used to get the signal in the range 0 - 2.5V for the analog-to-digital convertor.

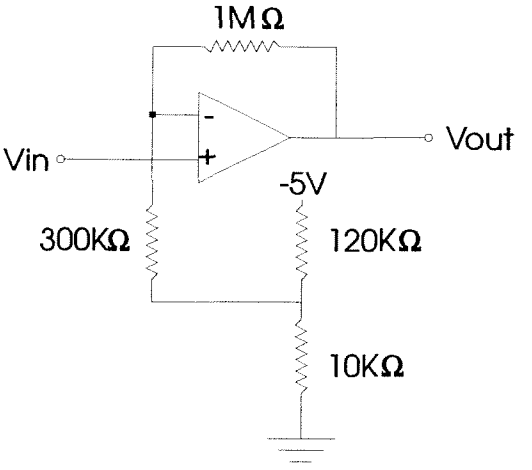

Figure G.4
Board Amplifier Stage 4